MINISTRY OF ENERGY AND MINERAL RESOURCES

Palu-Type Liquefaction

A Unique Natural Phenomenon in the World, A Comprehensive Geological Review

alu, Sulawesi Tengah 94221, Indonesia

PALU-TYPE LIQUEFACTION

(A Unique Natural Phenomenon in the World, A Comprehensive Geological Review)

PALU-TYPE LIQUEFACTION

(A Unique Natural Phenomenon in the World, A Comprehensive Geological Review)

MINISTRY OF ENERGY AND MINERAL RESOURCES
2025

ISBN : 978-634-96502-1-2

PALU-TYPE LIQUEFACTION

(A Unique Natural Phenomenon in the World, A Comprehensive Geological Review)

Authors
Muhammad Wafid A.N., Suyono, Taufiq Wira Buana, Sukahar Eka Adi Saputra, Akbar Cita, Munib Ikhwatun Iman, Supartoyo, Rio Alcanadre Tanjung M., Luli Gustiantini, Firman Maliki, Ryan Nur Rahdiana, Wawan Hermawan, William Pradana Solu, Athanasius Cipta, Merry Christina Natali, Imam Catur Priambodo, Risna Widyaningrum, Amalfi Omang, Purnomo Rahardjo, Joko Wahyudiono, Yudhicara, Irwan Hidayat Suherman, Akhmad Solikhin, Taat Setiawan, Abdullah Husna, Fadlianto Nurfalah, Ex Marwanto, Ibrahim Mandi, Nurmaliah, Rohman

Editors
Hermes Panggabean, Wahyu Wilopo, Sri Hidayati

Copy Editors
Nenen Adriyani, Atep Kurnia

Design Cover
Agus Soma

Artistics & Layout
Muhamad Iqbal

Managing Publisher
Joko Parwata, Rian Koswara, Ivan Ferdian

Published by:
Ministry of Energy and Mineral Resources
Jl. Merdeka Selatan No. 18, Jakarta Pusat 10110 - Indonesia

Printed by:
Geological Agency
Jl. Diponegoro No. 57 Bandung 40122 - Indonesia
Phone : 022 - 7215297
Fax : 022 - 7216444/021-5228372
Website : www.geologi@esdm.go.id

First Printing, November 2025
Copyright @2025 by Geological Agency
All right reserved.
No part of this book may be reproduced in any form, electronic, or mechanical, without permission in writing from publisher or authors.

ADDRESS
MINISTER OF ENERGY AND MINERAL RESOURCES

Praise and gratitude be to God Almighty. By His blessings and grace, the Ministry of Energy and Mineral Resources (ESDM), through the Geological Agency, has successfully completed the preparation and publication of the book *of Palu-Type Liquefaction*.

This publication reflects the Ministry of ESDM's duties and functions. As stipulated in Ministerial Regulation No. 12 of 2025 concerning the Organization and Work Procedures of the Ministry of Energy and Mineral Resources, the Ministry is responsible for administering government affairs in the energy and mineral resources sector to assist the President in managing state governance. In carrying out this mandate, the Ministry undertakes strategic functions, including investigations and services in geology, volcanology, geological hazard mitigation, groundwater, environmental geology, and geological surveys.

As a first-echelon unit within the Ministry, the Geological Agency plays a pivotal role in promoting public welfare through geological resource investigations and services, while safeguarding the public through hazard mitigation efforts. The liquefaction event triggered by the major earthquake in Palu and its surrounding areas underscores the Agency's direct involvement in disaster management, including scientific studies, hazard mapping, emergency response, and technical recommendations for future mitigation.

In this context, the publication of *Palu-Type Liquefaction* holds critical importance. The book serves not only as scientific documentation of the disaster but also as a strategic reference for the development of geological hazard mitigation policies. It is hoped that this work will be utilized by local governments, technical institutions, academics, and the public to strengthen awareness, understanding, and preparedness regarding potential liquefaction hazards in Indonesia.

Finally, I extend my sincere appreciation to the Geological Agency, the entire writing team, and all who contributed to this book. May this publication stand as a concrete demonstration of the Ministry of Energy and Mineral Resources' commitment to safeguarding the safety and welfare of the Indonesian people.

Jakarta, November 2025
Ministry of Energy and Mineral Resources

Bahlil Lahadalia

FOREWORD
HEAD OF THE GEOLOGICAL AGENCY

We express our gratitude to God Almighty, for by His grace and blessings, this book on *Palu-type liquefaction* has been successfully published. This work is the result of the dedication, determination, and collaboration of geoscientists, reviewers, and geologists within the Geological Agency, Ministry of Energy and Mineral Resources.

As mandated by Minister of Energy and Mineral Resources Regulation No. 12 of 2025, the Geological Agency is responsible for conducting research and providing services in geological resources, volcanology, geological disaster mitigation, groundwater, environmental geology, and geological surveys. Its functions encompass the formulation of technical policies, research implementation, monitoring, analysis, evaluation, and technical guidance, all aimed at supporting disaster risk reduction and the sustainable utilization of geological resources.

The publication of this book represents a tangible realization of these duties, particularly in the field of geological hazard mitigation. The devastating earthquake that struck Palu and its surrounding areas on September 28, 2018, was accompanied by widespread liquefaction in Petobo, Balaroa, and Jono Oge, marking one of the largest geological events in modern Indonesian history.

The liquefaction phenomenon in Palu is exceptional both nationally and internationally. Therefore, the studies presented in this book are expected to make a significant contribution to the development of disaster science globally. This event is the first recorded instance of liquefaction exhibiting characteristics distinct from similar occurrences elsewhere in the world.

Palu-type liquefaction is a unique phenomenon, particularly in the Balaroa and Petobo areas, which involving massive land flows generated by the complex interaction of geological, hydrogeological, and tectonic factors. These events were triggered by a combination of alluvial fan conditions with loose lithology, the presence of pressurized aquifers, and vertical cracks formed by tectonic activity, collectively resulting in destructive post-earthquake landflows.

Through the geological, hydrogeological, and tectonic analyses presented in this book, it is hoped that it will serve as a strategic reference for policymakers, academics, disaster practitioners, and the broader public in understanding liquefaction risks and developing effective mitigation measures. This aligns with the Geological Agency's commitment, as part of the Ministry of Energy and Mineral Resources, to investigate and manage energy and mineral resources while actively striving to protect the public from geological hazards.

Bandung, November 2025
Head of the Geological Agency

Muhammad Wafid, A.N.

PREFACE

On Friday afternoon, September 28, 2018, at 5:02 PM WIB (Western Indonesian Time), Central Sulawesi was struck by a powerful earthquake. The epicenter, located at 0.18° South Latitude and 119.85° East Longitude, approximately 27 kilometers northeast of Donggala, triggered a series of disasters that left extraordinary destruction in its wake. This event later became known as the Pasigala Earthquake.

The earthquake generated multiple associated hazards, including tsunamis, fault surface ruptures, ground cracks, land subsidence, landslides, and liquefaction. The tsunami affected the coastlines of Palu City, Donggala Regency, and parts of Sirenja. Liquefaction was notably widespread in Palu City, Sigi Regency, and Donggala Regency, while landslides predominantly occurred on steep slopes and weathered rock areas, particularly in Sigi and Donggala Regencies.

This book is the result of comprehensive investigations and analyses conducted on the disaster. These studies revealed that the liquefaction in Palu was a unique geological event. Unlike other liquefaction occurrences worldwide, this event manifested as a flow-type liquefaction with extensive damage, earning the designation *Palu-Type Liquefaction*.

The book provides a thorough description of the geological and geophysical dynamics of Central Sulawesi, emphasizing the complexity of tectonic activity and its implications for geological hazards. The highly active Palu-Koro Fault is highlighted for its central role in triggering destructive earthquakes that repeatedly affect Palu and its surrounding areas. Historical seismic activity, coupled with associated hazards such as tsunamis and ground deformation, underscores that the Palu-Donggala region is among Indonesia's most geologically disaster-prone areas.

The study further explores the evolution of Quaternary sediments and the development of alluvial fans, which significantly increase vulnerability to liquefaction. Loose, unconsolidated sediments amplify the potential for soil liquefaction during large earthquakes. The hydrogeological system and groundwater presence are also critical, as increased pore pressure triggered massive land flows in locations such as Balaroa, Petobo, and Jono Oge.

This book synthesizes the Palu-type liquefaction phenomenon as the result of a unique combination of geological, tectonic, hydrogeological, and human-related factors, distinguishing it from other liquefaction events worldwide. By providing a holistic perspective, the book illustrates the vulnerability of the Palu-Donggala region and deepens understanding of the interconnected natural processes that led to one of Indonesia's most complex geological disasters.

We hope this book will serve as scientific documentation of the 2018 disaster in Palu and its surroundings, as well as a practical and technical reference for liquefaction disaster mitigation, both nationally and globally. It is intended to expand knowledge of Indonesia's geological dynamics and provide a conceptual and empirical foundation for developing community strategies that are adaptive and resilient to future geological hazards.

Bandung, November 2025

Authors

PALU-TYPE LIQUEFACTION

(A Unique Natural Phenomenon in the World, A Comprehensive Geological Review)

CONTENTS

1. INTRODUCTION

The Indonesian archipelago was formed through the complex dynamics of tectonic processes resulting from the convergent interactions among three major plates: The Eurasian, The Indo-Australian, and The Pacific. These plate interactions not only generate unique geological conditions, but also render Indonesia to various geological hazards, such as earthquakes, ground movements, tsunamis, and other related geohazards (Atlas of Indonesia Liquefaction Susceptibility Zones, 2019). Large-scale earthquakes in Indonesia are often accompanied by collateral hazards, including tsunamis, liquefaction, and ground subsidence. One prominent example is the catastrophic earthquake in Aceh in 2004, with a magnitude of 9.3 on the Richter scale, which was accompanied by a major tsunami and ground movements. Although not directly documented, evidence suggests that liquefaction likely occurred during this event, despite subsequent erosion of traces due to the tsunami waves reaching far inland. Similar phenomena were observed during the 2006 Yogyakarta earthquake, which, although it did not generate a tsunami, exhibited signs of liquefaction in the form of sand boils, the formation of small sand volcanoes, and the subsidence of buildings into the ground, highlighting the characteristic manifestations of liquefaction processes.

The liquefaction disaster associated with the earthquake in Palu on September 28th, 2018, particularly in areas such as Petobo, Balaroa, and Jono Oge, demonstrated a high degree of destruction. These regions are depicted in several geological maps at a scale of 1:250,000, including the Palu Sheet (Sukamto *et al*., 1973), Pasangkayu Sheet (Sukido *et al*., 1993), and Poso Sheet (Simandjuntak, 1991), all published by the Centre for Geological Research and Development (P3G), Bandung, and compiled by Sukamto *et al*. (2003). This event was also documented visually through amateur video recordings by residents, which illustrate massive liquefaction accompanied by flow-type ground movements. These phenomena led to the destruction of buildings, subsidence and burial of houses and their contents, and the dragging of heavy vehicles such as trucks, cars, large trees, and communication towers. Such occurrences are extremely rare globally, as liquefaction generally manifests locally through sand boils or small sand volcanoes, or at larger scales through lateral spreading. The type of liquefaction involving flow slides, as observed in Palu, is exceedingly uncommon.

By comparison, the liquefaction event in Christchurch, New Zealand (2010), covered a broad area and caused significant damage, but did not involve flow liquefaction phenomena (Cubrinovski *et al*., 2011) (Figure 1.1). Similarly, other notable large-scale liquefaction events include the 1964 Niigata earthquake in Japan, which resulted in extensive urban liquefaction characterized by sand volcanoes and ground subsidence of approximately ±1.4 m, yet did not exhibit the large-scale flow-type ground movements seen in Palu (Ishihara and Koga, 1981; USGS/Wikipedia, 1964). During the Loma Prieta earthquake in California (October 17th, 1989), liquefaction was recorded at least at 134 locations along the coast from San Francisco to Monterey Bay, causing substantial infrastructure damage; however, the ground movements remained limited and did not evolve into massive flow slides (Holzer, 1998; USGS Professional Paper 1551).

Figure 1.1. Flow liquefaction occurring in Petobo (a) and Balaroa (b) as a result of the Palu earthquake in 2018.

The earthquake and collateral liquefaction hazards in Palu and surrounding areas on September 28th, 2018, resulted in severe impacts, particularly in Petobo, Balaroa, and Jono Oge. Post-disaster data report that the death toll reached 2,081, with the highest casualties in Palu City (1,706 persons), as reported by BNPB until October 25th, 2018 (BNPB, 2018). In Balaroa Subdistrict, the affected area spanned approximately 47.8 ha, with over 1,000 residential units suffering severe damage or being entirely swept away by ground flows. In Petobo, the affected zone extended around 180 ha, with an estimated over 2,000 houses damaged. The similar phenomena were recorded in other villages such as Tosale, Towale, and Loli in The Donggala District. In Jono Oge, Sigi Biromaru Subdistrict, the liquefaction-affected area covered roughly 202 ha, with documented damage to at least 36 to 168 buildings.

The damage caused by liquefaction in the affected area is highly significant, including road subsidence up to approximately 3 m deep (Figure 1.2), the formation of ground cracks as manifestations of lateral movements (lateral spreading) (Figure 1.3), and surface ground deformation resulting in wave-like undulations (ground surface undulation) (Figure 1.4). Field observations reveal that buildings, vehicles, and public infrastructure have experienced horizontal displacements ranging from tens to hundreds of meters from their original locations. Visual documentation from the field further corroborates the extreme damage inflicted by flow liquefaction phenomena during this event (Figure 1.5).

1.1. Basic Concept of Liquefaction

The initial concept regarding the phenomenon of liquefaction was first proposed by Karl Terzaghi in 1925 within his seminal work Erdbaumechanik auf Bodenphysikalischer Grundlage. This idea was later transliterated in 1956, stating

Figure 1.2. Road subsidence exceeding 3 m on the landslide crest caused by liquefaction in the Balaroa area.

Figure 1.3. Lateral spreading observed in the Jono Oge area.

Figure 1.4. Ground surface undulation observed in the Gumbasa area.

that "Liquefaction can only occur provided that most of the sediment deposit structure is metastable" (Seed and Idriss, 1971; Robertson and Wride, 1997). Under saturated soil conditions, during failure, the weight of the solid particles is no longer transmitted through intergranular contact, but is temporarily supported by pore water. This results in an increase in hydrostatic pressure at depth z from its normal value of z.γ_w, with uw approaching the submerged weight of soil, γ_s.z, where γ_w is the unit weight of water, uw is the pore water pressure, and γ_s is the unit weight of saturated soil.

Slope failure due to liquefaction was previously referred to by Terzaghi as Setzungsfliessung, which literally means "subsidence flow." In his writing, Terzaghi (1925) also introduced the term Beweglichkeit, which he translated as "mobility," to describe the condition of saturated sand that loses its shear strength during failure caused by liquefaction.

In Indonesian literature, the term "liquefaction" is sometimes translated as "pelulukan tanah" ("soil softening"). However, in this study, the term "likuefaksi" is maintained to ensure consistency with the technical terminology used in international literature.

Generally, liquefaction is defined as the significant loss of shear strength in soil (although not necessarily reaching zero) caused by an excess increase in pore water pressure, which leads to the disruption of the soil internal structure. This condition is closely related to the presence of

Figure 1.5. Damage caused by flow-type liquefaction phenomena.

weak soil structures or soils in a metastable state (Terzaghi, 1925). Under normal conditions, soil strength is supported by intergranular friction and effective stress-defined as the difference between total stress and pore water pressure-which diminishes drastically or even disappears during liquefaction.

Theoretically, soils that are highly susceptible to liquefaction are those with homogeneous textures, comprising clean fine sand, characterized by rounded grain shapes, and not yet subjected to optimal compaction, densification, or diagenesis.

However, field observations of liquefaction events in Palu, particularly in the areas of Petobo, Balaroa, and Jono Oge, demonstrate that the characteristics of the soil materials experiencing liquefaction do not always conform to the ideal conditions stipulated theoretically. Soil samples obtained from the affected locations exhibit a range of grain sizes, from silt to fine sand, with grain shapes varying from subangular (somewhat angular) to subrounded (somewhat rounded). Laboratory grain-size analysis results (Figure 1.6) of samples that emerged from within the soil to the surface due to liquefaction processes (very fine sand) are similar to the lithology in the Sm2 facies encountered in outcrops around the landslide crown (Figure 1.7). These findings indicate that liquefaction can still occur in materials that do not fully meet the ideal theoretical criteria, provided that the conditions of saturation, pore water pressure, and seismic energy are sufficient to disturb the soil internal structure.

1.2. Experimental Studies of Liquefaction in Laboratory Settings

Research on liquefaction phenomena has been extensively conducted through laboratory experiments using both field-derived soil samples and artificial soils (artificial sand). These tests employ various equipment, such as ring shear apparatus, triaxial compression tests, and flume tests, to simulate the dynamic conditions experienced during earthquakes.

Several foundational (fundamental?) studies have significantly contributed to this research, including the dissertation by Castro (1969), which specifically examined liquefaction behaviour in sandy soils. Subsequently, research by Poulos (1981) further enriched the understanding of the mechanisms and key parameters influencing the occurrence of liquefaction.

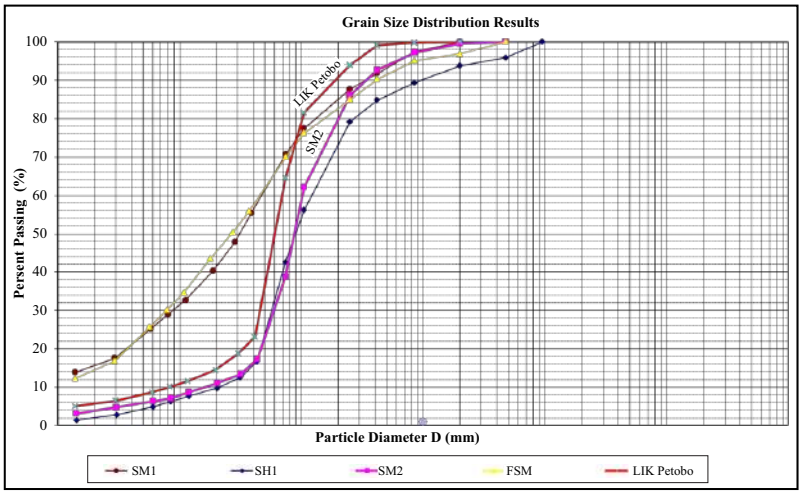

Figure 1.6. Grain size distribution of soil sample results from laboratory testing of material expelled due to liquefaction processes and outcrops in Petobo.

Figure 1.7. Depositional facies observed in the outcrop around the landslide crown in Petobo.

One of the main challenges in liquefaction testing is accurately replicating field conditions within the laboratory, especially when using field-derived soil samples. Field soils often exhibit high heterogeneity and initial conditions that are not ideally suited for liquefaction under controlled experiments. Consequently, researchers more frequently employ artificial soils, prepared with specific physical characteristics such as fine-grained particles (fine sand), uniform or poorly graded grain size distribution, grain shapes ranging from rounded to subrounded, and free from contaminants like clay minerals.

Sample preparation also plays a crucial role in the success of liquefaction experiments. Achieving high saturation levels and a loose soil structure require manipulating parameters such as the void ratio (e) and degree of saturation (Sr). Several common preparation methods employed in these experiments include dry deposition, wet tapping, and the settlement method. Among various studies, the dry deposition method has demonstrated the most consistent results in producing samples with a uniform density distribution, effectively representing field conditions susceptible to liquefaction.

1.2.1. Procedures and Methods Employed

This procedure is part of the S-O-B-O method (Wafid *et al*., 2004b), which is designed to conduct laboratory tests in soil mechanics using a ring shear apparatus. The method aims to investigate the deformation processes in sandy soils (SS-8), applied to soil samples in both dense and loose states, as well as drained and undrained conditions, utilizing the ring shear device.

1. The procedure for placing soil samples into the ring chamber is conducted using the dry deposition method, which involves pouring oven-dried soil in layers without compaction (tamping), as described by Ishihara (1993). Compaction was not performed, because the test aims to replicate loose soil conditions, which are more susceptible to liquefaction.
2. After the placement is complete, carbon dioxide (CO_2) gas was flowed into the chamber for approximately 60 minutes to displace air from the soil pores. Subsequently, de-aired distilled water was slowly circulated into the chamber over approximately 15 hours until the desired saturation condition is achieved.
3. The next stage involves initial isotropic consolidation at a normal stress of 50 kPa. Following consolidation, the B-value (BD), calculated as the ratio of pore water pressure increase to total stress increase ($BD = \Delta u / \Delta\sigma$), was monitored until it reaches a value of at least 0.95. This value serves as an indicator of full saturation, in accorandce with the standards established by Sassa (1985) and Wang and Sassa (2000).
4. After the B-value (BD) exceeds 0.95, the specimen is regarded as fully saturated, in accorandce with the criteria established by Sassa (1985), allowing the testing to proceed immediately. The next stage involves consolidating the specimen at an initial normal

stress of 200 kPa. Overall, the entire testing sequence is conducted through two main series, performed sequentially.

5. The first series involves monotonic stress-controlled testing using three different methods: undrained conditions, drained conditions, and a combination of drained and undrained conditions. During this phase, shear stress is applied gradually at a loading rate of 0.098 kPa/sec, and the process is halted when the shear displacement reaches 10 m.
6. Following the completion of each test in the first series, the second series was conducted, involving strain rate-controlled testing using three different shear rates: 25 mm/sec, 78 mm/sec, and 104 mm/sec.
7. The three testing methods in the first series (undrained, drained, and drain–undrained) are conducted until a shear displacement of 10 m is achieved. Subsequently, without altering the specimen or performing reconsolidation, strain rate-controlled testing was carried out under undrained conditions using three shear rates: one rate below the steady-state shear velocity (determined from stress-controlled tests) and two additional rates above this steady-state condition.
8. For all undrained (U) tests, whether in the first or second series, pore water is not permitted to exit the specimen. Consequently, all testing stages are conducted under strictly undrained conditions throughout.

The ring shear apparatus is a specialized shear testing device designed to determine the residual shear strength of soil samples, as described by Bishop *et al*. (1971). Similar to other direct shear testing equipment, it features a predetermined failure plane located at the interface between the upper and lower parts of the specimen mold. The mold has a ring (donut) shape, enabling continuous shear movement without limits, making it highly suitable for testing until the soil reaches its residual shear strength condition.

This device was first introduced by Hvorslev (1934) and subsequently gained considerable popularity in Europe. It has undergone several modifications tailored to specific research objectives, including adaptations by Broemhead (1936), Bishop *et al*. (1971), Mandl (1971), Lupini *et al.* (1981), Tika *et al.* (1996), and Sassa (1997).

At The Geodynamics Laboratory of The Research Centre on Landslides (RCL) at the Disaster Prevention Research Institute (DPRI), Kyoto University, where this research was conducted, there exists a diverse range of ring shear apparatuses in terms of size, features, and capabilities. Some of these devices are equipped to perform both undrained and cyclic tests, which are essential for studying liquefaction-induced slide phenomena and debris flows. One apparatus, in particular, can achieve maximum shear velocities of up to 3 m/sec (DPRI version 7), and is used for debris flow simulations. For this study, the version 5 (DPRI ver. 5) ring shear apparatus was employed. A schematic of the equipment is shown in Figure 1.8.

Ring shear testing with the DPRI-5 apparatus on saturated SS-8 sand specimens was conducted to evaluate the shear response of soil under different drainage conditions. This testing involved two main scenarios: undrained and drained conditions. The resulting graphs reveal significant contrasts in soil behaviour, directly related to the potential for liquefaction and dilatancy during shear processes. Figure 1.9 displays the results of ring shear tests (DPRI-5) on SS-8 specimens under undrained (liquefaction) and drained (dilatancy) conditions (Wafid *et al.,* 2004c). Figure 10 presents typical stress paths and stress–strain relationships derived from tests on noncohesive soil specimens using the DPRI-5 ring shear device. Additionally, the figure compares stress path trajectories between dense and loose specimens (Wafid *et al*., 2004c). Shear testing with the ring shear apparatus is an effective method for evaluating soil shear behaviour, particularly under large deformations beyond the peak strength and progressing toward residual conditions. For granular soils, such as saturated sand, shear characteristics are highly influenced by the drainage conditions

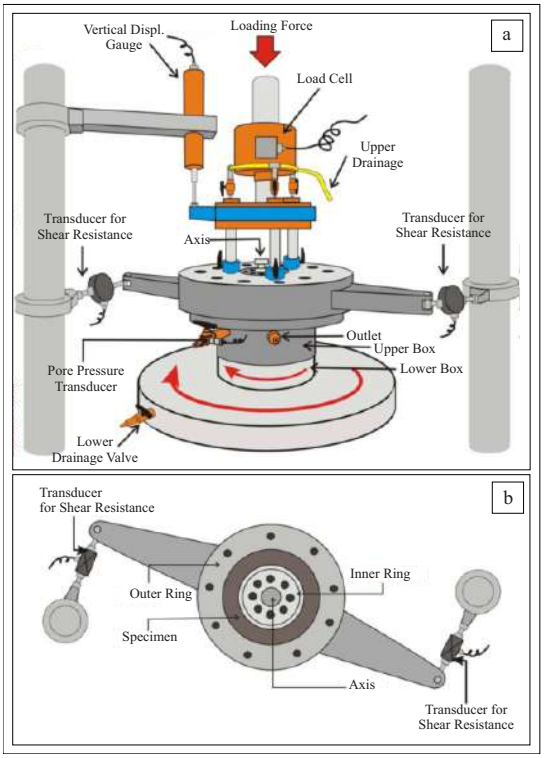

Figure 1.8. Sketch of the ring shear apparatus (DPRI Ver.5). a) The ring shear device along with its components. b) An example of a donut-shaped test specimen within the mold, accompanied by several transducers used to complete the setup (Wafid *et al*., 2004a).

during loading, broadly classified into two types: drained (drained condition) and undrained (undrained condition). Figure 1.11 shows typical shear behaviour graphs obtained from ring shear tests on saturated sand specimens under drained and undrained conditions.

Experimental testing using the torque-controlled ring shear apparatus was conducted on loose, saturated, undrained sand samples to assess liquefaction potential and shear weakening characteristics. The test results depict the soil response to sustained shear controlled by torque, enabling evaluation of effective stress behaviour, pore water pressure, and shear strength associated with large deformations. Figure 1.12 presents the experimental outcomes of liquefaction using the torque-controlled ring shear test on loose, saturated, undrained sand specimens.

Key parameters:

RFL = Residual Failure Line

φ'p = Peak effective friction angle

φ'r = Residual effective friction angle

Δu = Increase in pore water pressure

a) Effective stress patp.

b) Variations in normal stress, shear strength, and pore water pressure relative to shear displacement.

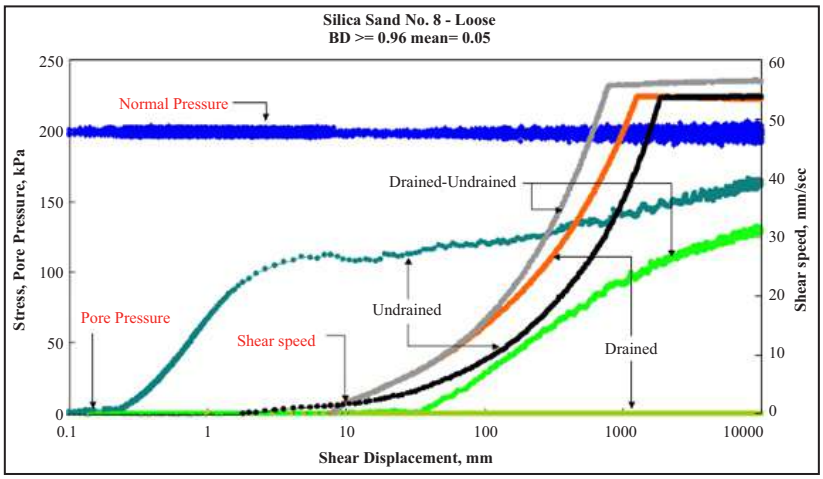

Figure 1.9. Graph illustrating the results of ring shear tests (DPRI-5) on SS-8 specimens under undrained (liquefaction) and drained (dilatancy) conditions (Wafid *et al*., 2004c).

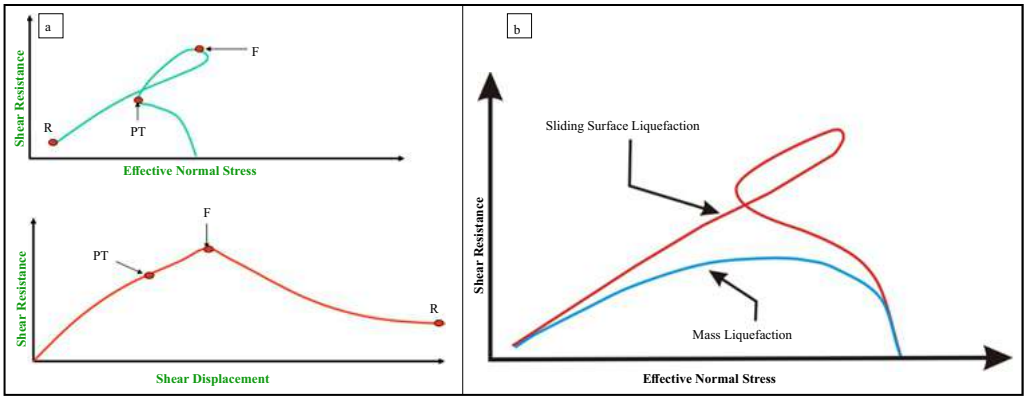

Figure 1.10. a) Displays the typical stress path and stress-strain relationship obtained from testing noncohesive soil specimens using the DPRI-5 ring shear apparatus. b) Shows the differences in stress paths between dense and loose specimens (Wafid *et al*., 2004c).

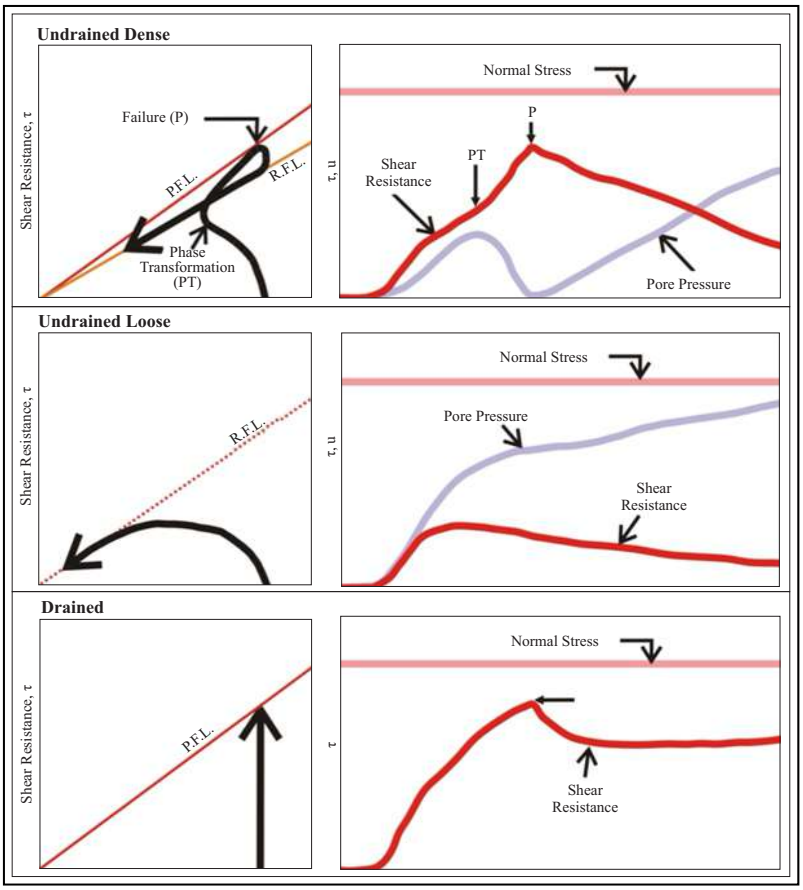

Figure 1.11. Typical shear behaviour observed from ring shear tests on saturated sand specimens under drained and undrained conditions.

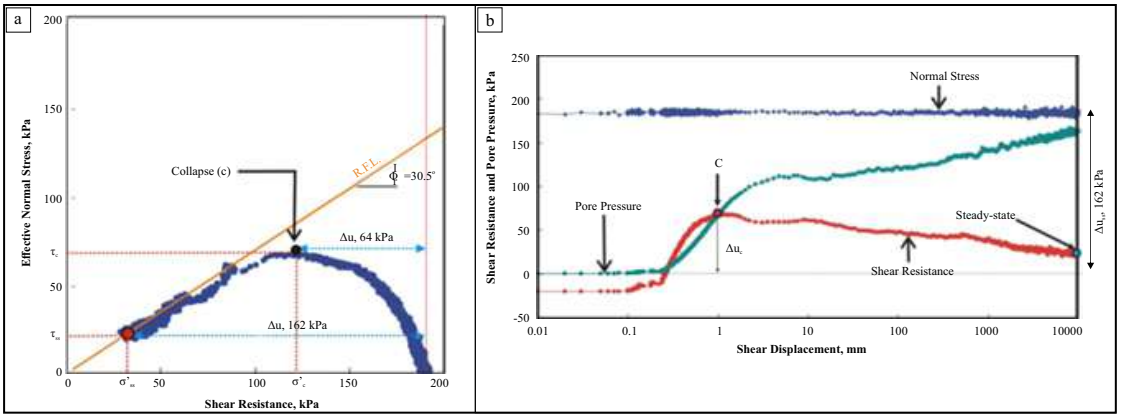

Figure 1.12. Experimental liquefaction results using a torque-controlled ring shear test on loose, saturated, undrained sand.RFL= Residual Failure Line, φ'p= Peak effective friction angle, φ'r= Residual effective friction angle Δu = Increase in pore water pressure. a) Effective stress patp; b) Variations in normal stress, shear resistance, and pore water pressure in relation to shear displacement.

Three sets of experimental tests were conducted using the torque-controlled ring shear apparatus on saturated loose sand under undrained conditions to examine liquefaction behaviour and the attainment of residual state at various shear displacement lengths. Figure 1.13 presents the results of these three liquefaction and residual-state experiments with different shear displacement lengths using the torque-controlled ring shear test on saturated, loose sand.
(Uji UND211:
D_r=65,6 %,
B_D=0,96,
L=17,7 mm;
UND212:
D_r=65,6 %,
B_D=0,95,
L=530,6 mm;
UND213:
D_r=69,8%,
B_D=0,98,
L=10.000 mm).

1.2.2. Characteristics of Test Specimens

The test specimens utilized in this study are silica sand obtained from the mechanical crushing of silica sandstone rocks to achieve specific grain sizes. In this research, the silica sand ranges from very fine to fine sand, with a D50 of approximately 0.041 mm (grain size distribution is shown in Figure 1.14). The composition consists of 80 % quartz mineral and 20 % feldspar, with a specific gravity (Gs) of 2.65, a maximum dry density (Dr dry-max) of 1.49 g/cm³, and a minimum dry density (Dr dry-min) of 1.05 g/cm³. Figure 1.15 illustrates the sketch of the sand sample testing results and a picture of the sample taken after testing using The Shear Zone Sampler.

1.3. Phenomena and Dynamics of Liquefaction: Global Perspectives And The Indonesian Context

Liquefaction events have caused significant damage across various regions worldwide. Notable major incidents include those in Niigata (Japan, 1964), Alaska (USA, 1964), Loma Prieta (USA, 1989), and Christchurch (New Zealand, 2010). Among these, the liquefaction disaster in Palu, Indonesia, in 2018 stands out as one of the most destructive, not only on a national scale but also in a global context.

Historically, liquefaction phenomena have been documented in various regions across Indonesia (Table 1.1). Notably, this phenomenon also occurred in Yogyakarta and Klaten during the

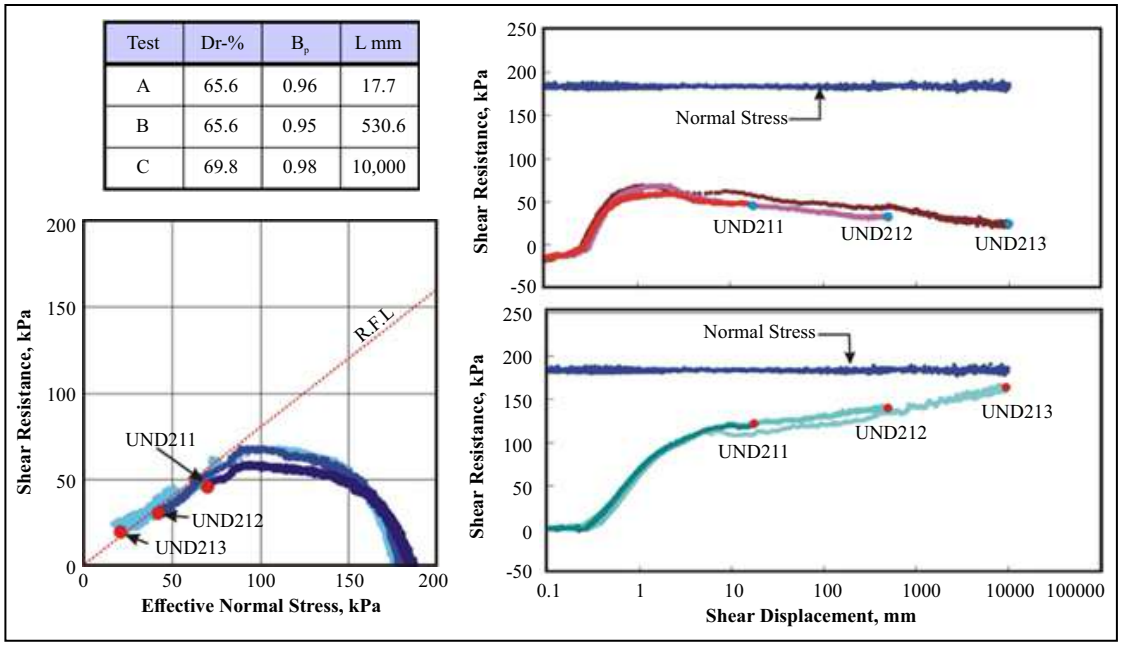

Figure 1.13. Results of three liquefaction and residual state experiments with varying shear displacement lengths using the torque-controlled ring shear device on saturated, loose sand under undrained conditions (Under test UND211: Dr=65.6 %, BD=0.96, L=17.7 mm; UND212: Dr=65. 6%, BD=0.95, L=530.6 mm; UND213: Dr=69.8 %, BD=0.98, L=10,000 mm).

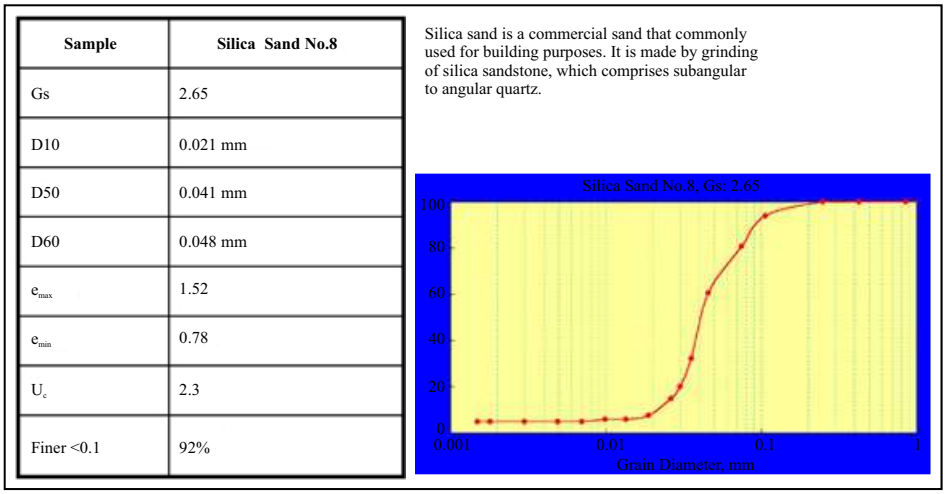

Figure 1.14. Figure 8. Displays the index properties of the test specimen used in this study (SS-8).

2006 Yogyakarta earthquake, which was triggered by the Opak Fault activity. Generally, liquefaction events in Indonesia tend to be relatively localized, characterized by features such as sand boils, small sand volcanoes, and lateral ground movements (lateral spreading). Lateral spreading is particu-

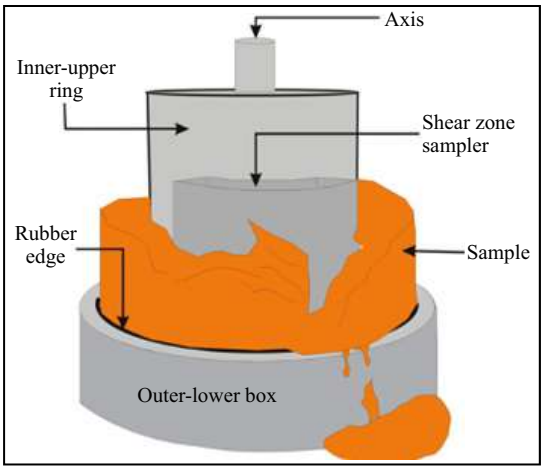

Figure 1.15. Sketch of the sand sample testing process and the sampling method after testing using The Shear Zone Sampler.

larly prevalent in areas with slope gradients, such as riverbanks and coastal zones.

However, the event in Palu demonstrated a highly destructive phenomenon where liquefaction evolved into flow liquefaction, a rare but extreme form of ground failure. This type represents an advanced stage of liquefaction, characterized by a sudden and significant loss of shear strength in saturated soil layers, resulting in the mass movement of soil as a flowing mass. Such flow events can devastate infrastructure and buildings, leading to substantial loss of life.

1.4. Geological Conditions Leading to Flow Liquefaction in Palu

The occurrence of flow liquefaction in Palu is closely linked to the area unique geological and hydrogeological conditions, including:

1. Formation of Quaternary Sedimentary Basin (Pull-Apart Basin):
   The Palu Valley was formed due to the activity of The Palu–Koro Fault, a sinistral strike-slip fault. This tectonic activity has created a pull-apart basin structure that functions as a "reservoir" for Quaternary sediment deposition.
2. Sedimentation Processes and Material Characteristics:
   The Palu Basin (Badan Geologi, 2009) receives sediments from alluvial fan sedimentation originating from the west and east. These deposits are predominantly fluvial sediments with a range of grain sizes from fine to coarse. Some layers contain subrounded grains, indicating that these materials have undergone transportation from distant sources, resulting in sediments with physical characteristics that tend to favour liquefaction.
3. Active Tectonic Dynamics and Complex Hydrogeological System:
   The Palu–Koro Fault (Sukamto *et al.*, 2003) is part of an active tectonic system that periodically releases seismic energy. This tectonic activity influences the hydrogeology of Palu, forming confined aquifers at certain depths. High surface water infiltration rates in some areas exacerbate soil saturation, creating conditions of excess pore water pressure, especially in zones with fractures or joints within the subsurface.

It is estimated that high pore water pressures accumulated prior to the earthquake were further amplified by seismic shaking, ultimately disrupting the internal soil structure and inducing liquefaction. In certain areas-particularly at the distal ends of alluvial fan deposits with landau?-sloping terrains-geotechnical assessments identify these zones as weak zones where flow liquefaction has been observed. Conversely, in some locations, only the formation of sand volcanoes was noted without subsequent flow liquefaction; this is likely due to insufficient soil layer thickness to develop a large enough soil mass capable of lateral and mass movement.

1.5. Impact of Liquefaction Events

Liquefaction phenomena have caused significant damage across various regions worldwide,

Table 1.1. Historical Occurrences of Liquefaction in Indonesia

No	Gempa Bumi	Tanggal	Magnitudo	Intensitas	Kejadian Likuefaksi
1	Lhok Seumawe, Sigli	4-Dec-1967	M6,2	VIII	Lhok Seumawe
2	Tarutung	27-Apr-1987	M6,6	VII	Tarutung
3	Gorontalo	18-Apr-1990	M6,2	IX	Gorontalo
4	Blangkajeren	15-Nov-1990	M6,8	VIII	Blangkajeren
5	Alor	7-Apr-1991	M6,9	VIII	P. Alor
6	Flores	12-Dec-1992	M7,5	VIII	Pantai Utara P. Flores
7	Liwa	15-Feb-1994	M7,0	IX	Liwa
8	P. Obi	10-Aug-1994	M6,3	VI	Desa Sambiki, P. Obi
9	Parigi	20-May-1995	M5,8	VII	Sausu-trans, Mekarsari, Balingi, Tolai, Torue
10	Kerinci	10-Jul-1995	M7,0	IX	Kec. Sitinjau Laut
11	Biak	17-Feb-1996	M8,2	VIII	Ds. Bosnik, Warsa, Aman, Sawai, Wasari
12	Bengkulu	6-Apr-2000	M7,9	IX	Kota Bengkulu
13	Ransiki	10-Oct-2002	M7,6	VIII	Ransiki
14	Manggarai	25-Mar-2003	M6,5	VI	Manggarai
15	Nabire	2-Jun-2004	M7,0	VIII	Ds. Sanoba, Kab.Nabire
16	Nabire	11-Jun-2004	M7,0	VIII	Ds Kimi, Kab. Nabire
17	Alor	11-Dec-2004	M7,5	IX	Air Mancur P. Alor
18	Palolo-Donggala	24-Jan-2005	M6,2	VII	Ds. Sintuwu, Palolo, Donggala
19	Gunung Sitoli	28-Mar-2005	M8,7	IX	Gunung Sitoli
20	P. Buru	14-Mar-2006	M6,7	VI	Desa Pela & Waimorat
21	Bantul	27-May-2006	M6,2	VIII	Bantul, Sleman, Klaten
22	Solok	3-Jul-2007	M6,3	VII	Solok
23	Bengkulu	9-Dec-2007	M8,4	VI	Bengkulu, Seblat
24	Pesisir Selatan	13-Sep-2007	M7,9	VII	Pesisir Selatan
25	Gorontalo	17-Nov-2008	M7,7	VIII	Molangato
26	Manokwari	1-Apr-2009	M7,6	VII	Kordakel
27	Padang Pariaman	30-Sep-2009	M7,9	VIII	Padang Pariaman, Kota Padang
28	Serui	16-Jun-2010	M7,1	VIII	Aitiri, Angkaisera, Kab. Yapen.
29	P. Obi	14-Mar-2010	M7,0	VII	Desa Kelo, P. Obi
30	Kendari	25-Apr-2011	M6,0	VI	Kecamatan Moramo
31	Sorong	25-Sep-2015	M6,8	VI	Kota Sorong
32	Tarakan	21-Dec-2015	M6,1	V	Tarakan
33	Pidie Jaya	12-Jul-2016	M6,5	VIII	Pidie Jaya
34	Lembah Napu, Poso	29-May-2017	M6,6	VI	lembah Napu
35	Lombok Utara	8-May-2018	M7,0	VIII	Lombok Utara
36	Lombok Timur	19-Aug-2018	M7,0	VIII	Lombok Timur
37	Pasigala	28-Sep-2018	M7,5	IX	Balaroa, Petobo, Sibalaya (Flow Likuifaksi)

including Christchurch, New Zealand, in 2010. The impacts included foundation cracking, structural deformations, and flooding due to water channels and pipes being uplifted to the surface and broken. The soil experienced uneven deformation, with substantial vertical displacements, ground fractures, and the extrusion of sand, mud, and water in large quantities. Thousands of homes were destroyed, and the eastern part of Christchurch became uninhabitable again, with estimated economic losses exceeding USD 52.2 billion.

Liquefaction effects induced by earthquakes have also been documented in several other major events, such as flow slide landslides at Lake Merced following the 1957 San Francisco earthquake, and tension cracks along with thousands of landslides triggered by the 1976 Guatemala earthquake magnitude 7.5. In Kobe, Japan, liquefaction caused by the Hyogo-ken Nanbu earthquake (1995) damaged ports by causing ground surface subsidence of 1.2 to 2 m and lateral displacement of pier structures. This earthquake resulted in over 6,000 fatalities and economic losses estimated at approximately USD 200 billion.

In Japan, the Niigata earthquake of 1964 (magnitude 7.5) triggered widespread liquefaction, leading to damage in approximately 2,000 homes. The apartment buildings in Kawagishi-cho experienced a reduction in bearing capacity, and severe tilting due to soil strength loss. Similar phenomena also occurred during the 1964 Alaskan earthquake (magnitude 9.2), which caused liquefaction and major landslides in Anchorage, along with lateral spreading that damaged road embankments. Meanwhile, the Loma Prieta earthquake in California (1989, magnitude 7.1) provided strong evidence of liquefaction, indicated by numerous sand boils at Oakland Airport, Moss Landing, and along The Salinas River. In Indonesia, extreme liquefaction events were observed during the Palu earthquake in 2018 (magnitude 7.4), caused by a combination of fine-grained soil conditions, high saturation levels, dynamic pore water pressures within confined aquifers, and geological structures such as The Palu–Koro Fault, which moves approximately 35 mm per year. The disaster resulted in 4,340 fatalities, 10,679 injuries, 667 missing persons, and over 82,000 displaced individuals, with economic losses reaching around USD 1.5 billion.

Liquefaction phenomena were observed in Yogyakarta during the May 27, 2006, earthquake (magnitude 6.2). Liquefaction occurred locally, primarily in the Bantul and Klaten regions, manifesting as sand boils and ground subsidence, although the effects were less severe than those in Palu. This earthquake resulted in 4,143 fatalities and caused severe damage to over 71,000 homes. Meanwhile, the 2004 Aceh earthquake (magnitude 9.3), which triggered a major tsunami, did not leave well-documented traces of liquefaction, because the affected areas were swept by the tsunami far inland, erasing the geological evidence of liquefaction.

2. GEOLOGICAL SETTING OF THE PALU-KORO FAULT SYSTEM

2.1. Tectonics

Tectonics refers to processes in the earth crust, which form structures and landforms (Keller and Pinter, 1996). Earthquakes are the result of tectonic activity around active margins or at the place where plates collide. However, some earthquakes have occurred in intraplate regions; for instance, the western United States is a tectonic province faced with the problem of large earthquakes caused by two main sources: The San Andreas Fault and the eastern Pacific subduction zone (Wallace, 1990).

Geologically, Indonesia can be divided into two major tectonic regions: western and eastern Indonesia. Eastern Indonesia is more tectonically complex than western Indonesia, because it lies at the junction of three tectonic plates: The Australian, Eurasian, and Pacific, which occurred over time during the Tertiary and Quaternary within the Cenozoic.

Sulawesi is located at the intersection of three major tectonic plates: The Eurasian Plate, The Australian Plate, and The Pacific Plate. This complex tectonic setting results in intense geological activity, including faulting, volcanism, and earthquakes. The Palu-Koro Fault is a left-lateral strike-slip fault that accommodates the relative motion between the northern and southern parts of Sulawesi. The Indonesian archipelago, especially eastern Indonesia, is formed by three main plates: The Eurasian Continental, Indo-Australian, and Pacific Plates. They have been converging since the Jurassic-Cretaceous period and actively interact at the edge of the Indonesian Archipelago.

Sulawesi Island, which is located in the central part of the Indonesian, and looks like the letter K, is strongly influenced by the activities of the three main plates above. Sukamto and Simanjuntak (1983) state that Sulawesi Island and its surrounding areas can be divided into several geological provinces. The East Sulawesi Geologic Province is referred to as the non-volcanic arc and covers The Southeast Arm of Sulawesi, the eastern part of Central Sulawesi, and The East Arm of Sulawesi. The western part of this province is characterized by the Tinondo-Pompangeo Metamorphics Belt, and the eastern part is characterised by The Hialu-Balantak Ophiolite Belt. Geologically, the eastern part of Sulawesi and some small islands around it are more complex. Thus, The East and Southeast Arms are composed of metamorphic rocks and are covered by sediments and ophiolites, which are the result of obduction processes during The Miocene (Smith and Silver, 1991). Surono (1998a) supposed that the metamorphic rocks and their covering sediments were a microcontinent, while the ophiolite rocks were The East Sulawesi Ophiolite Belt, often referred to as The Eastern Sulawesi Ophiolite Belt (Figure 2.1). The belt is dominated by ultramafic, mafic, and pelagic sediments (deep-sea sediments). Mafic rocks consist of gabbro, basalt, dolerite, microgabbro, and amphibolite, whereas deep-sea sediments are composed of deep-sea limestone and radiolarian.

However, the northern and southern arms are here referred to as “western Sulawesi’ for simplicity. The east and south-east arms have an oceanic origin and are composed of Mesozoic and younger allochthonous metamorphic and ophiolitic rocks, which were obducted onto western Sulawesi during The Oligocene to Early Miocene. In addition, several small continental fragments have collided with eastern Sulawesi,

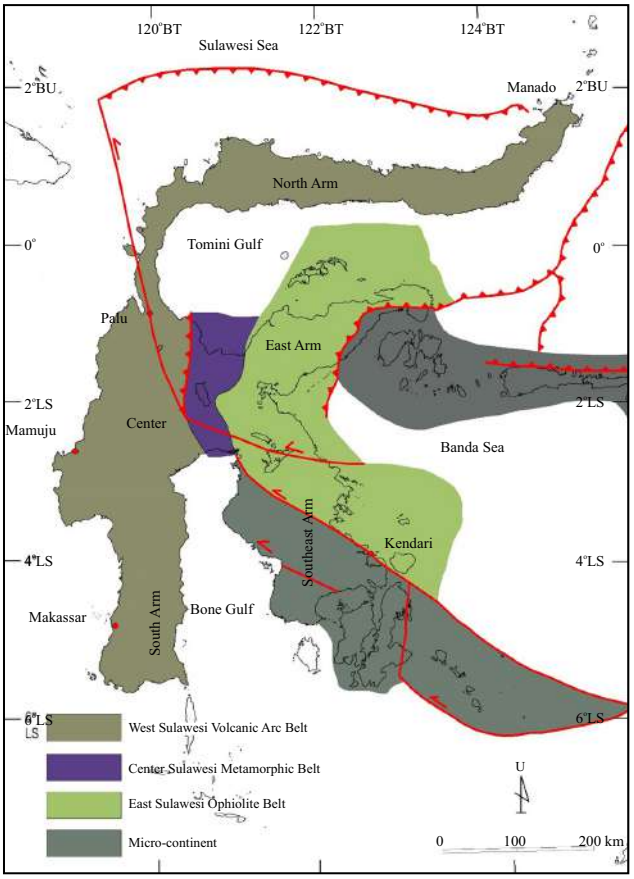

Figure 2.1. Geological provinces of Sulawesi Island and its surrounding area (modified from Surono, 2010).

including Banggai-Sula, Tukang Besi, and Buton. The Western Sulawesi Geologic Province is also known as The Volcanic-Plutonic Arc Belt and consists of The South Arm of Sulawesi, The Central Arm, the Neckline of Sulawesi, and The North Arm of Sulawesi. The pre-Tertiary metamorphic rocks are the oldest lithology in these provinces. Katili (1978) argued that the position of this line coincides with the eastern edge of Sundaland, while Hutchinson (1989) and Murphy (1979) in Situmorang (1984) supposed that this arm is part of The Southeast Eurasian Plate, which was separated from Sundaland during the pre-Tertiary. Even though Soesilo (2012) states that the Bantimala-Latimojong-Pompangeo Metamorphic Complex on Sulawesi Island until Luk Ulo on Java Island is a high-pressure metamorphic arc formed during The Cretaceous.

Furthermore, Wakita (2000) states that the tectonic events recorded in the Cretaceous accretionary-collision complexes in central Indonesia are subduction, accretion of fragments of an oceanic plate and microcontinents, sediment accretion and mélange formation, collixsion of continental blocks, exhumation of high P/T of metamorphic rocks, and obduction of oceanic plate (ophiolite). Also, the collision of a continental block is the key tectonic event noted in the Cretaceous accretionary-collision complexes (see Figures 1.2 and 1.3).

During The Early Eocene, a land connection existed between southwest Sulawesi, southern

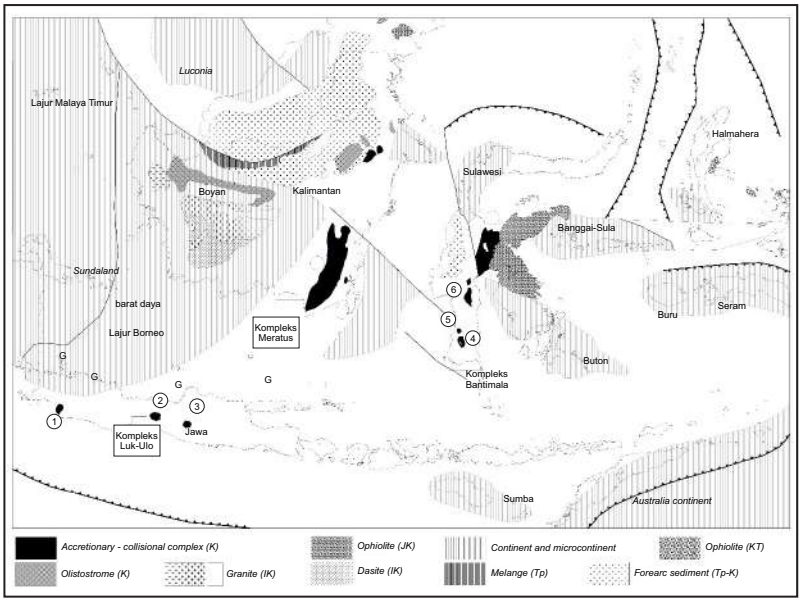

Figure 2.2. Major components of the Cretaceous accretionary-collision complex are distributed between a continent (Sundaland) and a microcontinent (Paternoster, Buton, *etc*.). Late Cretaceous accretionary-collision complexes are distributed in the following areas, *i.e.* 1. Cileutuh,2. Karangsambung,3. Jiwo Hills, 4. Bantimala, 5. Barru, 6. Pompangeo, 8. Meratus, and 9. Pulau Laut. Abbreviations of ages are as follows: JK: Jurassic to Cretaceous, K: Cretaceous, IK: Early Cretaceous, mK: Middle Cretaceous, uK: Late Cretaceous, Tp: Palaeogene, KT: Cretaceous to Tertiary (redrawn from Wakita, 2000).

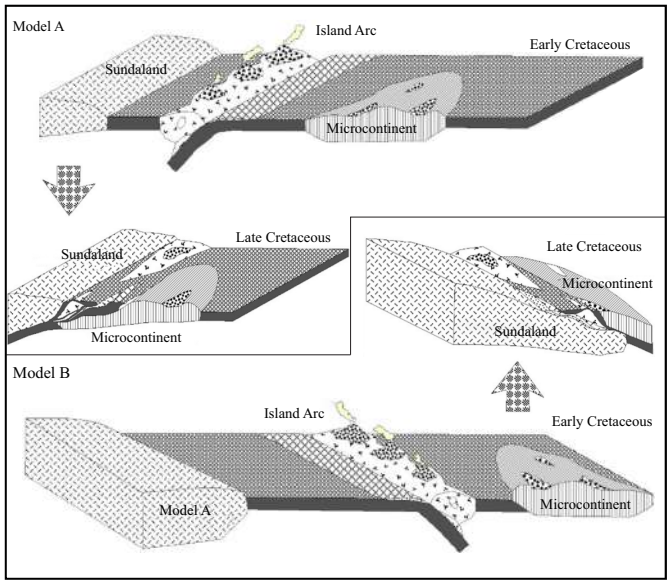

Figure 2.3. Two models for Cretaceous palaeogeography and tectonics in Central Indonesia: 1. Microcontinent collision, 2. Sundaland collision (Model A). On the other hand, the model B is: 1. The oceanic plate migrated northward and subducted under the island arc behind which the marginal sea was situated. 2. The oceanic plate moved southward and subducted under the volcanic arc along the margin of the oceanic crust to the south (redrawn from Wakita, 2000).

Kalimantan, and mainland Southeast Asia. However, later during The Middle Eocene, extension in The Makassar Strait region occurred, which led to the formation of a deep-water basin. However, based on gravity data modelling, it was found that The Makassar Strait is underlain by Eocene-aged oceanic crust in Katili (1978), Hall (1996), Wilson and Moss (1999), Clock *et al.* (1999), and Calvert (1999). The western part of Sulawesi was formed during The Early Cretaceous as a basement complex and apparently includes an old continental crust of Australian origin. This is supported by the presence of recycled ancient zircons from Miocene igneous rocks, which, based on their chemical composition, originated from northern Australia, not from south-east Sundaland. Possibly, these became accreted onto Sunda during the Oligocene to Miocene collision event (Priadi *et.al* 1993 and Bergman *et al*., 1996). Bergman *et al*. (1996) also state that The Northern Makassar Strait Basin is not the result of Tertiary rifting, but the basin is the result of shortening in north-west-south-east direction because of the collision of continents in The Neogene of West Sulawesi.

Charlton (2000) proposed that at 30 Ma, the Australian continental margin commenced a collision with the subduction zone in the northern region between Sulawesi in the west and Papua in the east (Figure 1.4). The ongoing discussion about how Kalimantan and Sulawesi rotated, and their positions relative to each other during The Paleogene, includes different views such as "no rotation," "clockwise rotation, "anticlockwise rotation", and "mixed rotations".

During The Oligocene, as a result of the collision between the microcontinent and the ophiolite complex in The Late Oligocene to Early Miocene, the ophiolite complex was uplifted above the microcontinent. The Sulawesi Molasse, which consists of clastic and carbonate sedimentary rocks, was deposited unconformably on top of the two major rock groups during the late and post-collision periods (Figure 1.5.A). In The Late Neogene, these two Sulawesi arms

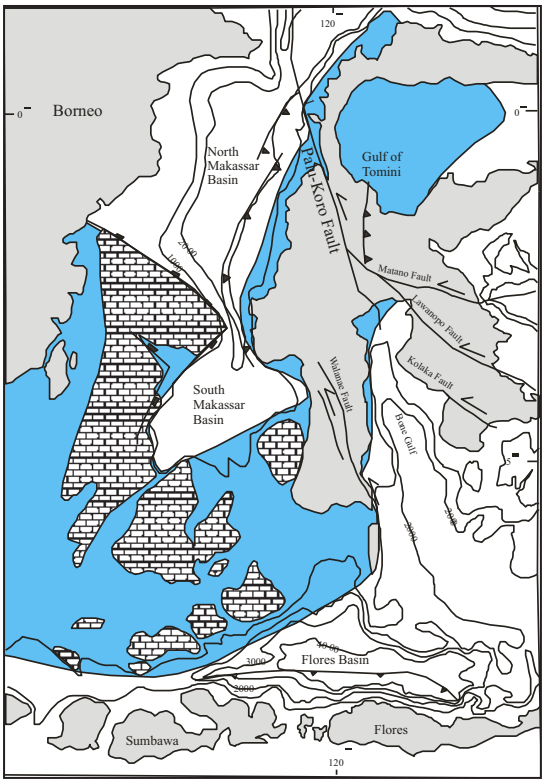

Figure 2.4. The tectonic setting of Kalimantan, Makassar Strait, and Sulawesi Island, modified from Letouzey *et al.,* 1990; Kavalieries *et al* 1992; Bergman *et al.,* 1996; Hall, 1996; Parkinson, 1996; and Charlton, 2000. The blue area represents terranes of presumed Sunda origin.

were torn apart by the regional Strike Slip Left Fault (Palu-Koro), Matano Fault, Pagaimana Fault, Mawanopo Fault, and Kolaka Fault and its couples.

The Sulawesi Molasse have significant variations in age, environment of deposition, and configuration of sedimentation history at the middle and eastern arms of Sulawesi. Nugraha *et al.* (2022), based on mineralogy, palaeontology, and *zircon geochronological analysis*, state that the molasse sediments have a range of ages from Early Miocene to Pleistocene based on Neogene sediment across Sulawesi. These mega sequences resulted from Early Miocene collision followed by extension, driven by subduction rollback, causing both uplift and subsidence.

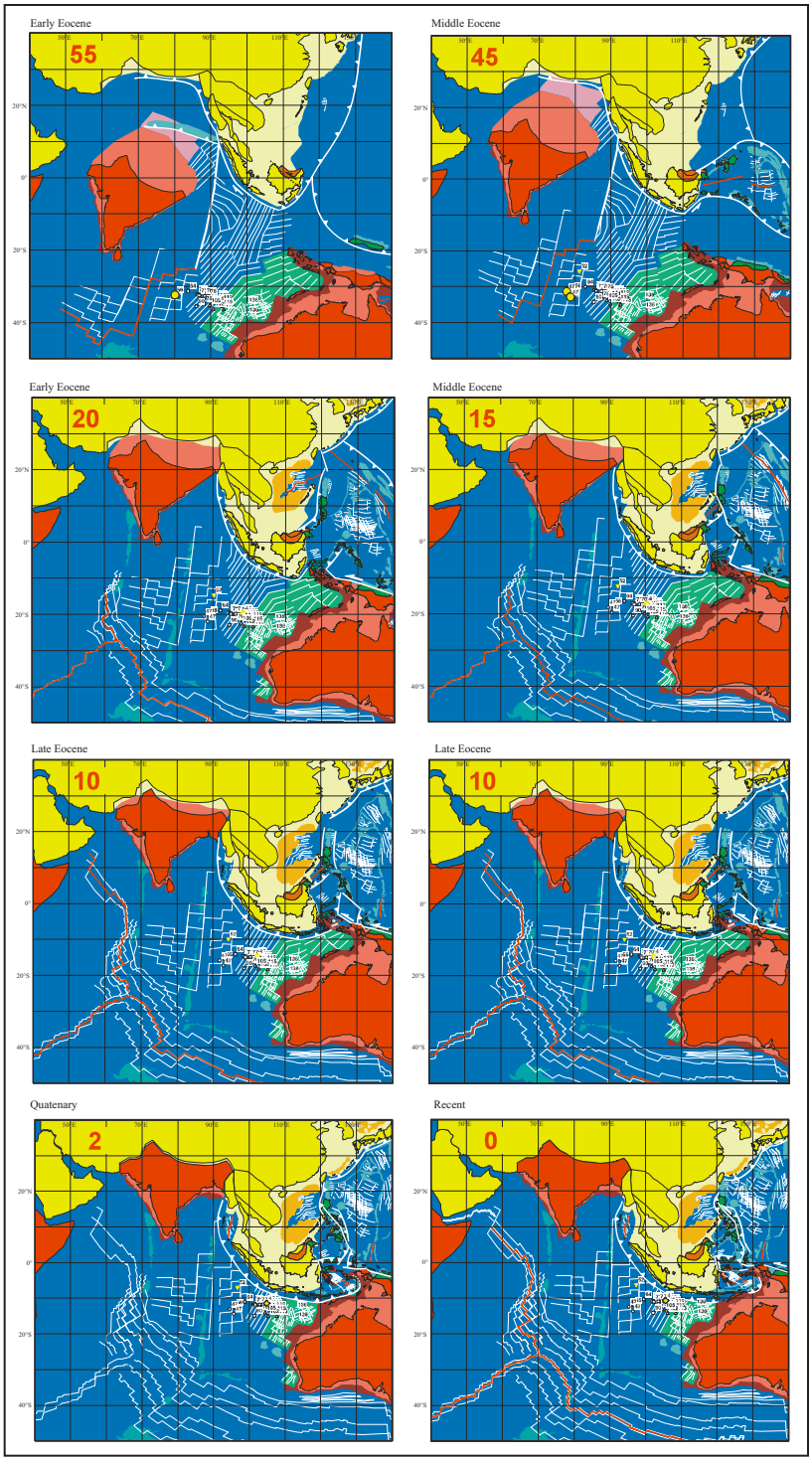

Figure 2.5. Tectonic evolution of Sulawesi Island since Early Eocene into the present (Source: Hall, 2002).

2.2. Tectonic Evolution Sulawesi Island

The geological activity and continental configurations of the Asian margin and surrounding regions around 55 Ma reveal significant tectonic transformations. The Asian margin stretching from Japan to the north showed a lot of geological activity, but the southern areas, like Taiwan and The South China Sea, were less clear and likely had quieter edges, because subduction had stopped earlier. The passive margin in South China began extending in The Late Cretaceous, while The Pacific edge remained an active margin.

India was moving closer to the Asian margin, anticipating a collision with Eurasia, while Australia had separated from Antarctica during The Cretaceous, experiencing slow rifting initially. By 55 Ma, The Tasman Sea had nearly fully opened, segregating Australia from its neighbouring continental fragments.

South-east Asia configurations depicted Kalimantan rotated clockwise, with remnants of oceanic crust indicating the proto-South China Sea formation during The Late Cretaceous. The oldest parts of The Luzon Arc in northern Sabah emerged post-45 Ma, showcasing geological connections between Luzon and Sabah.

Australia northern margin was situated at approximately 30°S, adjacent to the proto-Banda Sea, indicative of a failed Jurassic rift. An oceanic region of uncertain age lay between Australia and east Asia, featuring multiple ridge jumps prior to the end of India–Australia spreading. By 55 million years ago, these areas were interacting in different ways, with subduction affecting ophiolite formations and the movements of small plates playing a role in the coming together of the Australian margin.

In The Pacific, remnants of arc-derived crust, driven by rotating history as revealed through paleomagnetic data, underscore the complex interactions within the tectonic framework of the region, defining the boundaries of The Pacific and Northern New Guinea plates and illustrating a dynamic geological history leading into The Eocene epoch.

2.2.1 Reconstruction at 45 Ma

The geological reconstruction at 45 Ma reveals significant plate organisation changes across Southeast Asia, the western Pacific, and the Australian margins. During this period, from 50 to 40 Ma, India northward movement slowed, leading to its merger with Australia into a single tectonic plate. The cessation of activity at their mutual spreading centre saw the initiation of new spreading centres in the southern Indian Ocean, accelerating Australia northward motion.

The emplacement of ophiolites on Australia northern and eastern margins marked a change in subduction polarity east of New Guinea, giving rise to The Melanesian Arc system. This system formed as a result of rifting in the earlier arc crust, which established passive margins along the northern region of New Guinea. Meanwhile, southward subduction of the oceanic crust occurred south of The East Philippines–Halmahera Arc. By around 45 Ma, The Philippine Sea Plate had completed a significant clockwise rotation, leading to the propagation of The West Philippine Sea spreading system and the creation of a wide ocean basin in that area.

The period also saw the onset of southward subduction of the proto-South China Sea, resulting in a new active margin spanning from Sabah to Luzon. This shift played a crucial role in the opening of The South China Sea due to slab-pull forces, implicating subduction as a primary driver for the extension of the Indochina–South China margin.

Although the causes of these substantial changes remain uncertain, potential explanations include the collision of India and the resulting adjustments in plate boundaries, as well as the loss of the Kula–Pacific ridge, which may have affected subduction dynamics around the Pacific Plate. This hypothesis is linked to the bend seen in the Hawaiian-Emperor seamount chain, though the synchronisation of events across Southeast Asia, and the southwest Pacific during this time is still debated. Overall, the period around 45 Ma stands out as a pivotal epoch of plate reorganization in The Cenozoic era, significantly influencing the tectonic landscape of the region.

2.2.2. Reconstruction at 20 Ma

The rebuilding of The Melanesian Arc system and its back-arc basins during The Late Oligocene and Early Miocene shows that things were relatively stable, even though there were some uncertainties about how subduction was happening. The eastern boundary of the Australian Plate likely saw simultaneous opening and closing of several small ocean basins, highlighted by the formation of The South Norfolk Basin as a backarc behind the Three Kings Rise due to subduction effects.

By 20 Ma, the Ontong Java Plateau was partially coupled with the Australian margin, initiating southward subduction in The Solomon Sea and leading to the formation of The Maramuni Arc in eastern New Guinea. Concurrently, The Philippine and Caroline Sea Plates rotated clockwise along The Pacific Plate margin, with geological complexity evolving along the northern New Guinea margin. The Bird Head microcontinent began to fragment, contributing to uplift and convergence in eastern Sulawesi.

Within The Philippine Sea Plate, the widening of The Parece Vela and Shikoku Basins involved a significant eastward shift in the spreading centre, influenced by the plate rotation. Luzon experienced substantial rotation during The Early Miocene, complicating its surrounding plate boundaries.

In The South China Sea region, subduction continued north of Palawan, while southward subduction of the proto-South China Sea led to the opening of the Sulu Sea back-arc basin. North of Kalimantan, the proto-South China Sea closed, thrusting continental crust beneath Kalimantan and causing uplift and sedimentation changes.

The Burma Block began coupling with The Indian Plate, resulting in northward movement along The Sagaing Fault. Post-20 Ma, volcanic activity in Sumatra renewed as the subduction hinge retreated, while the Java-Sumba region experienced a decline in magmatism due to changes in subduction dynamics. Overall, these changes in the structure of Sundaland led to important geological changes, such as the flipping of basins and the reversal of fault movements.

2.2.3. Reconstruction at 15 Ma

By 15 million years ago (Ma), The Ontong Java Plateau had completely integrated with the Melanesian Arc system in the Solomon Islands, resulting in the cessation of subduction at the North Solomon Trench; however, minor local subduction and strike-slip faulting may have continued. The Solomon Sea was shrinking due to subduction beneath The Papuan Peninsula and eastern New Guinea, forming The Maramuni Arc, with possible local northward subduction under The South Caroline Arc, primarily a strike-slip zone.

In The Philippine Sea Plate, spreading had halted in The Shikoku and Parece Vela Basins, while slow spreading began in The Ayu Trough, accompanied by potential minor subduction due to interactions with The Caroline Plate. Complex strike-slip motions and minor subduction were also evident along the western edge of the plate within The Philippines.

The Cagayan Arc system collided with the Palawan margin, halting its spread in The Sulu Sea. During this time, I-type granites formed in Palawan, showing that the crust got thicker because of the collision and earlier rocks from The Mesozoic era, not just from volcanic activity after the seafloor spreading stopped in The South China Sea. This collision initiated south-dipping subduction of The Sulu Sea beneath The Sulu Arc and temporarily coupled The Luzon Arc to Mindoro, resulting in slowed subduction at The Manila Trench.

Further north, ocean crust had formed in The Japan Sea region, which was nearly fully opened by 15 Ma, characterized by extended continental and some oceanic crust. The South China Sea also ceased spreading, stabilizing The Indochina Block current position with limited movements on The Red River Fault since The Miocene.

At the southern and eastern margins of Sundaland, there was erosion and potential minor collisions within The Bird Head microcontinent. 11 Ma detached the Buton–Tukang Besi Block from the Bird Head and linked it to SE Sulawesi, although this oversimplifies more complex

geological events. Carbonate deposition continued in South Sulawesi, while clastic deposition persisted in shallow shelf environments.

Significant inversion events throughout Sundaland have been identified through seismic data, with an uplift of The Sunda Shelf occurring around 15 Ma. This uplift is associated with thick Neogene sediments in offshore NW Java Basins, likely sourced from The Singapore Platform.

2.2.4. Reconstruction at 10 Ma

By 10 Ma, the connection between The Ontong Java Plateau and The Melanesian Arc initiated a new subduction zone on the north and east sides of The Solomon Sea, transitioning from south-west-directed subduction linked to magmatic activity in eastern New Guinea to east-dipping subduction, which formed The New Hebrides Arc. This caused The Solomon Sea to quickly shrink because of subduction happening on both the eastern and western sides, along with a complicated history of changes and the creation of ocean crust in The North Fiji Basin, which included shifts in ridges and major rotation of The Fiji Islands.

The movement of The South Caroline Arc along The New Guinea edge included occasional shifts of arc pieces, helping The New Hebrides Trench move north, which started subduction under The Solomons and The New Britain Arc. This reconfiguration also triggered spreading in The Woodlark Basin, which now rifts westward into The Papuan Peninsula, while also being subducted at the New Britain–San Cristobal Trench. The oldest ocean crust in The Woodlark Basin formed around 6 Ma, indicating that ocean spreading may have started as early as 10 Ma.

The Philippine Sea Plate, rotating clockwise, underwent strike-slip motion and possibly minor subduction at Luzon from 15 to 10 Ma. Collision between Luzon and The Visayan Islands at 10 Ma terminated south-dipping subduction of The Sulu Sea and led to northward subduction along the northern Sulawesi Sea margin, forming The Dent-Semporna-Sulu Arc, which has ceased activity recently.

Subduction began in The Maluku Sea around 15 Ma, with older subduction on the west side and the initiation of east-dipping subduction indicated by volcanic activity around 11 Ma. In eastern Sulawesi, geological activity included significant strike-slip movement. By 10 Ma, the coupling of The Burma Block to The Indian Plate resulted in the opening of The Mergui Basin and the establishment of a spreading centre in The Andaman Sea.

Notable geological events occurred at The Java Trench, driven by the counter-clockwise rotation of Kalimantan, which reduced volcanic activity from Java and surrounding islands until 10 Ma, when magmatism resumed with increased intensity. The Java Trench propagated eastward due to deformation and differences in ocean crust ages, leading to the initiation of The Banda volcanic arc and the opening of The Flores and South Banda Seas.

The rotation of Sumba happened because of the spreading in The Flores Sea, and this led to the formation of metamorphic rocks in Seram, indicating that high temperatures caused changes in the rocks due to rifting. This volcanic activity in The Banda Arc around 5 Ma was characterized by contamination with continental crustal materials. Additionally, different volcanic activity began in western Sulawesi around 11 Ma, resembling post-subduction volcanics formed in an extensional setting, influenced by previous subduction enrichment.

2.2.5. Reconstruction at 5 Ma

Around 5 Ma, significant changes in plate motions marked the onset of present-day geological configurations. Subduction under The Solomons and New Hebrides Arcs caused The New Hebrides Arc system to rotate significantly and complicated the opening of The North Fiji Basin, with a simpler model showing it has rotated 22° clockwise since 12 Ma. The Solomon Sea nearly closed, ceasing subduction along its southern edge, while subduction shifted northward, creating an inverted U-shaped slab underneath eastern New Guinea and causing rapid spreading in The Woodlark Basin.

The Manus plume stabilized in its present position, promoting rapid spreading in The Bismarck Sea in a tectonic setting resembling a pull-apart. By 5 Ma, major terranes in New Guinea were approaching their current positions, resulting in rotation and minor translation within a transpressional fault zone. Limited subduction at The New Guinea Trench is suggested to have started during this time. Ongoing convergence between The Pacific and Australia has been absorbed through distributed deformation across a wide zone, contributing to the elevation and sedimentation patterns of northern New Guinea.

In western Sulawesi, a left-lateral fault system led to the collision of The Banggai–Sulu Block with The East Sulawesi Ophiolite, triggering uplift across Sulawesi and initiating the rise of western mountains due to thrusting. This uplift and erosion began later than documented in previous literature, with sedimentation patterns in South Sulawesi changing from carbonate platform deposition to foreland basin types.

The rapid retreat of the subduction hinge south of The Bird Head microcontinent caused further extension in The Banda Sea region, leading to the cessation of activity in The Banda Arc and the beginning of spreading in The South Banda Sea. Uplift in Seram challenged previous interpretations of it as a fold and thrust belt, suggesting that the area experienced extension more akin to core complex development.

By about 3 Ma, the eastern Banda volcanic arc collided with the Australian margin near Timor, halting spreading in The South Banda Sea. Concurrently, rifting and spreading began in the Mariana Trough, with subduction beneath The Luzon Arc and collision in Taiwan occurring as the pole of rotation for The Philippine Sea Plate stabilized north of the plate.

In Indochina, deformation continued along strike-slip faults, while The Andaman Sea opened at a low rate amid ongoing northward movement of The Burma Block. Offshore regions south of the gulf of Thailand and The Sunda Shelf experienced renewed extension, likely reflecting intricate deformation dynamics rather than classic plate tectonics, despite a general decline in global sea levels.

2.2.6. Reconstruction at 2 Ma

Since around 5 Ma, significant changes have occurred in the plate boundaries along the eastern Australian margin, eastern Indonesia, and The Philippines. The dramatic rotation of Fiji halted, and The Solomon Sea nearly vanished due to subduction along its northern margin beneath the New Britain and New Hebrides Arcs, while The North Fiji Basin continued to widen. The current Australia–Pacific relative motion vectors are now relevant for understanding tectonic activity in New Guinea, where there has been notable uplift from the docked arc terranes of the South Caroline Arc.

The Bird Head region remains complex and poorly understood, having possibly formed a partial connection to The Pacific Plate in the past million years. After The Banda volcanic arc crashed into the Australian margin, new plate boundaries formed to the north of the arc, causing the land to compress and possibly leading to subduction within the Bird Head microcontinent.

Subduction on both sides is eliminating The Maluku Sea to the north, as The Sangihe–North Sulawesi Arc thrusts over The Halmahera Arc. Meanwhile, subduction north of The Philippine Sea Plate has induced extension in The Okinawa Trough, linked to significant contraction in Taiwan due to The Luzon Arc collision with The Asian continental margin.

Spreading continues in The Mariana Trough, and rapid spreading above the Manus plume is creating a new ocean basin in The Bismarck Sea. In Indochina and Sundaland, deformation persists, with some basins in Sumatra experiencing inversion. While contraction and uplift have been significant in Java, complexities in forearc regions suggest a more intricate geological history than previously understood.

Predicting future changes in the region is challenging; however, it is expected that Australia will continue moving north, and The Pacific will shift westward relative to Eurasia. The anticipated

formation of a convergent mountain belt from Japan to northern New Guinea contrasts with the complex geological evolution observed, shaped largely by subduction processes. The interactions of these major plates have resulted in new ocean basins and significant geological displacements, underscoring the dynamic nature of the region tectonics.

2.3. Neotectonics of The Palu-Koro Fault System

The Palu-Koro Fault System is an active strike-slip fault that runs through the central part of Sulawesi, Indonesia. This fault system is a significant geological feature that plays a crucial role in the region tectonic landscape. It is responsible for some of the most devastating seismic activities recorded in Indonesia, including the catastrophic earthquake and tsunami that struck Palu in 2018.

2.3.1. History of The Palu-Koro Fault System

The Palu-Koro Fault has been active for millions of years, shaping the landscape and influencing the tectonic evolution of Sulawesi. Geological evidence suggests that the fault has experienced multiple phases of activity, with significant periods of movement occurring during The Late Cenozoic era. Paleo-seismological studies have identified numerous large-magnitude earthquakes associated with the fault system, indicating its long history of seismicity.

Previous work in Central Sulawesi, especially in The Palu-Koro region, has described evidence of fault movement (Tjia, 1974; Katili, 1978). However, the seismicity of this region is low (Beaudoin, 1998, in Bellier, 2001).

Nevertheless, although the area has low seismicity, the fault zone has high slip rates. Walpersdorf *et al.* (1998) argued that slip rates of The Palu-Koro Fault are 40−50 mm per year as measured by GPS on geodynamic activity. In addition, Surmont *et al*. (1994) pointed out that, based on paleomagnetics, The Palu-Koro Fault movement was affected by clockwise rotation in the north arm of Sulawesi. Furthermore, Stevens *et al*. (1999) calculated that slip rates of The Palu-Koro Fault are 38±8 mm per year by monitoring GPS within 3 years (1992−1995). Active fault research also takes into account the displacement of Holocene deposits, formed approximately 10,000−11,000 years ago. Bellier *et al*. (2001) argued that The Palu-Koro Fault has a left-lateral strike-slip system with 370+10 m displacement of Holocene deposit.

Even though there are not many shallow earthquakes along The Palu-Koro Fault Zone, some very damaging earthquakes have happened there, as noted by Kertapati *et al.* (1991). For instance, the 1968 and 1993 earthquakes, which have magnitudes of 6.7 and 5.7, respectively, have occurred in central Sulawesi and might represent Palu-Koro reactivation (Kertapati *et al.*, 1991). Moreover, Soehaimi (1985) reported that the Lawe Earthquake (1985) was associated with Palu-Koro Fault activity at shallow depth. The recent earthquake that occurred along the fault zone was the Palolo earthquake (2005), with a magnitude > 5 and causing area damage (Soehaimi *et al*., 2005).

Neotectonics refers to the study of tectonic processes that have occurred in the geologically recent past, typically within the last few million years. The Palu-Koro Fault System is an excellent example of an active neotectonic feature. Recent studies have utilized various techniques, including GPS measurements, remote sensing, and field observations to monitor and understand the ongoing tectonic activity along the fault. Neotectonics is a subfield of tectonics that examines recent tectonic deformations and the evolution of landscapes. The primary emphasis of neotectonics study is the geodynamics of a specific region. It often manifests in geological processes that occurred from millions of years ago (Ma) to thousands of years ago (Ka). This paper delineates neotectonics research concentrating on geological and geomorphological occurrences during The Quaternary and Holocene epochs. The text discusses present and prospective tectonic deformation in The Palu-Koro Fault, which bisects the central region of Sulawesi Island, Indonesia.

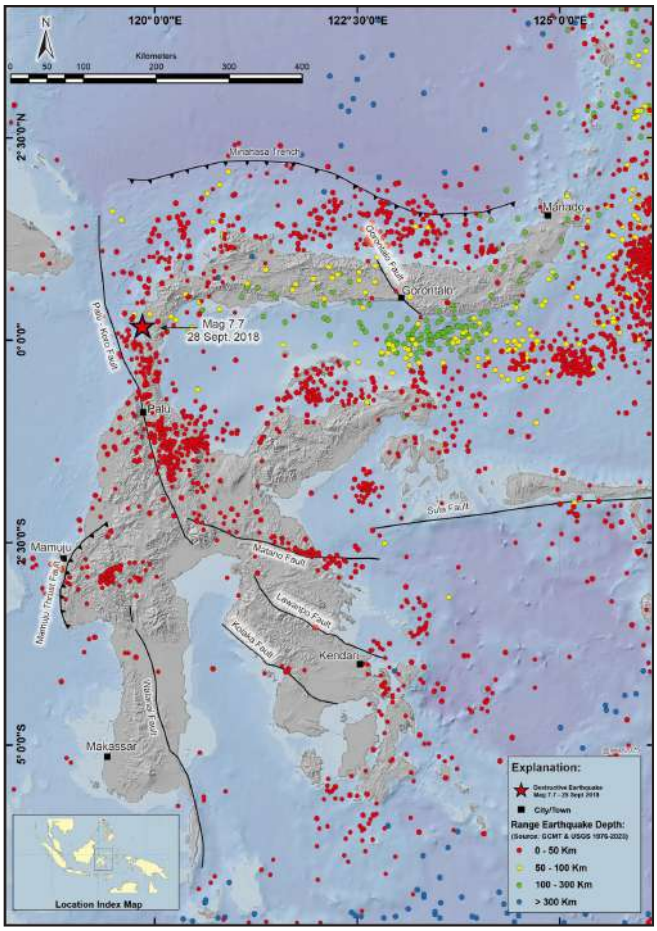

Gambar 2.6. The map of Sulawesi Island depicts seismicity based on the GCMT and USGS catalogues from 1976 to 2023. Surono (2010) and Jaya *et al*. (2023) depicted the major fault.

Tectonics refers to processes in the earth crust, which result in structures and landforms formation (Keller and Pinter, 1996). Earthquakes are the result of tectonic activity around active margins or at the place where plates collide. However, some earthquakes have occurred in intraplate regions; for instance, the western United States is a tectonic province faced with the problem of large earthquakes caused by two main sources: The San Andreas Fault and the eastern Pacific subduction zone (Wallace, 1990).

Neotectonics, which is related to the effects of tectonic processes such as earthquakes, is used to define active faults. Obruchev (1948) argued that neotectonics is the study of recent movements of the earth surface established during the Late Tertiary or Early Quaternary. Similarly, Zoback (1991) and Wood and Mallard (1992 say that neotectonics, which happened after The Miocene period, includes changes in the earth structure within stable areas, along with new formations that are happening now. In contrast, Morner's (2004) position is that the phase of neotectonics starts when the tectonic regime of an area begins to happen. Thus, it can be inferred from the definitions that neotectonics is a branch of tectonics that occurred in the past and continues to the present day (Stewart and Hancock, 1994). Furthermore,

the terminology of neotectonics relates to processes that produce crustal deformations over time and scale, with considerable significance to human society (Wallace, 1986).

2.3.2. GPS Measurements

Global Positioning System (GPS) data have been instrumental in measuring the rate of slip along The Palu-Koro Fault. Studies have indicated that the fault accommodates a significant portion of the relative motion between the tectonic plates, with slip rates estimated to be around 40 mm per year. These measurements offer invaluable information about the dynamics of the fault and help in assessing the seismic hazard associated with it.

2.3.3. Remote Sensing and InSAR

Remote sensing techniques, including Interferometric Synthetic Aperture Radar (InSAR), have been used to detect and measure ground deformation caused by tectonic activity along The Palu-Koro Fault. InSAR data have revealed patterns of surface displacement that correlate with fault movement, allowing scientists to map the extent and magnitude of recent fault activity. These techniques have proven invaluable in monitoring the fault and assessing the potential for future seismic events.

2.3.4. Paleoseismological Studies

In terms of neotectonic study, paleoseismology is an optional method to observe active data, which provide historical earthquake information (location, time, and size). Wesnousky *et al*. (1984) identified that paleoseismology can describe the behaviours and deformations of major faults, in particular for short periods during The Quaternary. In addition, a branch of earth science that focuses on earthquakes related to tectonics is seismotectonics, which relates geological structures and seismicity, including crustal deformation, analysis of fault behaviours, and recent earthquakes. Crustal deformation, which resulted from tectonic processes, will express the morphological landform. For a deep understanding of morphology and landform, morphotectonics offers the study of all aspects of horizontal and vertical movements and erosional and depositional processes in time and scale (Stewart and Hancock, 1994). In other words, morphotectonics involves cross-relational studies of neotectonics and landforms.

Paleoseismology involves the study of past earthquakes through the examination of geological and geomorphological evidence. Trenching and coring along The Palu-Koro Fault have uncovered evidence of past surface ruptures and fault displacements. By analyzing these features, scientists can reconstruct the history of seismic activity along the fault, offering explanations for the frequency and magnitude of past earthquakes. This information is crucial for understanding the seismic hazard posed by the fault and for developing effective mitigation strategies.

2.3.5. Seismic Hazard and Risk

The Palu-Koro Fault System poses a significant seismic hazard to the region. The 2018 Palu earthquake, with a magnitude of 7.5, was a clear example of the destructive potential of this fault system. The earthquake caused widespread devastation, including a deadly tsunami, landslides, and soil liquefaction. The event highlighted the need for a comprehensive understanding of the fault behaviour and the development of strategies to mitigate the risks associated with it.

2.3.6. Earthquake Hazard Assessment

Assessing the seismic hazard associated with The Palu-Koro Fault involves evaluating the probability of future earthquakes and their potential impact on the region. This requires a detailed understanding of the fault behaviour, including its slip rate and recurrence interval, as well as the potential for multi-segment ruptures. By integrating geological, geophysical, and historical data, scientists can develop probabilistic seismic hazard models that estimate the likelihood of future earthquakes and their expected magnitudes.

2.3.7. Risk Mitigation Strategies

Effective risk mitigation strategies are essential for reducing the impact of future earthquakes along The Palu-Koro Fault. These strategies include improving building codes and construction practices, developing early warning systems, and enhancing public awareness and preparedness. Additionally, land-use planning and infrastructure development should consider the fault location and potential for seismic activity to minimize the exposure of vulnerable populations and critical facilities to earthquake hazards.

The Palu-Koro Fault System is a dynamic and active tectonic feature that plays a crucial role in the geological landscape of Sulawesi. Understanding its neotectonic activity is essential for assessing the seismic hazard and developing effective risk mitigation strategies. Ongoing research, utilising advanced techniques such as GPS measurements, remote sensing, and paleoseismology, continues to offer important clues about the behaviour of this fault system. By integrating these findings into comprehensive hazard assessments and risk reduction efforts, the resilience of communities can be enhanced in the region and reduce the impact of future seismic events.

2.4. Regional Scale Geology

2.4.1. Geology of Sulawesi Island

Sulawesi can be split into three main geological areas based on rock types and how they formed: (1) the Western Sulawesi Plutonic-Volcanic Arc, (2) the Sulawesi Ophiolite Belt in the east, which is linked to deep-sea sedimentary rocks, and (3) pieces of land that came from the Australian continent. According to the tectonic setting map of Sulawesi (Hamilton, 1979), the contacts of the three major geological provinces are fault systems.

2.4.2. Western Sulawesi Plutonic-Volcanic Arc

The Sulawesi Volcanic Arc spreads over from The South Arm through the north arm (Figure 1.1), and consists mainly of plutonic-volcanic, sedimentary, and metamorphic rocks. The plutonic-volcanic rocks were formed from The Paleogene through The Quaternary, while sedimentary rocks were formed during The Mesozoic through The Tertiary. Metamorphic rocks were formed from The Permo-Triassic until The Paleogene (Sukamto, 1975; Hall and Wilson, 2000; Watkinson, 2011).

The South Arm Sulawesi mainly consists of metamorphic, ultramafic, and sedimentary rocks as basement. The metamorphic rocks include amphibolite, mica-schist, eclogite, and quartz, chlorite-feldspar, and graphite phyllites (Sukamto, 1982). These rocks have an Early Cretaceous age based on K/Ar dating of schist samples from Bantimala and Barru (the south arm region), which yielded ages of 132−114 Ma and 106 Ma, respectively (Wakita *et al*., 1996). Sedimentary processes of the south arm dominantly occurred in open marine environments from neritic to bathyal since The Late Cretaceous, as observed in The Balangburu and Marada Formations (Sukamto, 1982). Volcanism has also occurred since The Palaeocene to the recent, and this might be caused by the west-dipping subduction zone that was formed 63 Ma ago based on fission track dating of tuff (Leeuwen, 1981).

The Central Sulawesi area, which is situated between the south arm and north arm, is mostly made up of granitoids found along The Palu – Koro Fault zone and is made of quartz, K-feldspar, muscovite, and plagioclase. The collision process between the microcontinent (Banggai-Sula) and Sulawesi Island caused these granitoids to appear on the surface since the Middle Miocene (Priadi *et al*., 1994).

Mainly composed of Lower Miocene rocks, the north arm exhibits two distinct tectonic setting evolutions. First is westward subduction during The Early Miocene along The Sangihe Thrust. Secondly, rifting and uplift from The Late Miocene until The Quaternary caused collision between oceanic and continental crust along The North Sulawesi Trench (Yuwono *et al*., 1985; Leterrier *et al*., 1990; Priadi *et al*., 1994). However, the north arm of Sulawesi has several different geological features, in particular the

volcanism process. Volcanism in this arm was still active until recent times, which is proven by several active volcanoes at the end edge of this arm and Tomini Bay (Figure 1.1).

2.4.3. Eastern Sulawesi Ophiolite Belt

The Sulawesi Ophiolite Belt is located in the northern part of the southeast arm of Sulawesi. Surono and Sukarna (1995) contended that a mid-oceanic ridge was responsible for this ophiolite formation. The ophiolite belt mainly comprises mafic and ultramafic rocks at the east arm and-east arm, respectively (Fortuin, 1990; Simandjuntak, 1996). Surono and Sukarna (1995) argued that the basement of south-east Sulawesi terrain comprises low-grade metamorphic rocks with fewer aplitic intrusions. Pillow lavas present in the east arm melange are a definite sign of the ophiolite belt. Further, limestone and bedded chert are dominant in this belt and show deep-sea sedimentation (Simandjuntak and Barber, 1996). Moreover, this ophiolite belt was also highly folded and faulted; for instance, The Lawanopo Fault (north-west-south-east) forms the contact between the ophiolite belt and ultramafic/mafic rock unit (Figure 1.1).

Nevertheless, the east arm of Sulawesi also comprises sedimentary rocks that were formed during The Mesozoic. For example, The Meluhu Formation consists of sandstone, shale, and mudstone (Surono and Sukarna, 1995). It is also reported that metamorphic rocks were a source of The Melulu Formation due to metamorphic fragment occurrence in the sandstone, although as a thin layer in this formation (Surono and Sukarna, 1995). Furthermore, the southeast arm has Paleogene limestone belonging to The Tampakkura Formation, for instance, which consists of oolite, mudstone, wackestone, grainstone, and packstone. This formation was formed during The Late Eocene–Early Oligocene, because it contains foraminifera, indicating that period (Surono and Sukarna, 1995).

The ophiolite complex is also found in the east arm of Sulawesi. Simandjuntak and Barber (1996) reported this ophiolite complex as a complete sequence in this arm and that it was formed at oceanic crust during The Late Jurassic to Eocene. The complex might be in tectonic contact with Mesozoic sediment and mafic/ultramafic rocks (harburgite, pyroxenite, serpentinite, and dunite).

Molasse deposit occurrence is the proof of collision between the continental plate and ophiolite belt in Sulawesi Island. This deposit is widely distributed in the eastern and southern arms of Sulawesi. Simandjuntak and Barber (1986) argued that the east arm molasse was formed by the collision between continental terrane (Banggai-Sula) and The East Sulawesi Ophiolite Belt during The Late Miocene. The east arm molasse is dominated by shallow marine carbonates with coarse- to fine-grained clastic rocks. However, in the southern arm of Sulawesi, the molasse deposit is dominated by conglomerates (Alangga and Padua Formations) and marl-limestone sequences (Boepinang Formation, Eemoiko Formation). In addition, the southern arm molasse is Early Miocene; hence, it is older than the east arm.

2.4.4. Continental Fragments

Continental fragments occupying Central and South-east Sulawesi were derived from the northern part of The Australian Continent (Metcalfe, 1988; Metcalfe and Irving, 1990; Audley-Charles, 1991; Surono, 1997). The continental fragments consist of metamorphic rocks, including amphibolite, epidote-amphibolite facies, and alow-grade dynamo-metamorphic group of blueschist facies (Davidson, 1991). Silver *et al*. (1983) pointed out that the Indonesia-Australian microcontinent collided with The Ophiolite Sulawesi Complex with a westward-moving direction during Late Oligocene-Middle Miocene times. As a result, a local sedimentary basin was formed and produced a mélange complex. The basin became widely developed after the collision, and sedimentation began in the southeast arm and east arm during the Early Miocene and Late Miocene, respectively. This sedimentation led to molasse deposits, which contain major clastic and minor limestone.

The molasse deposit occurred in a marine environment, dominantly fluvial to partly transitional (Surono *et al*., 1993; Surono, 1996).

2.4.5. Major Tectonics of Sulawesi Island

As mentioned above, the Sulawesi region is a meeting point, or triple junction, of convergent plates; consequently, the region has complex geology. Simandjuntak (1992) argued that interaction of the plate occurred in The Neogene. The interaction of those plates led to several types of structures, such as subduction, collision zones, folding, thrust, and faults. Researchers believed the structures are still active or are being reactivated. The structures on the island can be divided into five major types: 1) The Minahasa Trench, which represents The Sulawesi Sea Crust collision with the Sulawesi continental crust and subduction beneath the north arm Sulawesi, formed during Paleogene times (McCaffrey *et al*., 1983). This trench led to the formation of the volcanic arc in the eastern part of north arm. 2) The Palu-Koro Fault, which occupies central Sulawesi, has a north-east trend and is approximately 250 km in length (Sudrajat, 1981), and is a strike-slip system (Katili, 1978; Walpersdorf *et al*., 1998). Historical earthquakes along this fault indicate that active tectonics have been continuing since the Neogene period (Simandjuntak, 1996) and are manifested by various tectonic movements such as uplift of coral reefs within the fault (Tjia, 1981) and reactivation of this fault (Kertapati *et al.*, 1992). 3). The Batui Thrust is a major geological feature representing the collision zone between The Banggai-Sula Platform and Eastern Sulawesi Ophiolite Belt in The Neogene (Simandjuntak and Barber, 1996). This thrust system is also active due to the intensity of seismicity within the thrust (Kertapati *et al*., 1992) and the occurrence of coralline reefs, which were cut by thrust movement in The Quaternary (Simandjuntak and Barber, 1996). 4) The Posos Thrust in the Central Sulawesi is a structural contact zone between The Central Sulawesi Metamorphic Belt and The Western Sulawesi Magmatic Belt (Hamilton, 1979; Simandjuntak, 1992). Several earthquakes that occurred in The Tomini Bay indicate that this tectonic system (thrust) is reactivated. 5) The Walanae Fault, which is located at the south arm Sulawesi, is a wrench fault system (strike-slip) with north-west-south-east direction. Jaya and Nishikawa (2013) mentioned that the paleostresses of the fault were influenced by the collision between eastern Sulawesi and Australian fragments and occurred since The Pliocene. The seismicity along the fault shows low seismicity; hence, the fault is inactive.

2.4.6. The Tectonic Development of Sulawesi Island

The triple junction of plate convergence has led Sulawesi Island to have several types and periods of tectonism. According to Simandjuntak and Barber (1996), the tectonic development of Sulawesi Island can be broken down into four main stages: "Cretaceous Cordilleran subduction", "Mesozoic tectonic divergence", "Neogene Tethyan type collision", and "Quaternary double opposing collision".

The "Cretaceous Cordilleran subduction" is represented by the subduction zone between the Banda Sea and The Sunda Shield in the western part of the island. Cretaceous-Paleogene flysch sediment with basaltic lava in the upper part of the trench are indications of plate convergence. The flysch sediment was observed in The Central Sulawesi Metamorphic Belt, The Cretaceous-Paleogene mélange, and the Eastern Sulawesi Ophiolite Belt.

The time of "Mesozoic tectonic divergence" led to the crashing together of land masses with small continents, creating the ophiolite belt in the Western Banda Sea area. The micro-continents, such as The Banggai-Sula Platform and The Tukangbesi-Buton Platform, were the result of fragmentation of the northern Australian Continent (Piagram and Panggabean, 1984). Rusmana *et al*. (1993) pointed out that tectonic divergence of this period was associated with The Sorong Fault system, with displacement in the east–west direction followed by the splay system of this fault.

The next period of tectonic development is The Neogene "Tethyan" type collision that is indicated by the melange complex along The Batui Thrust in the eastern arm of Sulawesi (Simandjuntak and Barber, 1996). Mainly, the collision was the result of the movement of the micro-continents (Banggai-Sula Platform, Tukangbesi-Buton Platform) in a north-north-west direction and collision with ophiolite belts in The Neogene period. In addition, the collision has no volcanic arc and no development of forearc and backarc basinal settings (Simandjuntak and Barber, 1996), which are unique characteristics of this type of collision.

The last tectonic development of Sulawesi Island is The Quaternary double opposing collision that reactivated major structures during Neogene times. For instance, the active volcano (Minahasa-Sangihe Volcanic Arc) at north arm Sulawesi was developed by the double opposing collision. Furthermore, seismicity shows historical earthquakes that occurred along major structures. This indicates that tectonic activity has shaped the morphology of Sulawesi Island, and this process continues to the present day.

2.5. Local Scale Geology

The researched area is located in The Central Sulawesi Province along The Palu Koro Fault. The Palu-Koro Fault clearly appears to divide the studied area, as shown in Figure 1.8. The Palu-Koro Fault has a north-south trend with sinistral strike-slip displacement. The fault is assumed to represent the ductile deformation of metamorphic rock in terms of timing and kinematics, because it cuts the metamorphic basement. Along the fault is a metamorphic complex suggesting "non-coaxial ductile deformation". Watkinson (2011) argued that the ductilely deformed rocks are part of Australian Gondwana, which formed in Mesozoic-Precambrian time; the metamorphic rock consists of gneisses, amphibolites, and schists. Watkinson (2011) divided The Central Sulawesi into four categories of geological complexes (Figure 1.4): sedimentary rocks, volcanic rocks, plutonic rocks, and metamorphic rocks. Sedimentary rocks occupying the fault western and eastern parts were formed from The Upper Cretaceous until The Holocene. Interestingly, The Holocene sedimentary rocks are located close to the fault, and they seem to be cut by the fault; hence, it is assumed that activity of the fault also occurred during The Holocene.

Volcanic rocks formed as products of volcanic activity have been formed during Oligo-Miocene and Miocene times, and occupy the southwest parts of the fault. Plutonic rocks formed by intrusions are located along the fault. For instance, a granite complex is located close to the fault. The fault may serve as a fissure for magma intrusion. In terms of metamorphic rocks, the area has experienced some types of metamorphism based on age: The Permo-Triassic metamorphic complex at the eastern part of the fault, represented by granite dominantly with biotite schist, paraneisses, amphibolite, and schists (Watkinson, 2011). Triassic-Jurassic metamorphic complex composed of metapelites and metabasites (Leeuwen and Muhardjo, 2005) located at the eastern and western parts of The Palu-Koro Fault. Cretaceous-Paleogene metamorphic rock composed of quartz-mica schist, marble, metaconglomerate, and meta-tuff phyllite (Watkinson, 2011), which were affected by the "plutono-metamorphic belt" of central Sulawesi (Watkinson, 2011).

However, Sukamto *et al*. (1996) noted that the regions near The Palu-Koro Fault are made up of igneous rocks, sedimentary rocks, metamorphic rocks, sedimentary Molasa, alluvial deposits, and coastal sediment (Figure 1.8). Igneous rocks are composed of granite and granodiorite, whereas sedimentary rocks consist of sandstones, conglomerates, and limestone. Metamorphic rocks found in this area consist of phyllite, slate, and quartzite. Sediment Molasse, the most hardened sediment, is composed of conglomerate, sandstone, mudstone, limestone pebbles, and marl. There are also alluvial and coastal sediments consisting of gravel, sand, mud, and coral limestone.

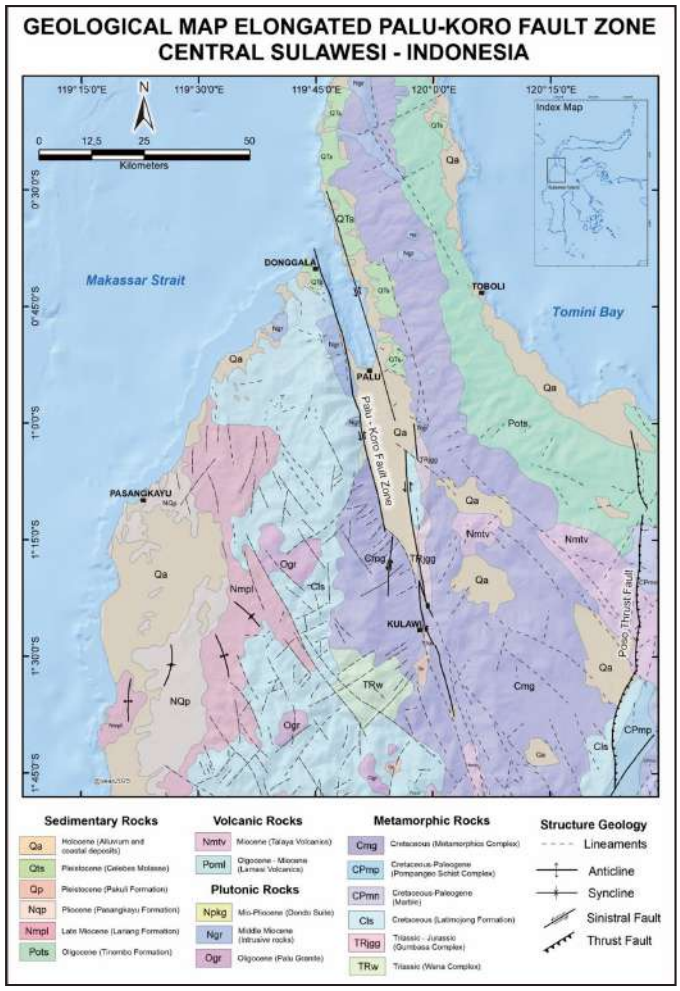

Figure 2.7. Geological map of the elongated Palu-Koro Fault, Central Sulawesi. The information has been adapted from the works of Sukamto in 1973, Simandjuntak *et al.* in 1997, and Sukido *et al*. in 2011.

Only the eastern study area exposes the oldest rocks in the mapped area, which are metamorphic rocks. The metamorphic complex consists of amphibolitic schist, mica schist, gneiss, and marble. The schists are more abundant on the western side, and gneiss with minor marble is dominant on the eastern side. Unmapped intrusive bodies, mostly less than 50 m across, intrude the metamorphic complex and range in composition from diorite to granodiorite (Sukamto *et al*., 1996). These intrusions are probably feeders for the volcanic rocks that occur in The Tinombo Formation. Small intrusions are mostly of diorite, diorite porphyry, microdiorite, and granodiorite, which intrude The Tinombo Formation, predate the molasse deposits, and are widely distributed throughout the area. The mapped intrusions have ages of 31.0 my by K/Ar analysis of feldspar. An unmapped intrusion about 15 km NE of Dinggala underlying Quaternary coral yielded an age of 8.6 my dated by K/Ar analysis of biotite (Sukamto *et al*., 1996).

The area also consists of a molasse complex (Sukamto *et al*., 1996). These rocks occur

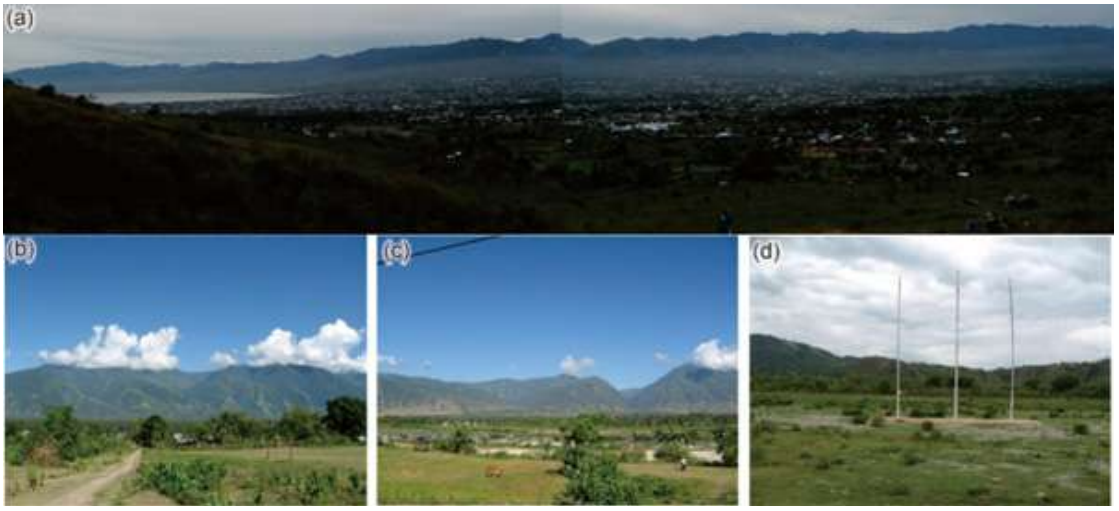

Figure 2.8 Morphology landscape of Palu Bay. (a) Morphology of Palu Bay, (b) Fault Scrap western side, (c) The Balane mountain ridges as the source of alluvial fans, (d) Fault scarp on the eastern side (Photo: Soehaimi, 2012).

Figure 2.9. Sulawesi Molasse outcrops are shown at Talise Village, Mantikulore Subdistrict, Palu District, Central Sulawesi.

at lower elevations along the flank of both ridges, unconformably overlying The Tinombo Formation and the metamorphic complex, and contain detritus derived from the older formations

and consist of weakly consolidated conglomerate, sandstone, mudstone, coral limestone, and marl. Near the metamorphic complex at the western part of the area, the deposits consist mainly of very coarse boulders, and seem to have been deposited close to the fault. The unit includes Quaternary fluvial deposits on both sides of Palu Bay and possibly elsewhere.

The young geological units of this area are alluvium and coastal deposits. The units composed of gravel, sand, mud, and coral limestone formed in fluvial, deltaic, and shallow marine environments are the youngest sediments in the area. They probably are entirely of the Holocene age. In the area near Labea and Tambo, coral reefs form small, low hills.

According to Sukamto *et al*. (1996), the geological structure in this area is dominated by the Palu Fault line, which has a north−south direction, and along The Palu Valley zone might be seen as a graben that was driven by active fault activity. Hot springs are found along the valley zone as an indicator of this fault. Some faults and other lineaments are parallel to the direction of The Palu Fault in the eastern part of Palu. Many other faults and lineament directions are roughly perpendicular to the line of the main Palu Fault. A reverse fault cutting the metamorphic rocks and Tinombo Formation indicates the nature of compression on older faults. The youngest recorded fault movement occurred in 1968 near Tambo, rising after the earthquake in the form of normal faults trending-west-south-east, causing 5 m of subsidence of the surface (Sukamto *et al*., 1996). In part of the subsidence, the beach area (approximately 5 km^2) sunk into the sea (Sukamto *et al*., 1996).

In terms of the tectonic regime, The Palu-Koro Fault has three periods of tectonism (Bellier *et al.*, 2006). Firstly, during The Late Miocene-Early Pliocene (5 Ma), it had a west-north-northwest direction and transpressional deformation. Secondly, in The Pliocene, the fault had a west direction, whereas “regional cooling” and “exhumation” also occurred around the fault. Thirdly, in The Quaternary period, block movement occurred adjacent to the fault.

3. SEISMICITY AND COLLATERAL HAZARD

3.1. Seismicity

Central Sulawesi Province is one of the earthquake prone areas in Indonesia that were sourced from onshore and offshore (Figures 3.1 and 3.2). The gulf regions of Palu, Central Sulawesi Province, are classified as having a high level of seismicity, especially the source from The Palu-Koro Fault that spread onshore to offshore. Another source of earthquakes comes from the subduction zone in the form of a megathrust in The North Sulawesi at shallow depths. In addition, it comes from the intraslab zones which are subduction zones with moderate to deep depths, that are rarely found in The Palu Gulf area. Figure 3.1 shows the distribution of earthquakes on Sulawesi Island from 1980 to 2024, dominated by shallow earthquakes, except in Tomini Gulf which also originates from the moderate to deep intraslab zone. The Palu-Koro Fault as the main earthquake source in the Palu area has caused disasters several times. Earthquakes on the land that originate from the movement of active faults are generally destructive, although the magnitude is small, but the depth is shallow.

3.2. History of The Destructive Earth-quake at Palu Gulf

Based on The Geological Agency destructive earthquake catalogue, The Palu Gulf has been hit by several destructive earthquakes. The Geological Agency records that there have been seventeen destructive earthquakes since 1950 until now (modified from Supartoyo *et al*., 2014). This destructive earthquake event had triggered tsunamis four times, in 1927, 1968, 1996, and 2018. The tsunami was assumed triggered by

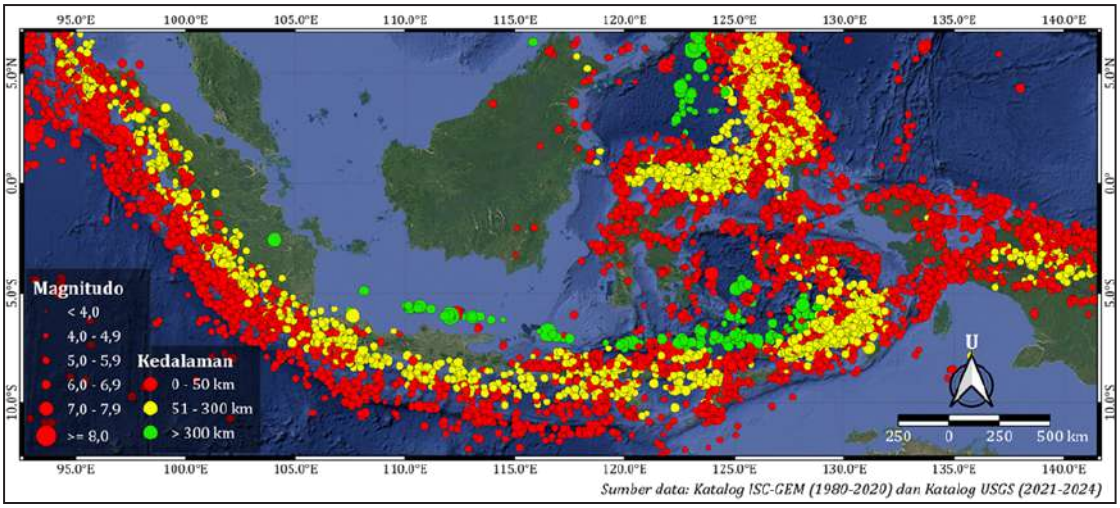

Figure 3.1. Seismicity in Indonesia region from 1980 to 2024 are sourced from ISC and USGS Catalogues.

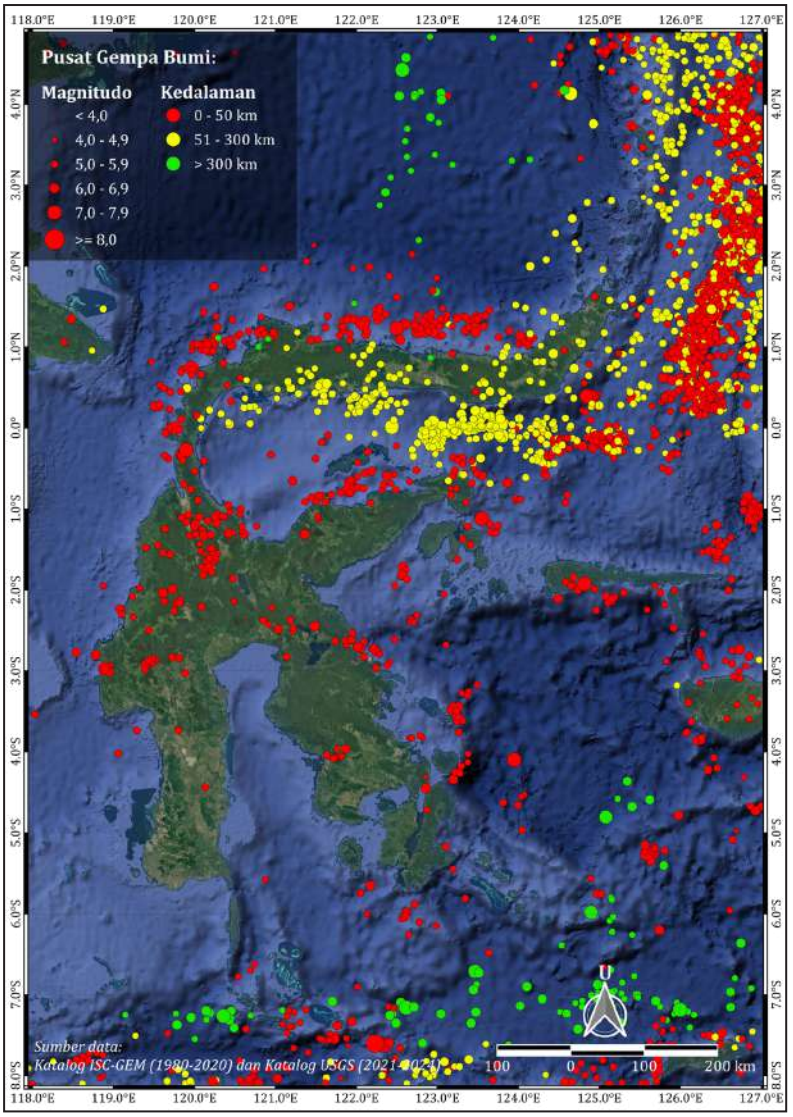

Figure 3.2. Seismicity of Sulawesi Island in 1980 until 2024 source from ISC and USGS Catalogue. It shows that in the northern arm of Sulawesi and Tomini Gulf, earthquakes originate from the intraslab zone, while in other areas they originate from active faults.

landslide on the coastal and or the bottom of the sea due to strong earthquake shaking.

The destructive earthquakes not only caused building damage, but also the collateral hazard (ground crack, landslide, liquefaction). Table 3.1 below presents the earthquake destructive events at Palu Gulf (Figure 3.3).

3.3. Earthquake Source

Sulawesi Island is one of the areas prone to earthquakes, because it has many earthquake sources (Cipta et al., 2016) (Figure 3.4) that spread onshore as well as offshore. Meanwhile, the main earthquake source on The Palu Gulf area is from The Palu-Koro Fault which spread

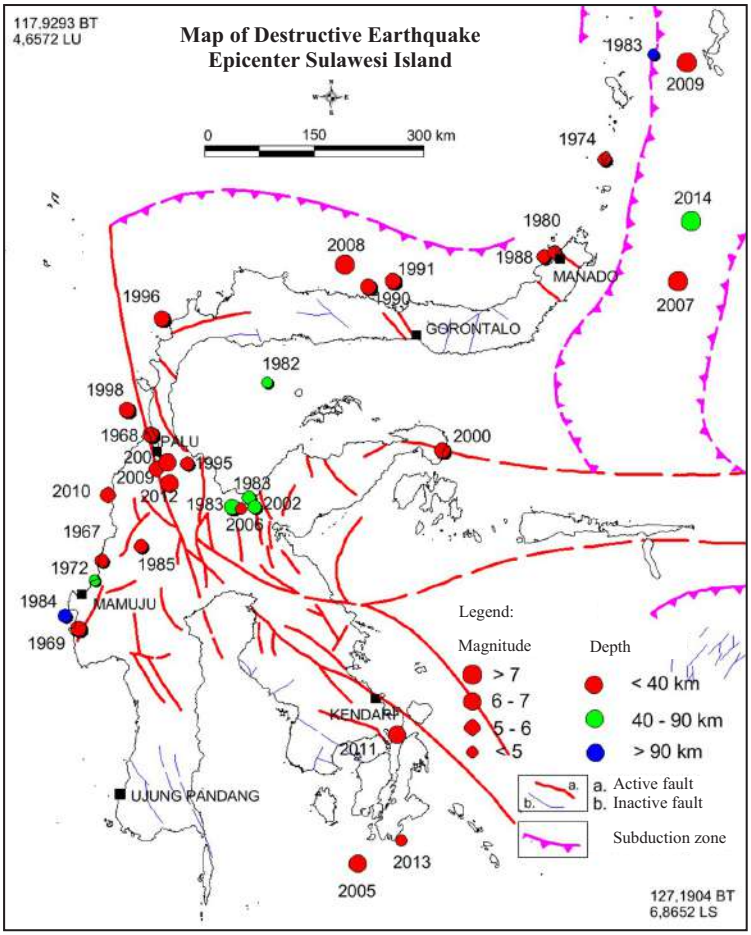

Figure 3.3. Map epicentre of destructive earthquake in Sulawesi Island (Supartoyo *et al*., 2014).

onshore to The Palu Gulf in the sea. Some researchers publish the existence, distribution, and activity of Palu-Koro Fault (Bellier et al., 2001; Daryono, 2016; Pusgen, 2017; Jaya et.al., 2019; Natawidjadja et.al., 2021).

Pusgen (2017) divides the distribution of The Palu-Koro Fault into four segments (Figure 3.5), namely from the north to south: The Makasar, Palu, Suliki, and Moa Strait segments. In addition, Natawidjaja et al. (2021) mapped the distribution of The Palu-Koro Fault offshore using high-resolution bathymetry data after The 2018 Pasigala Earthquake (Figure 3.6). In 2023, the Marine geology team of The Geological Agency also conducted bathymetric and Subbottom Profiler (SBP) surveys in The Palu Gulf. The results confirmed the continuity of The Palu-Koro Fault into The Palu Fault, shaped a pull-apart structure with a deep valley. This structure was limited by the east Palu Fault and the west Palu Fault, both kinematically dominated by left-trending normal faults (Figure 3.7).

It can be said that The Palu-Koro Fault is highly active. Several destructive earthquakes in Palu Gulf have been linked to the activity of Palu-Koro Fault (Table 3.1). The data from Quick Response Teams of Geological Agency shows that the earthquake of Palu Sigi Donggala in 2018

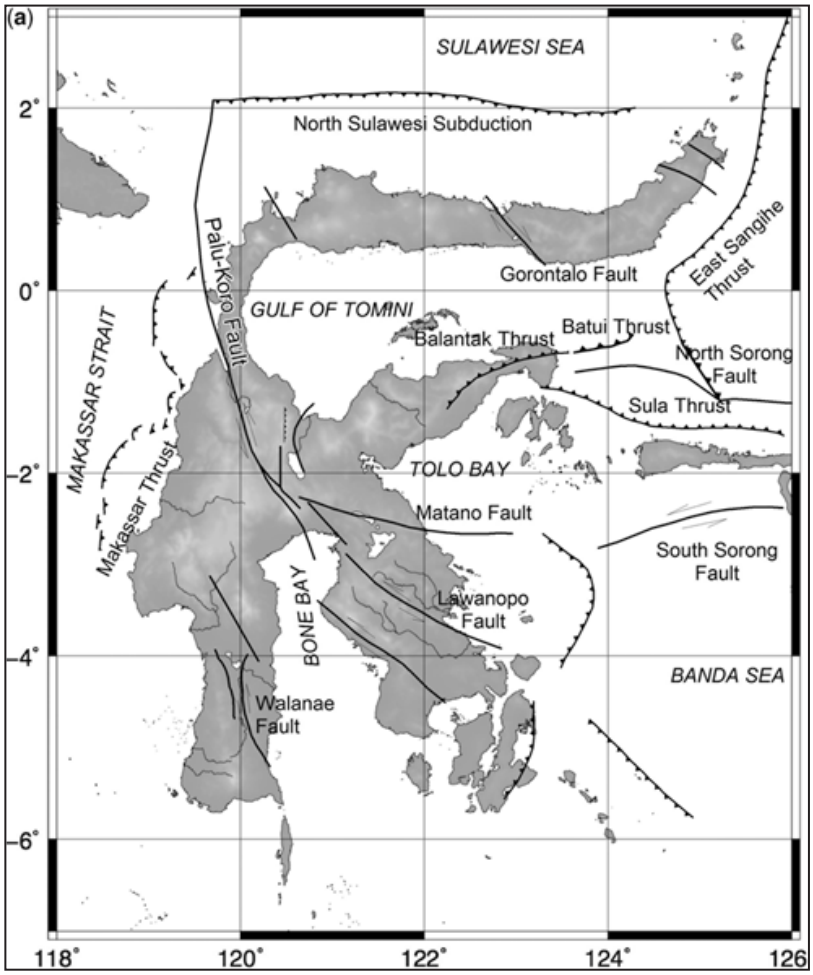

Figure 3.4. Earthquake source on Sulawesi Island (Cipta *et al*., 2016).

caused a maximum sinistral horizontal offset of 580 cm in the Pewunu area, West Dolo District, Sigi Regency. If it is assumed, the destructive earthquake in 2018 was equivalent to the 1907 earthquake, with a return period of 111 years, the slip rate of The Palu-Koro Fault is about 5,2 cm/year. This is certainly a significant slip rate (Slemmons and Depolo, 1968 in Wu and Hu, 2024).

3.4. The Palu Sigi Donggala Earthquake on September 28thth, 2018

The earthquake occured on September 28th, 2018 has caused disaster in Central Sulawesi, including Palu City, Donggala Regency, Sigi Regency, and Parigi Moutong Regency. This earthquake is named as Palu Sigi Donggala or Pasigala Earthquake. The massive disaster occurred at an area near of Palu-Koro Zone. This earthquake caused 4.845 people died, 172.999 people was evacuated and about 110.214 buildings were damaged (https://www.tempo.co/politik/tsunami-dan-gempa-palu-donggala-2018-dalam-angka-korban-daya-rusak-dan-lainnya-138090). The total loss reached IDR 18.48 trillion, which is a very large loss. Table 3.2 shows the loss by this earthquake at Palu City and surrounding areas.

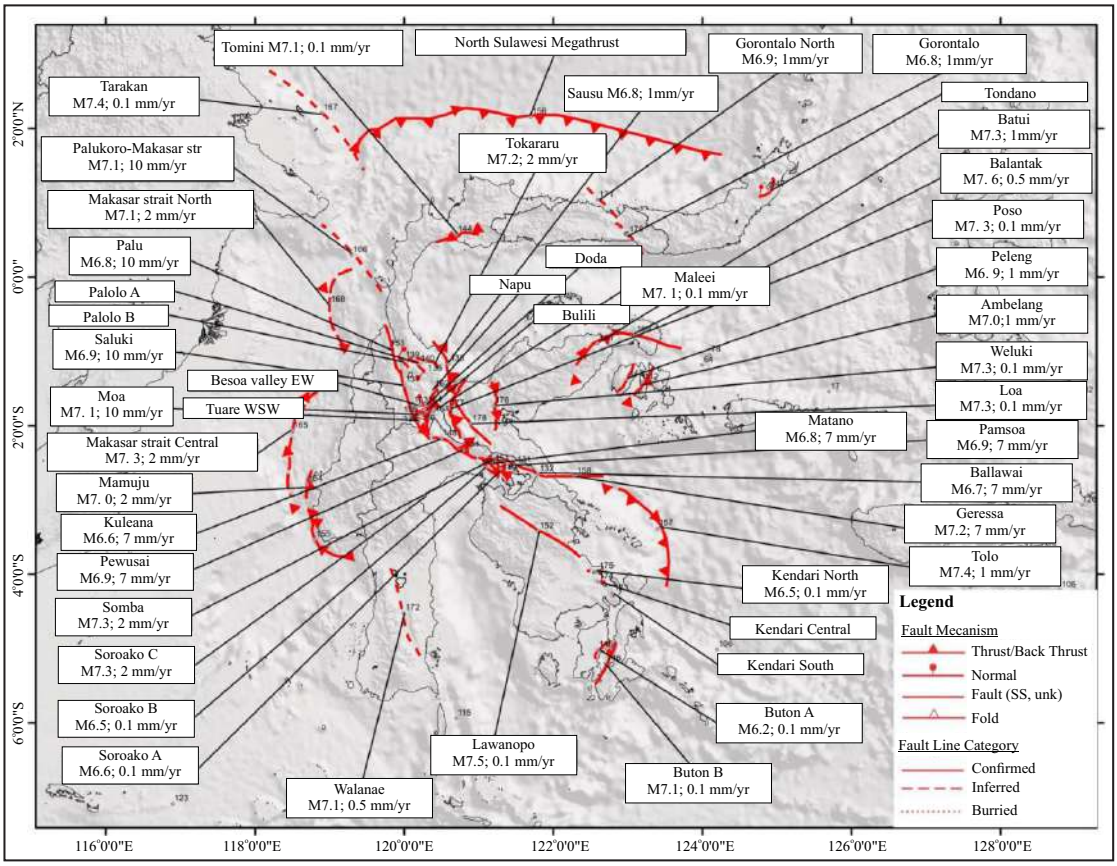

Figure 3.5. Distributions of earthquake sources on Sulawesi Island (Pusgen, 2017). The Palu-Koro Fault is divided into four segments, namely The Palu-Koro Makassar Strait segment located offshore and onshore Palu, Saluki, and Moa.

The results of a field observation by The Quick Response Team of Geological Agency (QRTGA) show that The Pasigala Earthquake on September 28th, 2018 has resulted in tsunami (Figure 3.8), Fault Surface Rupture (FSR), ground cracks, land subsidence, ground oscillation, liquefaction, and landslides. Tsunami striked along Palu Gulf included Palu City and Donggala Regency coastal, and a small part of the Sirenja area, Donggala Regency. The area in Palu Bay between the east coast of Palu Bay to Sirenja Beach, Donggala Regency (Figure 3.9), did not show tsunami material. Eyewitnesses also said there was no tsunami. The tsunami height reaches 6 m at yellow bridge of Gulf Palu. The results by QRTGA (Figure 3.10) shows that the flow depth around 0,65 – 5,3 m and the inundation distance reach 500 m from the coastal to the land. The maximum of flow depth (about 5,3 m) observed at Ulujadi, and the maximum of inundation distance observed around yellow bridge of Palu Gulf. Tsunami remains observed at Tanjung Padang and Tompe Village, Sirenja District, Donggala Regency, with flow depth 3,9 m (about 30 m from shoreline) and inundation distance reach 190 m. Flow depth at Tompe Village, Sirenja District, reached 2,6 m (about 36 m from shoreline), and inundation distance reached 88 m.

The data from Quick Response Teams of Geological Agency shows that there is Fault

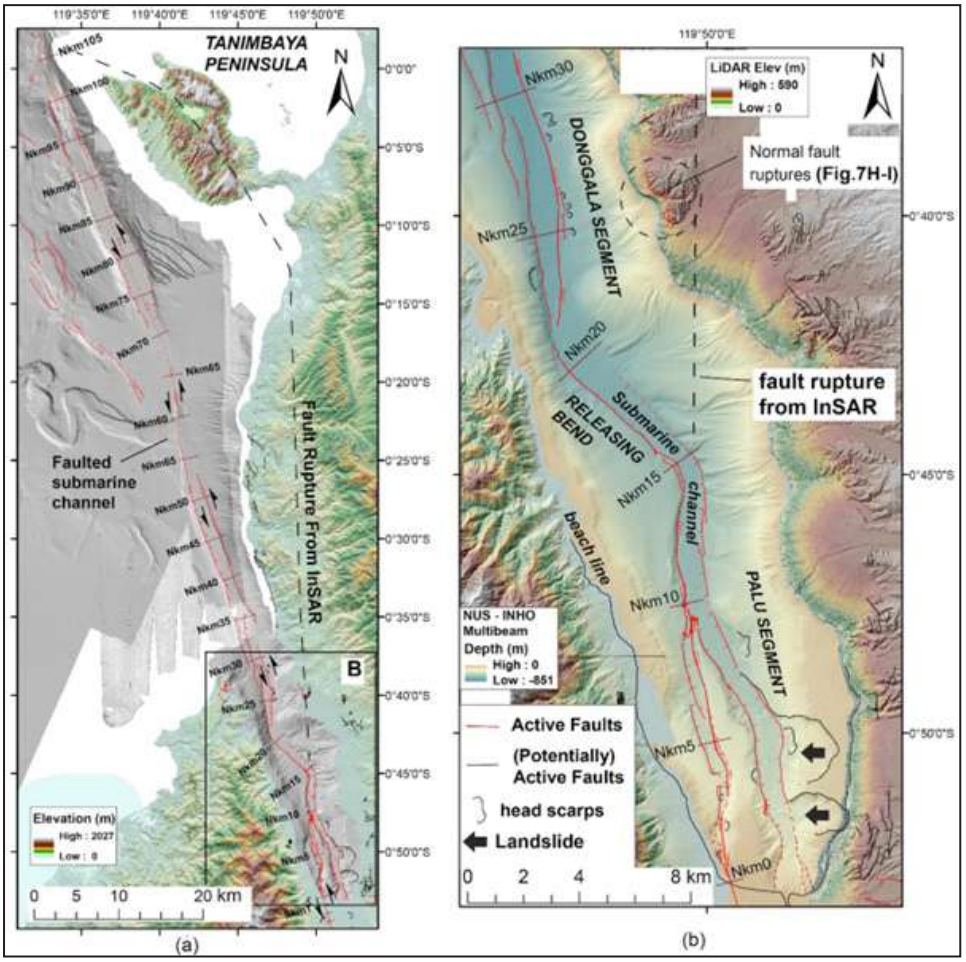

Figure 3.6. Distribution of The Palu-Koro Fault in the sea (Natawidjadja *et al.*, 2021).

Surface Rupture (FSR) in The Palu City to Sigi Regency. Indications of FSR (Figure 3.11) are the presence of horizontal and vertical offset, for example houses, roads, rice fields, and so on. In general, the offset dominated with sinistral offset found along the west Palu Koro Faults, the values vary between 6 cm and 580 cm. The sinistral offset in large dimensions found in the area, such as:

1) Pawunu Village, West Dolo District, Sigi Regency (about 460 cm to 580 m). This location as a large dimension of sinistral offset.
2) Cemara road, Donggala Kodi, Palu City (about 515 cm to 429 cm).
3) Sungai Manonda road, Balaroa Village (totally sinistral offset 488 cm).
4) Diponegoro road, West Palu (about 238 cm).
5) Binangga, Sigi Regency (129 cm to 246 cm with 34 cm vertical component).
6) Bolapapu, Kulawi District, Sigi Regency (about 82 cm to 125 cm).

This sinistral offset stretches from the western part of Palu Gulf to the southeast in the direction of N 330° E to 350° E passing through Palu City to the Kulawi area of Sigi Regency (Figures 3.10 and 3.12). The presence of this sinistral offset indicates a Palu-Koro Fault line that is actively czutting alluvial deposits. This position is not in

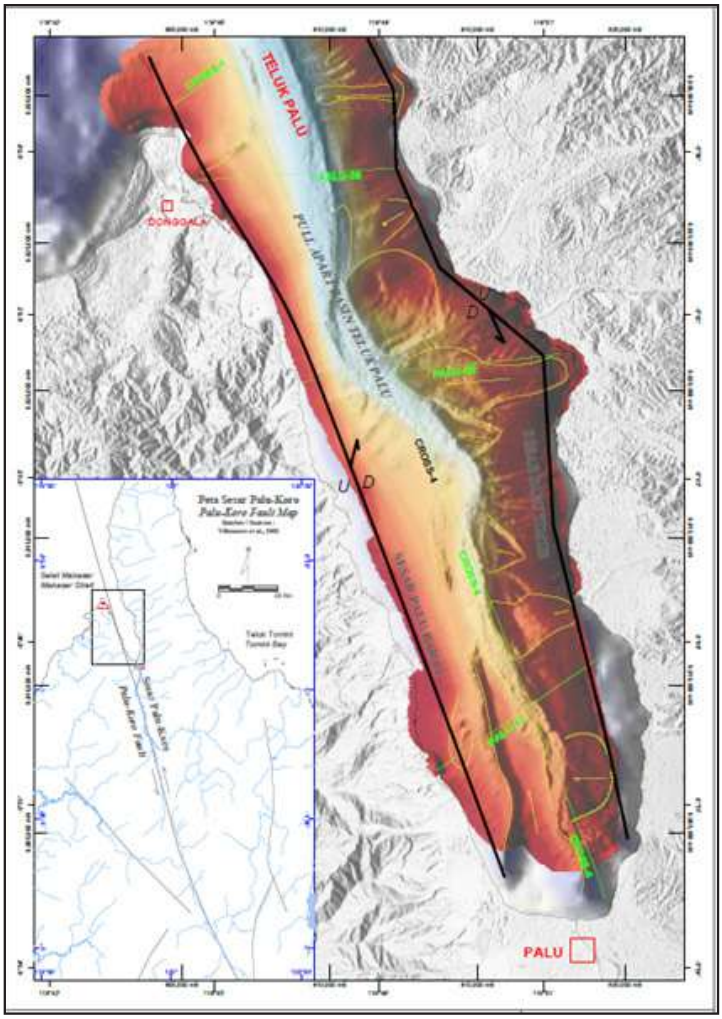

Gambar 3.7 Structural geology in Palu Gulf shows continuity of The Palu-Koro Fault in the sea that shaped as a full-apart structure (Gustiantini *et al*., 2024).

the mountain front zone, but further east towards the land. This fault caused severe building damage along its path (Figure 3.10). In the eastern region of Palu City, there was no sinistral offset. Other offset was found in small dimensions with a dextral offset and vertical less than 0.5 m, and generally in the west-east and northeast-southwest directions. The ground cracks were found in The Palu City and Donggala Regency with direction such as : north-south, west-east, northeast southwest and northwest-southeast direction (Figure 3.13).

The liquefaction is characterized by the appearance of fine sand along ground cracks, found in Palu City, Sigi Regency (Sigi Biromaru District), and Donggala Regency (Sindue, Sirenja and Balaesang Districts) (Figures 3.14 and 3.15). The type of this liquefaction is cyclic liquefaction, including lateral spreading and sand boil. The other liquefaction type is a flow liquefaction found at Balaroa, Petobo, Sibalaya, and Jono Oge. The flow liquefaction caused heavy damages at this area. At the bottom land uplift was showed

Table 3.1. The Catalogue of Destructive Earthquake at Palu Gulf, Central Sulawesi (modified from Supartoyo *et al*., 2014)

NO	Name of E-Quake	Date	Epi-Centre	Depth (Km)	Mag	MMI	Explanation
1.	Bada Valley	1905	-	-	-	-	Damages in Bada Valley.
2.	Kulawi-Lindu	30/07/1907 04:00 am	On land	-	-	VII	164 houses and 49 paddy storehouses were collapsed at Kulawi. Estimated there was ground crack
3.	Kulawi-Gimpu	18/03/1909 06:00 am	On land	-	-	VII-VIII	Disaster at Kulawi-Gimpu. Ground crack direction of N−S at Pabotoe-Namo.
4.	Lemo	30/07/1910	-	-	-	VIII	Hundreds of houses and many paddy storehouses were collapsed. Buildings were damaged at Colo, Anja, Olu Congko dan Palu.
5.	Donggala ***(Tsunami)***	1/12/1927	5,0° S-119,5° E	-	-	VIII-IX	50 people died, 50 people injured by tsunami. Damage building at Donggao. Tsunami strike at Palu City about 3 km from the coast.
6.	Lindu lake	1937	-	-	-	VI	Buildings were damaged at Tamado Village (the Lindu lakeside). Ground crack occurred.
7.	Tambu, Donggala ***(Tsunami)***	14/08/1968	0,7° S - 119,8° E	23	6	VII-VIII	Tsunami with runup ± 8−10 m. Landslide occured, and hot water appears. 200 people died, 790 houses were damaged at Mupaga Village. 7 houses moved to the NW direction at Tambu Village.
8.	Central Sulawesi	23/10/1983	1,6° S- 120,8° E	50	6	VII	2 people died, 4 people injured , 42 houses collapsed.
9.	Lawe, Sigi	1/3/1985	2,082º S & 119,67º E	17	5,7	V-VI	Slighty damage of building. Strong shakes at Palu. Earthquake occured and felt by people from 1st to 2nd of March 1985.
10.	Toli-Toli & Donggala ***(Tsunami)***	01/01/1996	0,729° S - 119,931° E	24	7	VII	9 people died. Tsunami with run up ± 2 m and inundation distance ± 400 m. Building were damaged at Bangkir Village (Toli-Toli) and Tonggolobibi Village (Donggala). On Pangalasean road the tsunami covered logs.
11.	Donggala	11/10/1998	0,4° S - 119,5° E	33	6,1	VI	Houses were damaged at village of Kabonga Besar, Kabonga Kecil, Boya, G. Bale, Labuan Bajo, Maleni, Ganti, Kola Kola and Lumbudolo (Banawa District, Donggala Regency).
12.	Palolo, Sigi	24/01/2005 04:10:08,8 Local Time	1,03° S - 119,99° E	30	6,2	VII	1 people died, 4 people injured. Worst damages at Palolo District, Sigi Regency. Building were damaged at Palu City, Sigi Biromaru Regency and Sigi Regency. Ground crack occured about ± 150 m at Kaleke Village. Fault surface rupture at Sintuwu Village ± 150 m length, at N 310º E. Liquefaction occured at Sintuwu Village. The major landslide at Sigimpuu Village.
13.	Palu	2/03/2009 08:30:00 Local Time	1,11° S - 119,85° E	30	5,7	V	1 people injured. A car show room and a preschool were damaged. Epicentre on the land.
14.	Kulawi, Sigi	18/08/2012 17:41:53 Local Time	1,29º S, 120,012º E	10	6,2	VII	5 people died, 16 people heavy injured, 37 people slighy injured, 303 houses were heavy damaged, 192 houses were moderate damaged, 464 houses were slighy damaged at Kulawi. Landslide and ground crack occured at Kulawi.
15.	Pasigala ***(Tsunami)***	28/9/2018 18:02:44 Local Time	119,85° E 0,18° S	10	7,5	VIII-IX	4845 people died, 4612 people injured, thousands of building were damaged in Palu City, Donggala, Sigi dan Parigi Moutong.

Table 3.1. continued...

NO	Name of E-Quake	Date	Epi-Centre	Depth (Km)	Mag	MMI	Explanation
16.	Sigi	06/08/2023 18:09:22 Local Time	120,16° E 1,14° S	10	5,3	V	Tsunami at Palu Gulf with FD 4-6 m, ID 600 m. Landslide and ground crack occurred in Palu City and Donggala Regency. Flow liquefaction occurred at Balaroa, Petobo, Jono Oge dan Sibalaya.
17.	Donggala	09/09/2023 22:43:24 Local Time	119,8° E 0,03° N	10	6,3	VI	3 houses were heavy damaged, 10 houses were slightly damaged at Lembangtongoa Village, Palolo District, Sigi Regency. 4 houses were damaged at Pomolulu Village, Balaesang Tanjung District, Donggala Regency.

Table 3.2. Total Loss by The Pasigala Earthquake on 2018 (https://www.tempo.co/politik/tsunami-dan-gempa-palu-donggala-2018-dalam-angka-korban-daya-rusak-dan-lainnya-138090)

No.	Location	Loss
1.	Palu City	Rp. 8,3 T
2.	Sigi Regency	Rp. 6,9 T
3.	Donggala Regency	Rp. 2,7 T
4.	Parigi Moutong Regency	Rp. 0,64 T

as a typical of landslide on the wedge of the toe zone. Many victims were caused by this flow liquefaction.

A lot of landslide events triggered by earthquakes are found especially on the steep slopes and rocks that have endured weathering. The landslide locations was in Sigi Regency (Gumbasa and Kulawi District) and Donggala Regency (Sindue, Sindue Tombusabora, Sindue Tobata, Sirenja, and Balaesang Districts) (Figure 3.15). On the southern part, Jono Oge area has a broken bridge caused by flow landslide type process that also caused a village in the area moved away.

3.4.1. Pasigala Earthquake Intensity Scale on September 28th, 2018

The quick response team of The Geological Agency recorded the earthquake intensity scale based on surveys in the field and objects affected by earthquakes. Based on the identification, the maximum intensity scale of the earthquake on September 28th, 2018 occurred in the Jono Oge area, Sigi Biromaru District, Sigi Regency (Fig-

Figure 3.8. Tsunami trace at IAIN campus in Palu City with the flow depth of 1 m (left), and on Sirenja District, Donggala Regency with the flow depth 2 m (right).

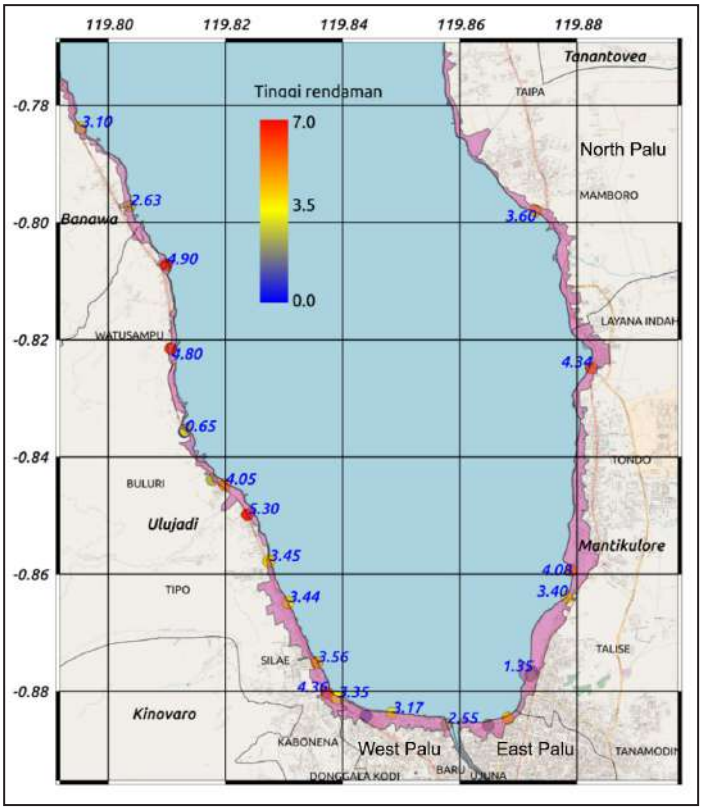

Figure 3.9. Map tsunami flow depth in Palu Gulf. The red circle indicates tsunami intensities and the number shows the tsunami flow depth. The pink colour shows the region that was hit by the tsunami (Geological Agency, 2018).

ure 3.16), which reached an intensity scale of IX MMI (Modified Mercally Intensity). This makes residents panic, ground oscillations (Figure 3.17), weak building collapse, strong buildings were severely damaged, foundation and building frames damaged, ground cracks (Figure 3.18) and large-scale liquefaction occurred. The ground oscillation axis runs west–east and north–south. All buildings on the ground oscillated in the Jono Oge was damaged.

In addition, the area around the epicentre of the earthquake, the coastal area of northern Donggala, parts of Sigi Regency and Palu City (Figure 3.16) were at the intensity of VIII MMI. This made drivers distracted, strong buildings were damaged due to some parts collapsing, water tanks that located upstairs rotated and collapsed, house frames moved from the foundation, improperly tied walls collapsed, tree branches broke, wet soil and steep slopes split, ground cracks, landslide, and liquefaction occurred. The surveys shows that the high prone area has a big potential to be affected by an earthquake with a scale greater than VIII MMI. This is in line with a map of earthquake-prone areas in Central Sulawesi published by PVMBG, Geological Agency in 2012 (Robiana *et al*., 2012) (Figure 3.19).

3.4.2. Earthquake Shaking in Balaroa, Petobo, Jono Oge, And Sibalaya

To recognize how large earthquakes caused the liquefaction flow type in Balaroa, Petobo, Jono Oge, and Sibalaya area, shaking modeling was carried out with the Deterministic Seismic

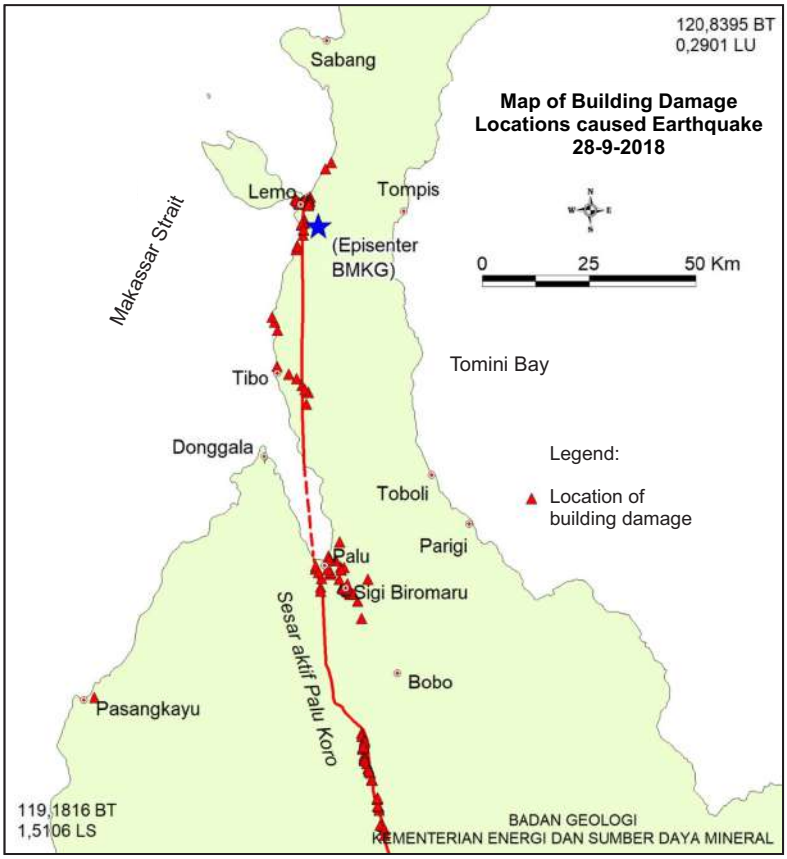

Figure 3.10. Building damage distribution caused by earthquake on September 28th, 2018 (Geological Agency, 2018).

Figure 3.11. Sinistral offset of fault surface rupture around 4,6 m to 5,8 m caused by earthquake on September 28th, 2018 in Pawunu Village, Dolo Barat District, Sigi Regency (Supartoyo *et al*., 2018).

Hazard Analysis (DSHA) method. The modeling was performed using OpenQuake software. OpenQuake is GEM (Global Earthquake Model Foundation) software that advance free, open source, and easily collaborative access to develop earthquake hazard models. This model uses the GFZ (German Research Centre for Geosciences) earthquake parameter data. The parameter is showed at Table 3.3 and downloaded on October 20th, 2018 from web http://geofon.gfz-potsdam.de/eqinfo/event.php?id=gfz2018tabt. Other data for input is the map of shear wae velocity of thickness 30 m depth (Vs30) (Figure 3.20).

Palu-Koro Fault geometry is a main source of Pasigala Earthquake on September 28th, 2018 (Figure 3.12), refer to Map of Source and

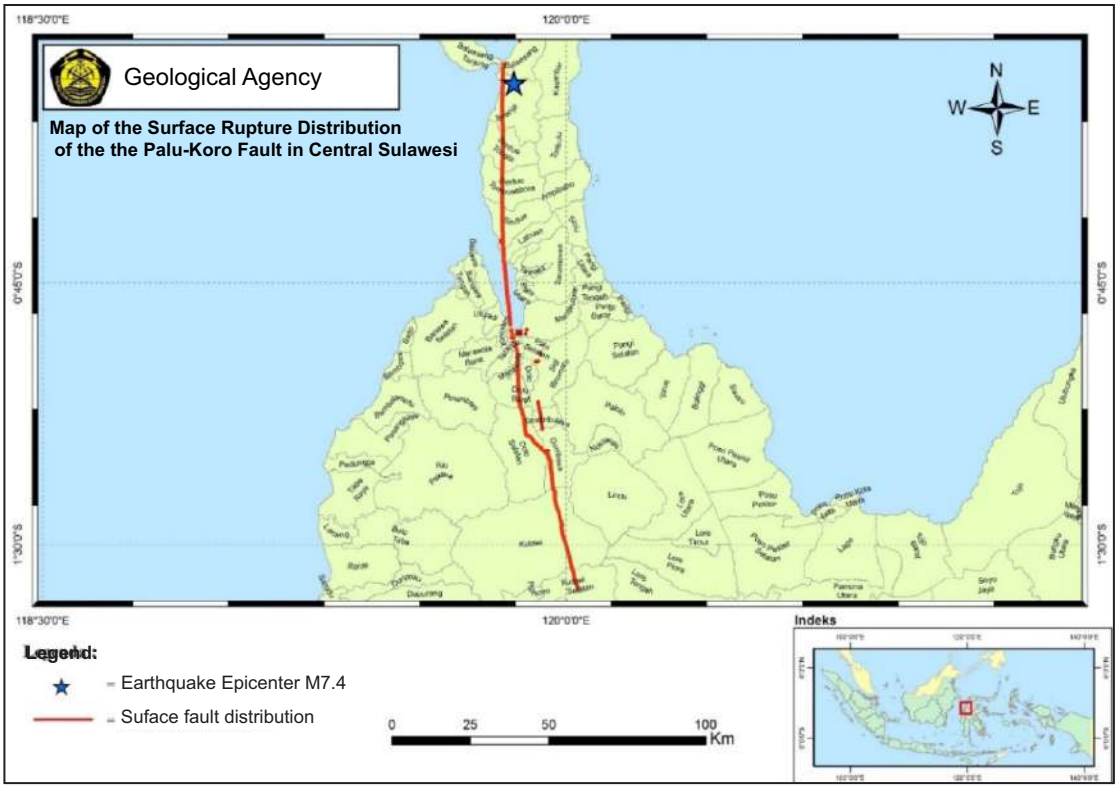

Figure 3.12. Map of Palu-Koro active fault based on fault surface rupture data (Supartoyo *et al*., 2018).

Hazard Earthquake Indonesia in 2017 (Pusgen, 2017). The distribution of the Palu – Koro fault to earthquake hazard analysis is modified by Quick Response Teams, Geological Agency, based on the field observation. The calculation of earthquake shaking in this model used three attenuation functions, namely: Boore *et al*., (2014), Campbell and Bozorgnia (2014), and Chiou and Youngs (2014) with each parameter of 1/3. The application of this attenuation function shows the epistemic uncertainty, because there were no application attenuation functions in Indonesia.

The result of the hazard earthquake shaking of Pasigala on September 28th, 2018, using DSHA methods is shown at bedrock (Figure 3.21), surface (Figure 3.22), and at Table 3.4. In general, PGA (Peak Ground Acceleration) value on the surface is bigger than on bedrock. In addition, the PGA value of bedrock and surface in Balaroa and Petobo is not significant. Based on the field observation, the earthquake intensity scale in Balaroa, Petobo and Sibalaya was of VIII MMI. As for the Jono Oge area, the intensity scale reaches IX MMI, shown by the ground oscillation and massive ground crack. In the Jono Oge area, all buildings had heavy damage (Figures 3.17 and 3.18).

Based on the profile of electricity used in Balaroa and Petobo areas (Buana *et al*., 2019), there is a geological structure pattern that has negative flower structure which is one of the characteristics of the geological structure strike slip fault (Figures 3.23 and 3.24). It is assumed that the strike slip fault is one of The Palu-Koro Fault zone parts. This local fault will add more

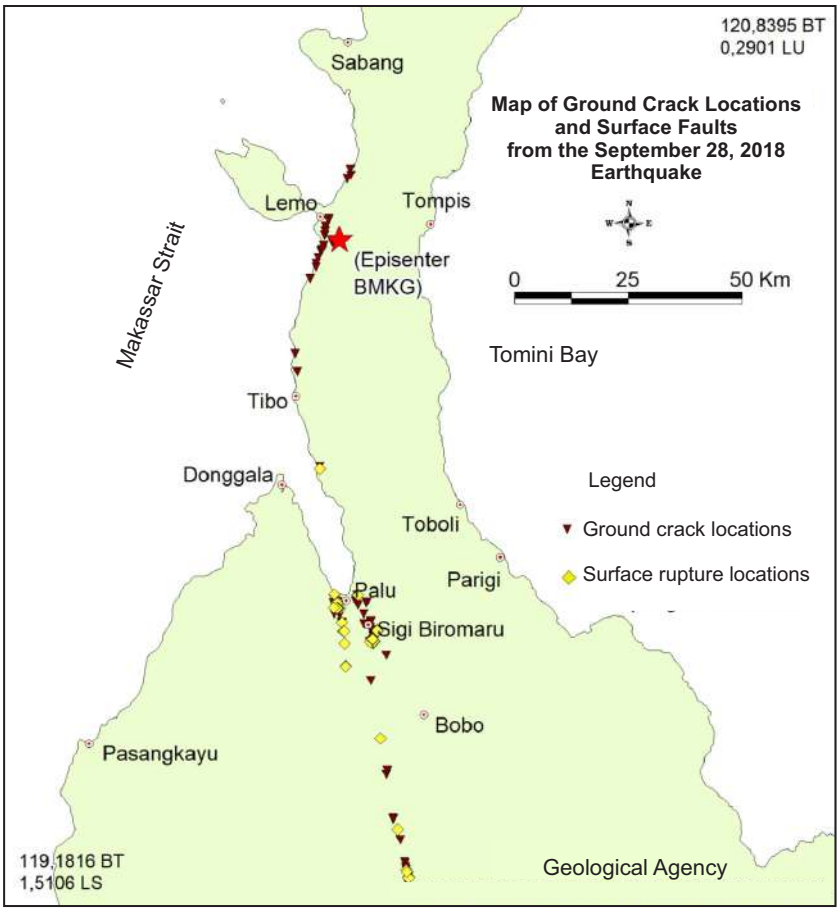

Gambar 3.13. Map of measurement of surface rupture and ground cracks (Supartoyo *et al.*, 2018).

Figure 3.14. The left figure: Liquefaction caused damaged to residents' houses due to the earthquake on September 28th, 2018 in Panau Village, Sigi Biromaru District, Sigi Regency. The right figure: Landslides and flow-type andslides threaten residents of Sungku Village, Kulawi District, Sigi Regency.

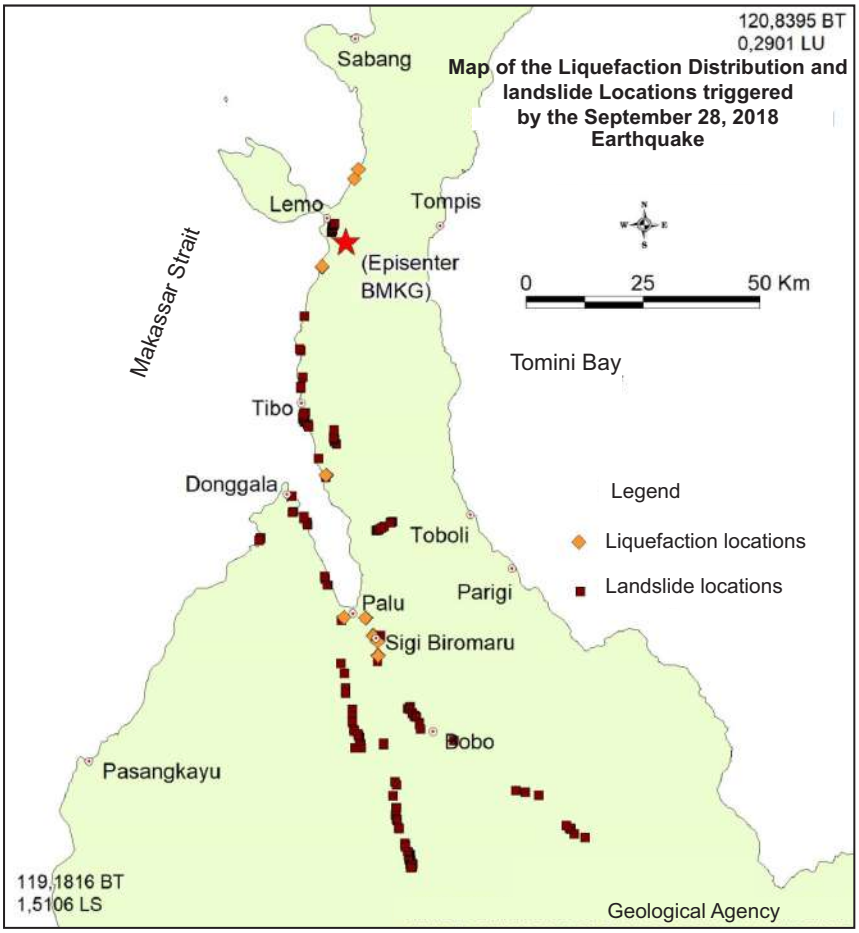

Figure 3.15. Map of the liquefaction distribution and landslide locations. triggered by the earthquake on September 28th, 2018 (Supartoyo *et al*., 2018).

cracks that have a potential to infiltrate water, so the soil becomes more saturated.

3.5. Analysis of Focal Mechanism of Fault Movement in the September 28, 2018 Earthquake

The focal mechanism of an earthquake describes how seismic energy is released from its source or fault. It is commonly illustrated through a *focal mechanism diagram* or *fault-plane solution*. The analysis of the focal mechanism of the Palu earthquake indicates that the source of the event was tectonic activity in the form of a slip movement along an active fault, specifically the Palu-Koro Fault. In general, this earthquake exhibited a strike-slip mechanism, in which two fault planes move horizontally relative to each other. The following presents the results of the focal mechanism analysis of the September 28, 2018 Palu earthquake.

The earthquake parameters used in this analysis were obtained from the United States Geological Survey (USGS) (Table 3.5). After conducting the analysis using a stereonet, the following results were obtained:

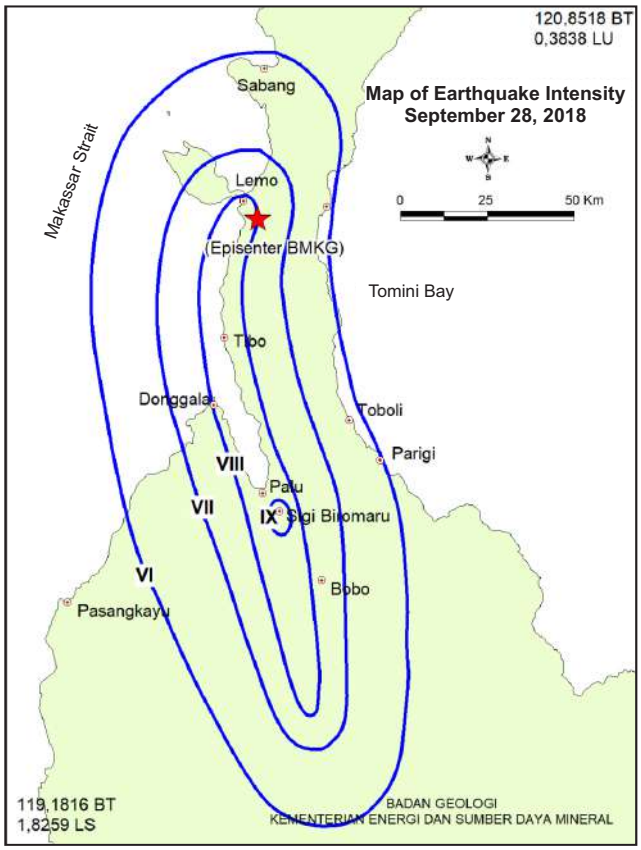

Figure 3.16. Earthquake intensity map on September 29th, 2018 (Supartoyo *et al*., 2018).

Figure 3.17. The ground oscillation caused buildings damaged by the earthquake in Jono Oge area, Sigi Biromaru District, Sigi Regency on September 28th, 2018. Earthquake intensity scale reaches IX MMI in Jono Oge area.

Figure 3.18. Massive ground crack direction north–south from the earthquake caused residents' houses damaged in Jono Oge area, Sigi Biromaru District, Sigi Regency, on September 28th, 2018.

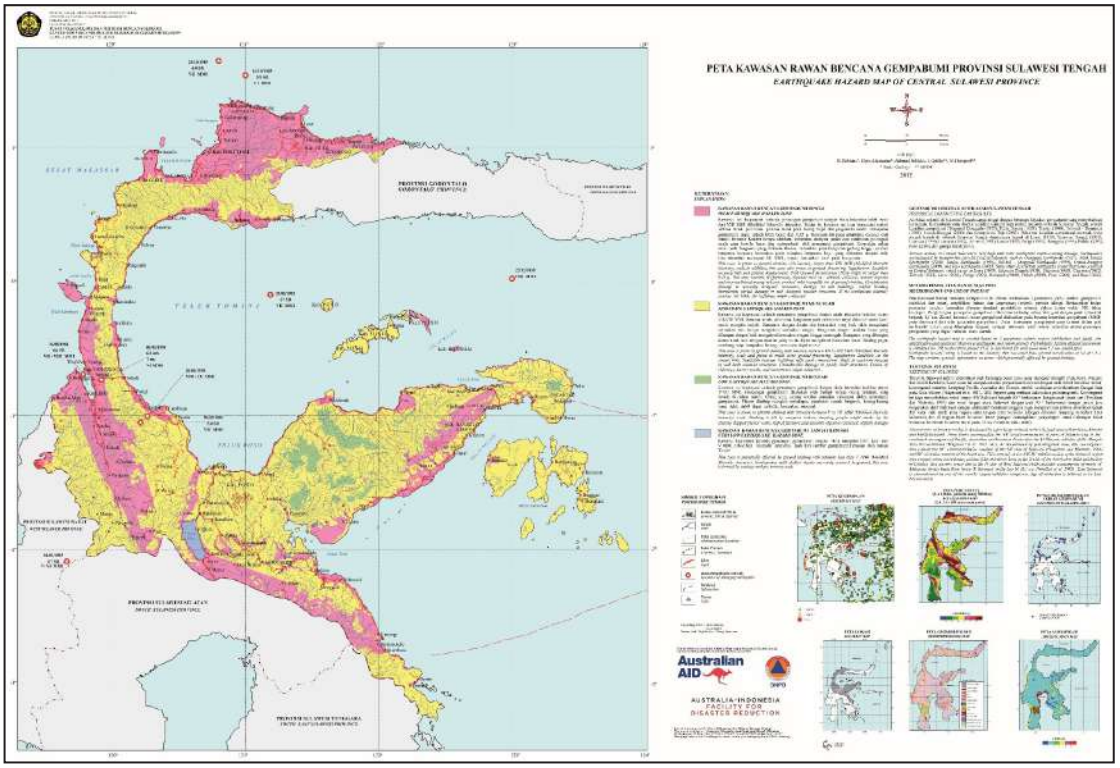

Figure 3.19. Map of earthquake-prone areas in Central Sulawesi (Robiana *et al*., 2012).

Table 3.3. Earthquake Parameter in Palu - Donggala on September 28th, 2018 based on GFZ Germany Data

East	South	Magnitude (Mw)	Depth	Strike	Dip	Rake
119.86	-0.22	7.5	10	351	76	-11

As shown in Figure 3.25, Nodal Plane 1 is oriented at N 87°E/74°, and Nodal Plane 2 is oriented at N 350°E/60°. The NP2 plane is interpreted as the fault plane responsible for the earthquake, which occurred at a depth of approximately 13.5 kilometers. The earthquake at this depth is interpreted to have taken place within a ductile deformation zone.

The earthquake occurring at a depth of 13.5 km caused significant surface deformation along the Palu–Koro Fault Zone. Based on the analysis (Figure 1), the fault orientation is N 343°E/69°, with a net slip of 19°, N350°E, and a rake of 20°. According to Rickard (1972), this fault is categorized as a normal left-slip fault. The fault movement is relatively sinistral (left-lateral), as observed from satellite imagery.

From this analysis (Table 3.6), the orientations of the maximum principal stress (σ_1), intermediate principal stress (σ_2), minimum principal stress (σ_3), and shear strain (η) were obtained. In addition, the associated maximum stress (σ_1'), intermediate stress (σ_2'), and minimum stress (σ_3') were determined. *Shear strain* represents the angular displacement between the principal and associated stresses.

The results show that σ_2 = 52°, N119°E indicates a relatively steep inclination compared

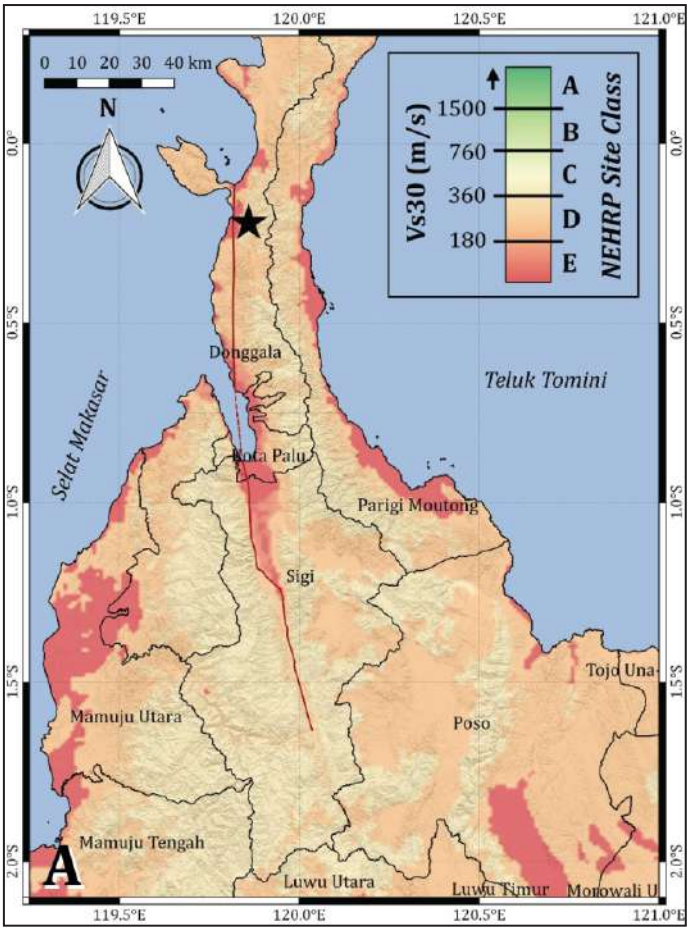

Figure 3.20. Map of shear wave velocity of thickness 30 m depth (Vs30) in Central Sulawesi Province and surrounding area. The red line is The Palu-Koro Fault that is used in deterministic hazard modeling, and the black star is an epicentre (Omang *et al.*, 2018).

to $\sigma_1 = 28°$, N309°E and $\sigma_3 = 4°$, N217°E, which are relatively shallow. Therefore, according to Anderson (1951), this fault is classified as a sinistral fault.

3.6. Collateral Hazard

Collateral hazard is a secondary, often cascading, geological event that is directly triggered by a primary geohazard. The 2018 Pasigala Earthquake had generated a complete collateral hazard, that are: ground cracks, land subsidence, undulated land, land movement/ landslide, liquefaction, and tsunamis. These secondary hazards are triggered by strong earthquake shocks. These secondary hazards are distributed across Palu City, Sigi and Donggala Regencies. Ground cracks and subsidence were observed ranging in small to large dimension. In the locations nearby the surface faults and flow-type liquefaction zones, massive ground cracks and subsidence were observed, controlling building damage. The pattern of the ground cracks located off the surface faults is relatively aligns with the strike of The Palu-Koro Fault. While the ground cracks located in the flow-type liquefaction zone formed a curved pattern.

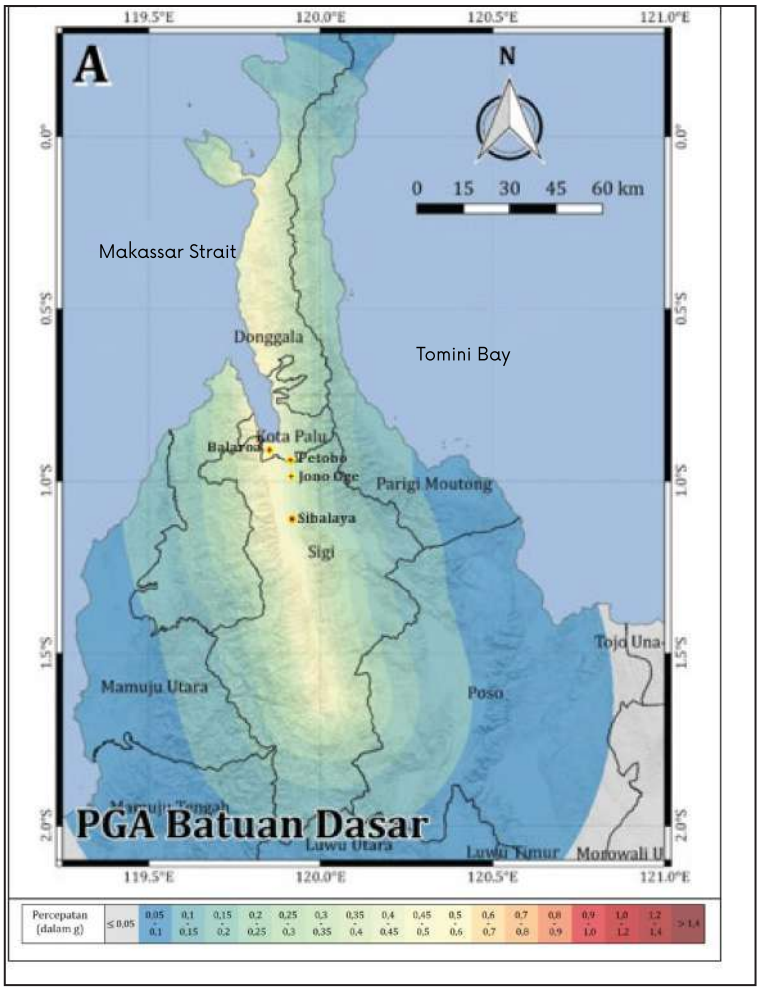

Figure 3.21. The earthquake shaking on bedrock (Omang *et al.*, 2018).

The undulating land phenomenon was identified in the Jono Oge area, Sigi Biromaru District, Sigi Regency. This phenomenon is suspected to be the onset of the flow-type liquefaction. In this undulated land area, buildings were damaged, the earthquake shock was very strong, reaching an intensity of IX on the MMI scale.

Earthquake-induced landslides were observed almost across Palu City, Donggala Regency, and Sigi Regency. These landslides occurred in hilly morphology, bordering valleys formed by The Palu-Koro Fault mechanism. The landslide types triggered by the 2018 earthquake included falls, landslides (rotational and translational), and flows. The landslide materials consisted of rocks, and debris composed of soil and rock mixture. In several locations, the landslide material blocked roads, causing road cuts, as observed in northern Donggala and Kulawi, Sigi Regency. The landslides in Kulawi were particularly massive due to their proximity to The Palu-Koro Fault zone. These landslides generally occured in weathered granite rocks.

Furthermore, the 2018 Pasigala Earthquake also triggered liquefaction. There are two

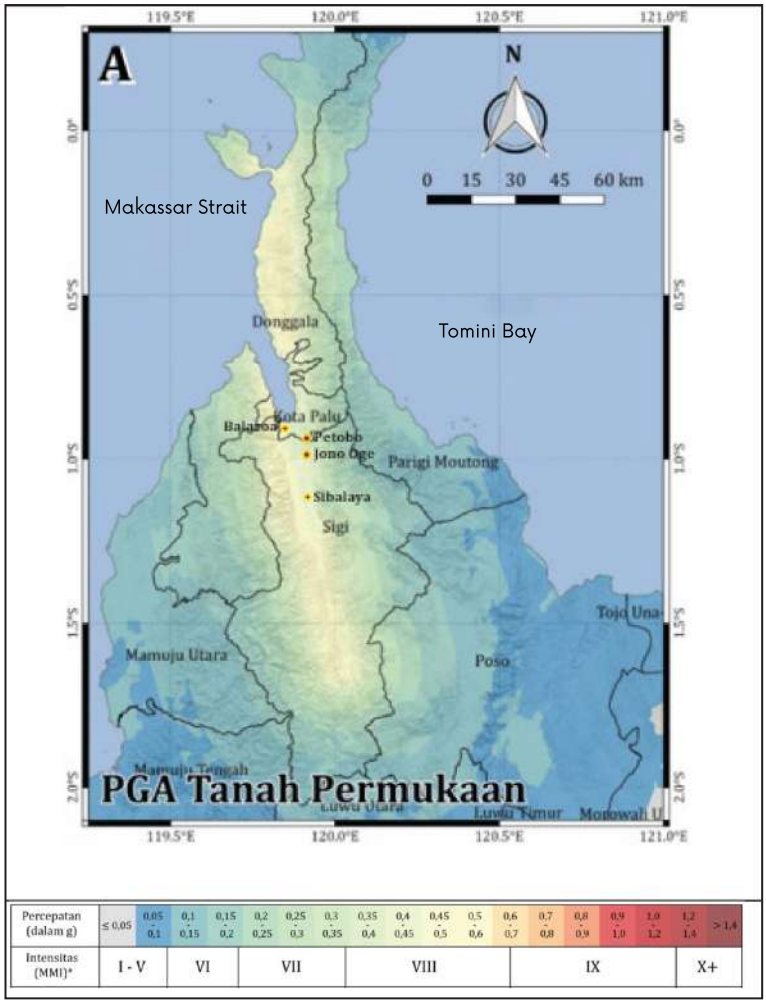

Figure 3.22. The earthquake shaking on surface (Omang *et al.*, 2018).

Table 3.4. The Result of Earthquake Hazard Analysis of Pasigala Earthquake on September 28th, 2018

No.	Location of flow Liquefaction	East	South	PGA at Bedrock (gravitasi/ g)	PGA at surface (g)
1.	Balaroa	119,839694	-0,906385	0,432	0,424
2.	Petobo	119,919641	-0,938269	0,364	0,335
3.	Jono Oge	119,917806	-0,982238	0,369	0,405
4.	Sibalaya	119,92113	-1,09541	0,383	0,418

liquefaction types: cyclic and flow types (Kramer, 1996). Flow-type liquefaction, also known as Palu-type liquefaction, occured in the Balaroa, Petobo, Jono Oge, and Sibalaya areas. Massive damages are identified in the areas affected by this Palu-type liquefaction. Heavy casualties occurred in Balaroa and Petobo. In Jono Oge area, undulating land was observed, which is

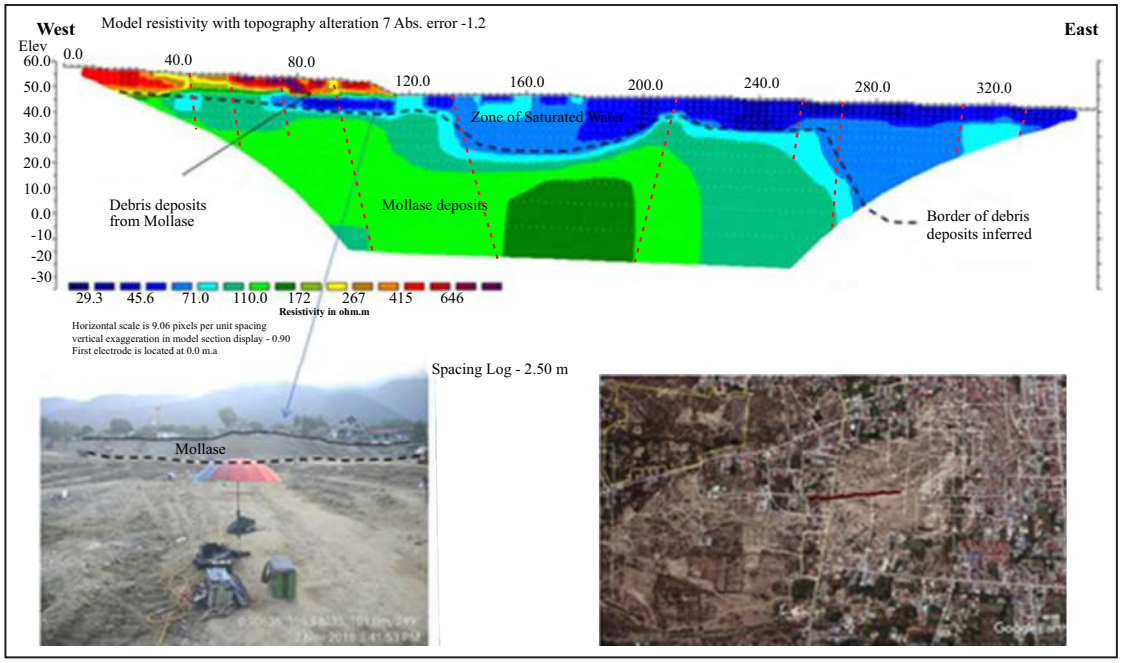

Figure 3.23. Interpretation of negative flower structure (red line dots) as a sign of strike slip fault based on electricity data from Taufiq *et al.* (2019).

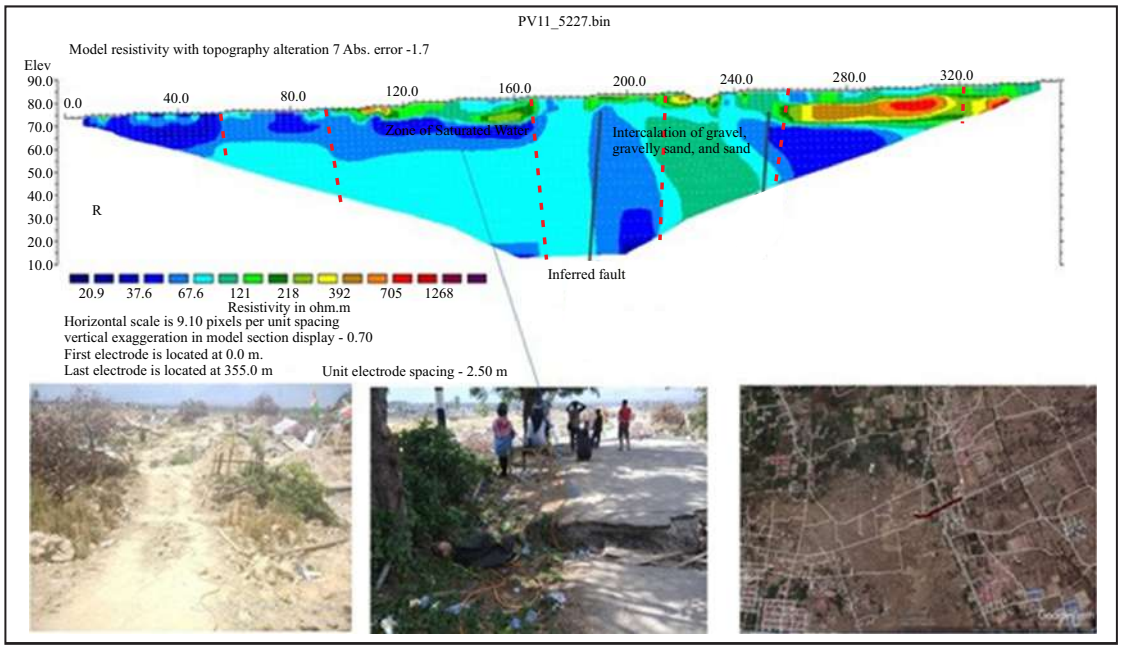

Figure 3.24. Interpretation of negative flower structure (dots red line) as a sign of strike slip fault based on electricity data from Buana *et al.* (2019).

Tabel 3.5. parameter gempabumi yang diperoleh dari laporan *United State Geological Survey* (USGS)

Location						
Longitude	119.85			Strike	Dip	Rake
Latitude	-0.256		Nodal Plane 1	87	74	-156
Depth	13.5 Km		Nodal Plane 2	350	67	-17
Magnitude	Mww 7.53					
	Plunge	Azimuth				
Pressure	28	309				
Tension	4	217				
Neutral	62	119				

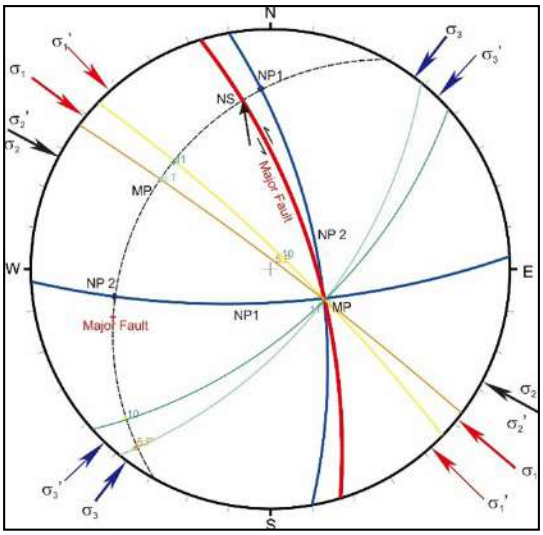

Figure 3.25. Stereonet analysus results of the Palu-Koro Fault Zone Movement MEchanism (Based on Earthquake Parameter Data from USGS).

a rare phenomenon. This occurrence damaged buildings, and is suspected to be the beginning of Palu-type liquefaction. This Palu-type liquefaction is likely to be the first in Indonesia. The Palu Bay area is classified into a high liquefaction prone area (Badan Geologi, 2019). This Palu-type liquefaction will be discussed in more detail in the next chapter.

Following the 2018 Pasigala Earthquake, a team from the Geological Agency and the UNDP conducted a paleoseismological study by digging a trench with a dimension of 17.5 m long, 1.5 m wide, and of 1.5 m average depth. The trench was located on Pipa Air Street, Palu City. At the initial location, the trench depth reached down to 2.5−3m. However, it then collapsed due to the loose sand lithology and shallow groundwater table. The trench analysis revealed paleo-liquefaction. Unfortunately, this paleoliquefaction age could

Tabel 3.6. Palu-Koro Fault properties based on stereonet analysis result

	Strike	Dip	Rake	net slip Plunge	net slip Bearing	
Major Fault	343	69	20	19	350	
	Plunge	Bearing			Plunge	Bearing
Σ_1	28	309		s_1'	27	318
Σ_2	62	119		s_2'	62	119
Σ_3	4	217		s_3'	8	223
η	8					
Classification	Normal left slip fault (Rickard, 1972)					
	Sinistral fault (Anderson, 1951)					

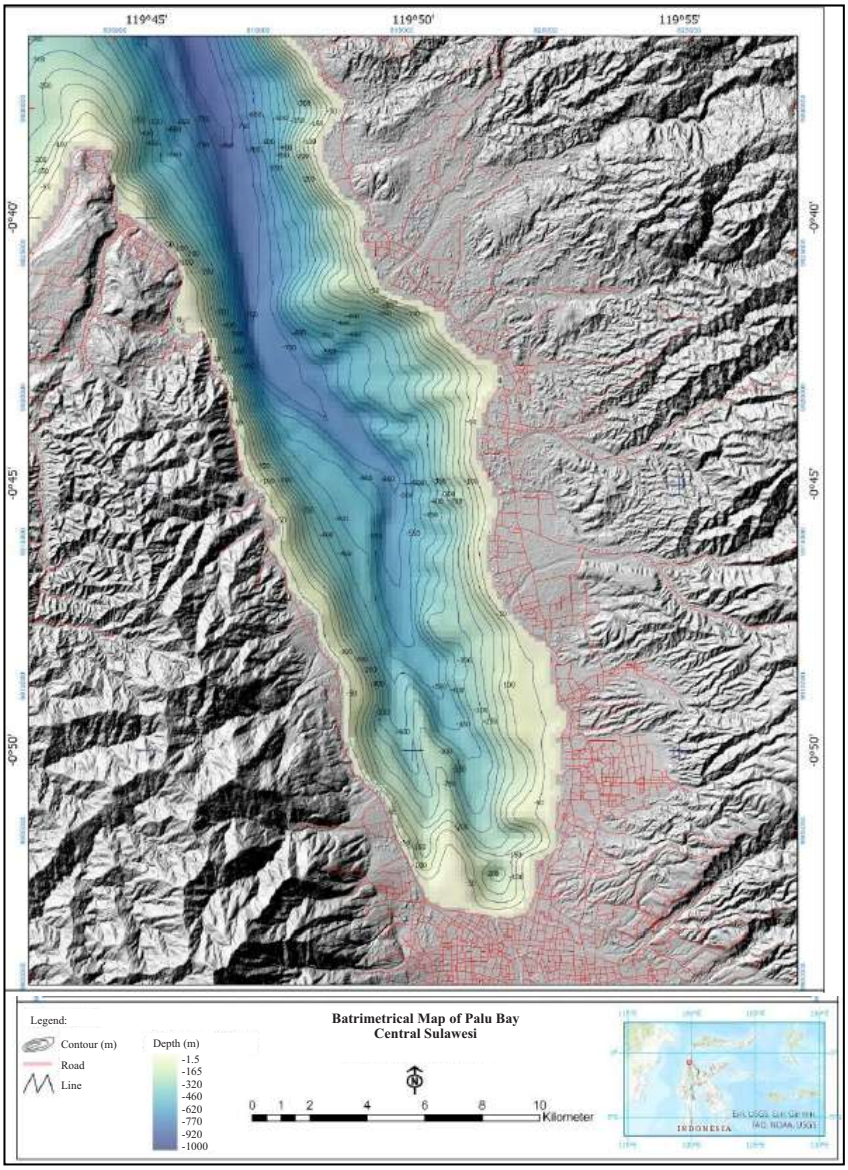

Figure 3.26. Bathymetry of Palu Bay (BBSPGL, 2023).

not be identified due to the lack of carbonaceous material contained in the paleosoil samples, that was analyzed at The Quaternary Laboratory of Geological Survey, Geological Agency.

As has been mentioned before that 2018 earthquake in Palu had triggered a tsunami, which was corraborated by a submarine landslide. This submarine landslide is also suspected to have triggered the tsunami occured during the 1927 earthquake and tsunami disaster in Palu. According to marine geological team of Geological Agency (Team from Marine Geological Institute (MGI), or BBSPGL in Bahasa Indonesia), the morphology of Palu Bay

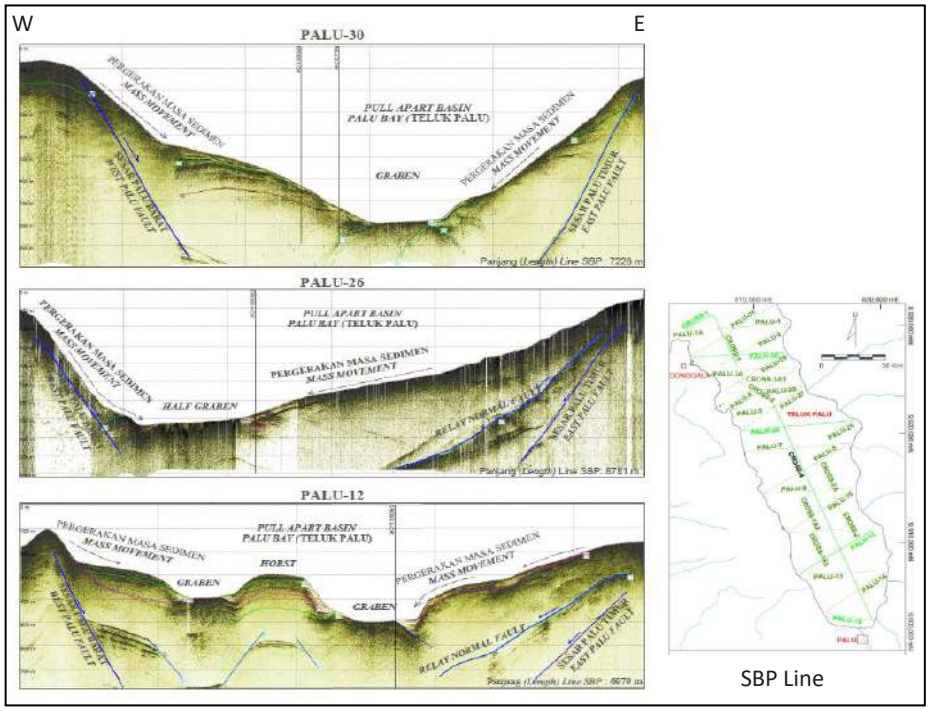

Figure 3.27. Shallow seismic line indicate submarine landslide area, as one of the tsunami triggers (Gustiantini *et al*., 2024).

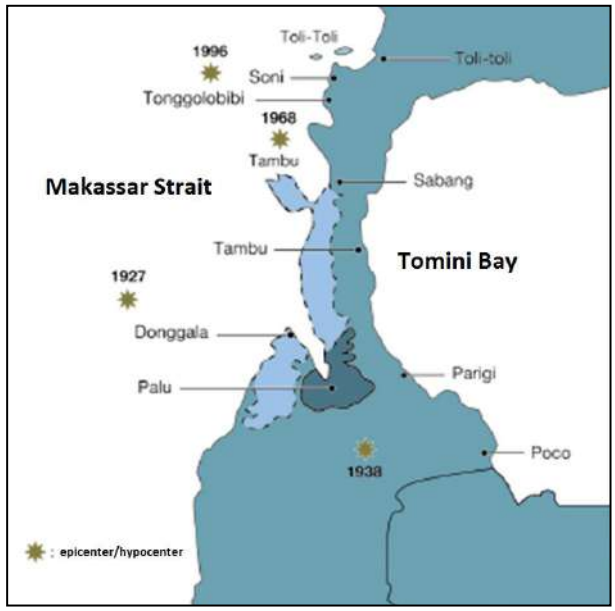

Figure 3.28. The earthquake epicentre resulting tsunami during one century occured in the westcoast of Sulawesi (left); The earthquake centre triggered tsunamis surround Palu Bay prior to 2018 tsunami (right) (Pelynovsky *et al*., 1997).

is gradually steep started from -50 m water depths nearby the coastline, getting deeper toward the open sea down to -800 m. As a consequence, it is prone to underwater landslides (Figure 3.26). Furthermore, the sediment layer on the coast of the bay is alluvial with a thickness of up to 125 m from the surface, increase the possibility of underwater landslide occurence (Thein *et al*., 2015).

Subbottom Profiler (SBP) data resulted from survey conducted by BBSPGL of The Geological Agency, indicated several underwater landslide features, that consistently recorded on the west and east coasts of Palu Bay (Figure 3.27).

Since 1927, there have been six tsunamis in The Makassar Strait. All the tsunamis resulted from the movement of Palu-Koro Fault System, Sulawesi subduction zone system in the north, and The Paternoster Fault Zone (Pelynovsky *et al*., 1997). The Palu – Koro Fault System had resulted in three tsunamis: the December 1927 tsunami (Palu Bay), the 14th August 1968 (Palu Bay), and the 1st January 1996 tsunami (Simuntu – Pangalaseang). The epicentre position is in the west coast of Sulawesi. Another three tsunamis resulted from The Paternoster Fault Zone are the April 11th 1967 tsunami (Tinambung), the February 23rd 1969 (Majene), and the January 8th 1984 (Mamuju). The earthquake epicentre lied in the southwest coast of Sulawesi (Figure 3.28).

According to the tsunami history, the tsunami source in The Makassar Strait is dominated by shallow earthquake (between 15-25 km). In general, the epicentre is located 10-100 km from the Sulawesi coastline, connecting The Palu-Koro and Paternoster. The earthquake depths is between 13-25 km, with the magnitude ranged between 5.5-7.7 (Prasetya *et al*., 2001). The earthquake strength resulted from Palu-Koro Fault is ranged between 6.3-7.7.

Based on a 2023 survey in Palu Bay, The Geological Agency's marine geology has created a simulation and evaluation of the wave generation and propagation model using tsunami sources derived from historical earthquakes that have occurred around Palu Bay, Donggala (6.4 – 7.8 SR). The Palu tsunami simulation was generated by an underwater landslide and earthquake scenario assumed to be the trigger for the tsunami. During The Palu Bay highest sea level or MHWL (Mean High Water Level) was 1 m, similar with the actual tsunami event (Pakoksung *et al*., 2019). Six sources of landslide parameters according to Gusman *et al*. (2019) and Nakata *et al*. (2020) are indicated in Figure 3.29 with the landslide scenario parameters presented in Table 3.7.

The earthquake data sources were obtained from The United States Geological Survey (USGS) reports as shown in Figure 3.30, and earthquake parameter input is presented in Table 3.8. The length and width parameters of the earthquake fault were obtained from the empirical equation of Well and Coppersmith (1994):

$$Log\ L = -2.142 + (0.58 \times M_w)$$

$$Log\ W = -1.61 + (0.41 \times M_w)$$

Notes:

Table 3.7. Landslide Scenario Parameters, *United State Geological Survey* (USGS)

	Landslide 1	Landslide 2	Landslide 3	Landslide 4	Landslide 5	Landslide 6
Length (m)	400	350	1500	250	350	100
Width (m)	800	650	2000	500	700	200
Thickness (m)	30	15	15	15	21	6
Slope steepness (deg)	15	15	10	8	11	8
Starting Point (deg)	119,840, -0,704	119,857, -0,789	119,876, -0,854	119,825, -0,845	119,808, -0,799	119,748, -0,658
End Point (deg)	119,933, -0,709	119,84, -0,793	119,864, -0,847	119,834, -0,844	119,814, -0,798	119,753, -0,650
Start Time (s)	60	60	60	60	60	60

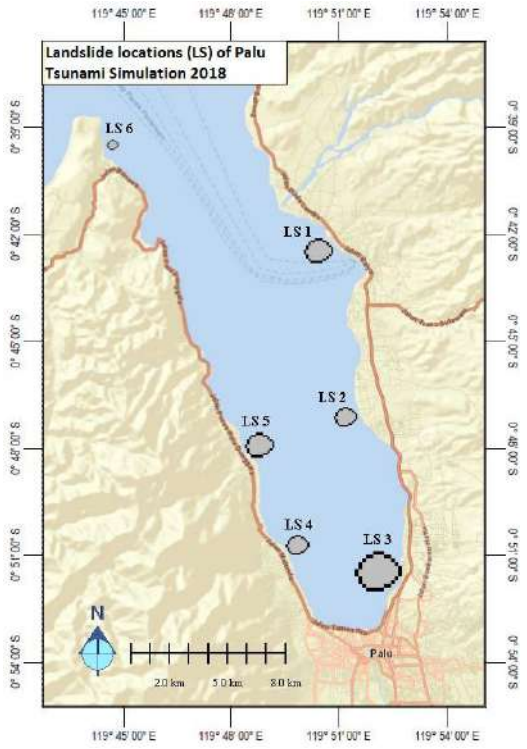

Figure 3.29. Landslide (LS) locations of the 2018 Palu Tsunami simulation according to Gusman *et al*. (2019) and Nakata *et al*. (2020).

Tabel 3.8. Earthquake Scenario Parameters

Eartquake Parameters	
Falt Length (km)	200
Fault Width (km)	30
Earthquake depth (km)	13,5
Strike (deg)	356
Dip (deg)	67
Slip (deg)	-17
Dislocation (m)	1,8
Magnitude Moment (Mw)	7,5
Epicentre (Longitude)	119,846
Epicentre (Latitude)	-0,256

L : Fault width
W : Fault Length
Mw : Magnitude Moment of earthquake

Tsunami simulations were conducted using The Cornell Multi-grid Coupled Tsunami (COMCOT) v. 1.7 model, based on shallow water equations and the FORTRAN 90 programme. The numerical model is based on The Shallow Water Equation (SWE) which is then averaged over depth (depth-average based models). In the COMCOT model, it is assumed that the water level changes are equal to the changes in the seabed.

The 2018 Palu Tsunami occurred during a Mean High Water Level (MWHL) of 1 m. The tides certainly affected the height of the tsunami run-up throughout the model domain area. The maximum tsunami run-up height is indicated by the red, green, yellow, orange, and blue colour contours, the value range of each colours are indicated in Figure 3.31.

The simulation results indicated at least five districts with the potential to be the most affected if a tsunami strikes again are: Ulujadi, West and East Palu, Mantikulore, North Palu, and Tawaeli District. The coastal area of West Palu District has a maximum tsunami run-up distribution ranging from 4 to 8 m, and in some areas, the maximum tsunami run-up reaches more than 10 m.

It is already known that the main factor forming a tsunami is landslides. Typically, the type of waves formed by landslides have short wavelengths, so the generated energy is not strong enough to penetrate the land. As a result, these waves do not create a significant large run-up distance from the shoreline. Run-up distances in this area range from 50 m −100 m from the shoreline.

In the coastal areas of Ulujadi and East Palu Districts, the maximum tsunami run-up height reached to 7.8 m. In this area, the distribution of maximum tsunami run-up is dominated by the range of 3 m – 7 m, and there are locations with maximum tsunami run-up heights reaching more than 10 m. In East Palu District, the distribution of maximum tsunami run-up heights is dominated by the range of 3 m – 5 m. Therefore, the distribution of maximum tsunami run-up heights in

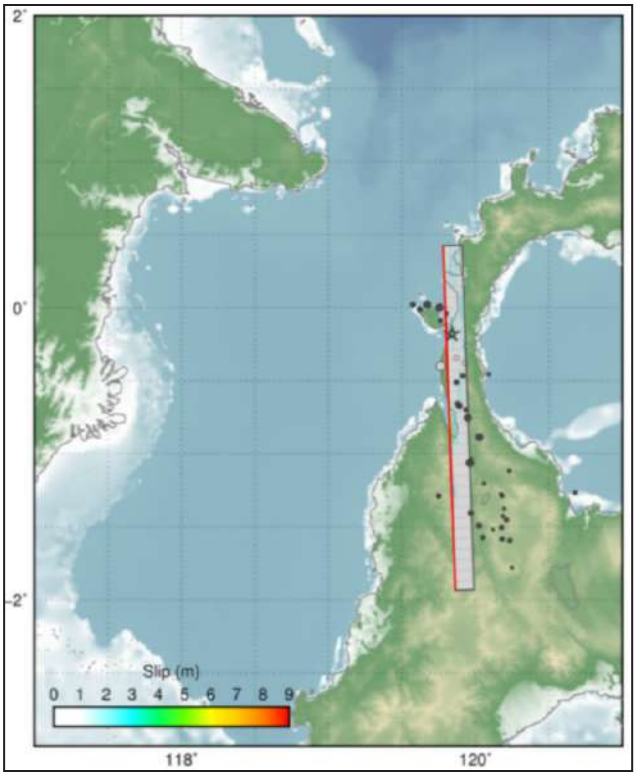

Figure 3.30. Earthquake fault sketch (Source: USGS, 2018).

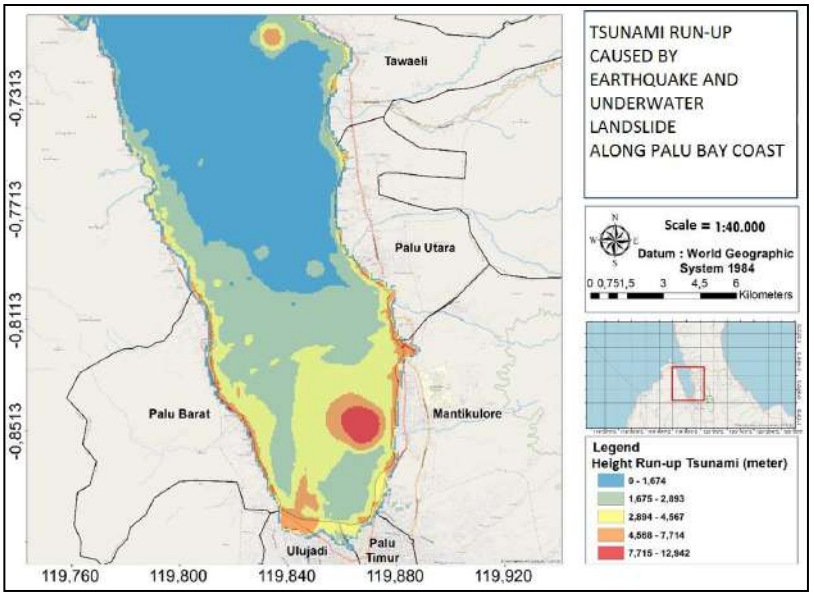

Figure 3.31. Map of tsunami run-up height and inundation area (BBSPGL, 2023).

Ulujadi District has a greater value with a wider inundation area compared to that of East Palu. In this district, the run-up distance reaches 700 m from the coastline located between the borders of Palu Ulujadi and East Palu Districts.

The distribution of the maximum tsunami run-up height in Mantikulore District, on the eastern coast of Palu Bay, dominated by the range of 4 m to 8 m. In general, the coastal area of this district does not have a large inundation area. However, in the northernmost and southernmost areas of Mantikulore District, run-up distances reach 600 m and 200 m from the shoreline, respectively. This is due to the relatively inland slope of the coast, which deflects the tsunami waves to be accumulated in these two areas. As a result, the tsunami can travel quite far inland in these two areas.

Similarly, in North Palu District, the coastline slopes are relatively toward the sea. Therefore, the wave energy generated by the tsunami will be refracted, or shifting its direction toward the coastal area, relatively more inclined toward the land. Consequently, the tsunami can travel inland and form inundation zones in these areas, specifically in the northernmost and southernmost areas, with a run-up distance of up to 300 m from the coastline. In general, the distribution of maximum tsunami run-up heights in this subdistrict ranges from 2 m to 5 m.

The coastal area of Tawaeli District has a maximum tsunami run-up height distribution ranging from 3 m–4.5 m. The coastal area in this district is relatively inclined towards the land, thus the refraction or the direction changes of tsunami propagation accumulated in the coastal area of Pantoloan Station (119.860, -0.721). As a result, inundation in this Pantoloan Station is relatively larger compared to that of the other coastal area, with a run-up distance of up to 300 m. In this district, the largest maximum run-up height reaches up to 6 m at several inundation locations farthest from the coastline.

4. QUATERNARY GEODYNAMICS OF THE PALU REGION AND ITS SURROUNDING AREA

4.1. Quaternary Geological Conditions of Palu and Its Surrounding Area

The Quaternary dynamics of the Palu region, Central Sulawesi, are strongly influenced by the active tectonics of The Palu–Koro Fault, which is the primary factor in the formation of sedimentary basins and local geomorphological evolution. This fault controls Quaternary deformation and sedimentation patterns, including the development of alluvial fan and over bank deposits (Bellier *et al.*, 2001; Watkinson and Hall, 2017). Tectonically derived detrital material constitutes the main source of Quaternary deposits in this region (Permana and Zen, 1991). Clear evidence of neotectonics is observed on the western side of Palu, particularly in Balane, where the fault dissects fan deposits dated to approximately 1790 ± 200 BP (Soehaimi *et al*., 2019).

Quaternary deposits in The Palu Valley developed within a complex alluvial–fluvial basin system that includes alluvial fans, fluvial channels, and marine deposits at the northern end of Palu Bay. Sedimentation processes in this area are primarily governed by allogenic factors, especially tectonic activity that influences accommodation space and drainage patterns (Miall, 1992; Moechtar, 1994).

The Palu alluvial fan exhibits facies zonation, reflecting variation in depositional energy, with coarse, poorly sorted sediments in the proximal zones, whereas the medial zones are dominated by finer, better-sorted sediments. Distal zones are characterized by the deposition of mud and fine sand due to reduced flow energy (Blair and McPherson, 1994; Nemec and Postma, 1993).
Material supply originates from the erosion of The Gawalise Mountains to the west and The Palu–Koro Mountains to the east, contributing gravel, sand, mud, and debris from landslides (Miall, 1992; Sidi *et al*., 2018; Permana and Zen, 1991). Grain-size variations demonstrate upward coarsening in proximal zones and upward fining in distal zones, indicating a decline in energy along depositional pathways (Boggs, 2006; Posamentier and Allen, 1999). Studies focused on Palu confirm this facies zonation pattern as the product of dynamic interaction between sedimentation and active tectonics, shaping the Quaternary stratigraphic characteristics of the area (Bellier *et al*., 2001; Watkinson and Hall, 2017).

4.1.1. Geodynamics of The Palu Area

Quaternary Alluvial And Fluvial Systems

The Quaternary depositional system in The Palu Valley encompasses two primary systems: the alluvial and the fluvial systems. Each is composed of facies that reflect depositional environments controlled by geomorphic and tectonic factors. In the alluvial system, two primary facies are recognized: Proximal Alluvial Fan and Medial Alluvial Fan, along with distinct deposits from debris flow processes.

The proximal facies are characterized by coarse clastic deposits consisting of boulders, cobbles, gravel, and very coarse sand, with poor sorting, massive structures, and angular to subangular grains. These features reflect high-energy,

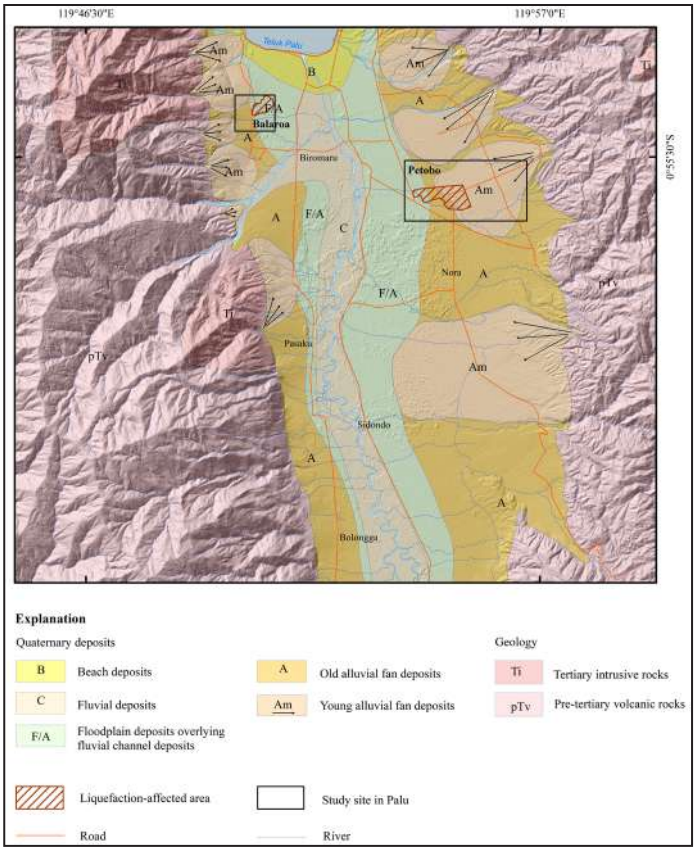

Figure 4.1.1. Distribution map of Quaternary depositional facies in Palu (modified from Suparan and Rimbaman, 1992)

short-distance gravity-driven deposition near the mountain front. Such deposits form immediately after flows exit the mountainous source areas, indicating rapid deposition with poor sorting.

The medial facies represent transitional depositional environments with more stable conditions, dominated by sand to silt deposits. Grains are finer, moderately to well-sorted, and subrounded to rounded. Sedimentary structures such as parallel lamination appear, reflecting a supply of finer material due to reduced slope gradients and decreasing flow energy.

Debris flow deposits develop as products of dense mass flows composed of an unsorted mixture ranging from large boulders to fine matrix material. These deposits are typically massive and heterogeneous, reflecting direct emplacement from rapid mass movements. Grains are angular to subangular, derived from mechanically disrupted slopes, such as those triggered by landslides caused by intense rainfall or tectonic events.

The proximal facies are characterized by coarse clastic deposits consisting of boulders, cobbles, gravel, and very coarse sand, with poor sorting, massive structures, and angular to subangular grain shapes. These characteristics reflect high-energy, short-distance, gravity-driven deposition near the mountain front, with transport occurring over very short distances from the source (Blair and McPherson, 1994). Such deposits form immediately after flows exit the mountainous source area, indicating rapid deposition with poor sorting.

The medial zone represents a transition to a

more stable depositional environment, dominated by sand to silt sediments. Grains are finer, with moderate to good sorting, and are subrounded to rounded. Sedimentary structures such as parallel lamination begin to appear, indicating the supply of finer sediments due to reduced slope gradients and decreasing flow energy.

Remobilized debris-flow material developed as a product of very dense mass-flow processes, consisting of an unsorted mixture ranging from large boulders to fine-grained matrix. The deposits are generally massive and heterogeneous, reflecting direct emplacement from rapid mass movements. Grain shapes are angular to subangular, reflecting the origin of material from mechanically disrupted active slopes, such as landslides triggered by intense rainfall or tectonic events. Debris-flow deposits are commonly found in the proximal to medial zones of the alluvial fan.

Within the fluvial system, two primary facies are recognized: floodplains and channels.

- Floodplain facies form when river discharge exceeds channel capacity, depositing fine-grained material onto adjacent plains. The deposits are dominated by clayey silts with fine lamination, occasionally containing interbeds of fine sand and organic matter. This process occurs repeatedly, particularly during seasonal flooding events.
- Channel facies are primarily composed of sand deposits with interbeds of gravel and silt. Sorting is generally good, and grains show moderate abrasion (subangular to subrounded). Sedimentary structures such as cross-bedding and planar lamination reflect the variable flow dynamics in this facies. The composition is dominated by quartz and feldspar, with sediment colours ranging from yellowish-brown to grayish-brown depending on oxidation conditions and mineral content.

Laterally, fluvial systems in The Palu Valley are more developed on the western side compared to the eastern side. This asymmetry is influenced by geomorphic and structural factors such as gentler topography, wider accommodation space due to localized subsidence, and drainage patterns that tend to concentrate toward the west under the influence of the active fault. Conversely, the eastern side of the valley is dominated by alluvial fans and gravitational processes (debris flows) from steep slopes, limiting the lateral expansion of the fluvial system. As a result, fluvial sedimentation—particularly floodplain and channel deposits—develops more extensively and accumulates significantly in the western part of the valley.

The presence of these facies indicates a strong relationship between surface sedimentation processes and active tectonic control along the Palu–Koro Fault Zone. Lateral and vertical facies variations demonstrate a complex stratigraphic evolution resulting from the interplay

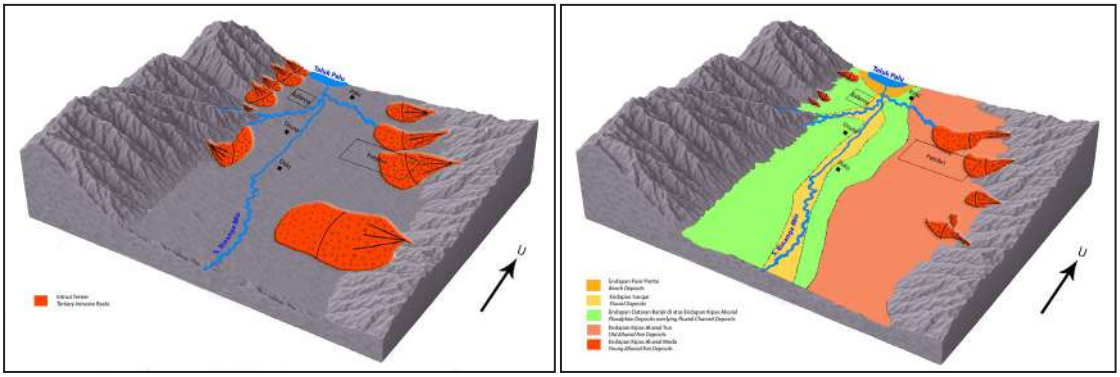

Figure 4.1.2. Evolution of old fans (left) to young fans (right) during The Quaternary Period.

between fluvial depositional mechanisms, gravitational processes, and tectonic dynamics that control accommodation space and depositional patterns across both spatial and chronostratigraphic dimensions. The continuous interaction between gravitational, fluvial, and tectonic processes has produced a complex stratigraphic architecture in The Palu Valley, reflecting the distinctive characteristics of sedimentary systems in tectonically active environments.

Evolution of Alluvial Fans

The Palu–Koro Fault plays a key role in the formation of Quaternary deposits in the Palu Valley by creating tectonic depressions that serve as accommodation space for sediments (Watkinson and Hall, 2017). Coarse to medium sediments were cyclically deposited on the older alluvial fans in proximal and medial zones, reflecting high-energy depositional phases near the source and a decrease in energy toward the medial zone (Harvey, 2012; Allen and Hovius, 1998).

Continuous tectonic activity caused deformation of older alluvial fans, including local uplift, subsidence, and fracturing, resulting in remobilization and redistribution of sediments through landslides and debris flows (Costa, 1984). These processes triggered the formation of new alluvial fans that developed on or around the older ones, with changes in flow patterns and sediment facies due to local deformation and topographic modification (Prasetya *et al*., 2019).

Alluvial fan deposition in this area was episodic, influenced by tectonic activity cycles that altered slope gradients, accommodation space, and sediment transport pathways (Burbank and Anderson, 2011). Distal zones did not develop significantly due to limited accommodation space and high flow energy in proximal and medial zones (Blum and Törnqvist, 2000). Fault-induced river channel shifts restricted sediment distribution to distal zones, focusing deposition closer to the sediment source (Schumm *et al*., 2000).

Drilling data from Palu, up to a depth of 60 m (Hidayat, 2000), reveal three vertically stacked alluvial fan systems, each showing alternating high-energy coarse facies (gravel to very coarse sand) and low-energy fine facies (silt and sandy

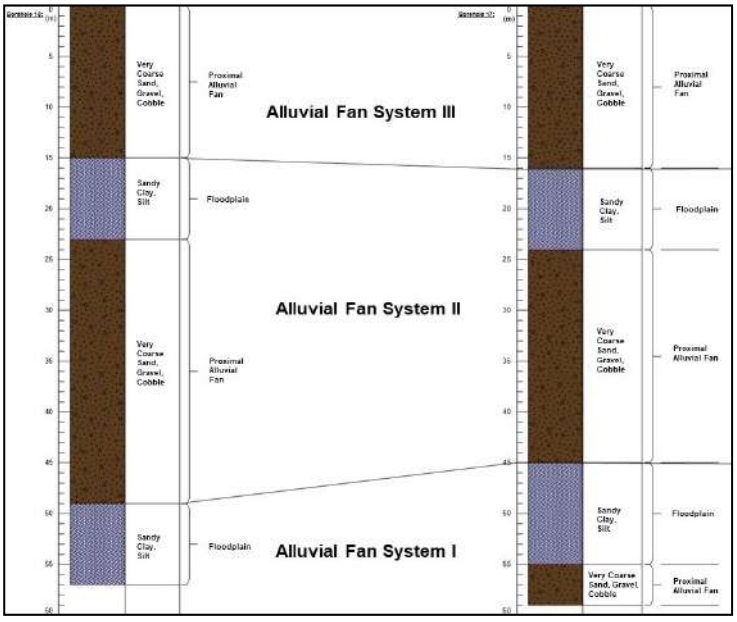

Figure 4.1.3. Borehole correlation up to 60 m depth in the western Palu Valley.

clay). This pattern indicates recurring cycles of alluvial fan development closely tied to the dynamics of the depositional environment.

Vertical repetition of fan systems reflects the significant influence of tectonic activity in controlling sedimentation. In tectonically active areas such as Palu, fault movements trigger local uplift and subsidence, modifying topography and river flow patterns. These conditions lead to shifts in sedimentation loci and channel avulsion, resulting in the episodic formation of new fan systems atop older ones (Harvey, 2012; Allen and Hovius, 1998).

Active tectonics in Palu, including deformation from the main fault and secondary structures, play a major role in regulating fan morphology and sedimentation dynamics. Deformation modifies slope gradients and stability, triggering mass wasting and increasing sediment supply to the fan system. Additionally, variations in flow energy and hydrological conditions caused by tectonic activity contribute to the formation of floodplain facies interbedded with coarse deposits, marking interseismic periods of lower depositional energy (Watkinson and Hall, 2017).

The presence of three stratigraphically distinct fan systems also indicates changes in slope geometry due to deformation, resulting in shifts in fan depositional positions over time. Morphotectonic fan models in active fault zones explain that alluvial fans evolve through local uplift, valley-floor subsidence, and channel migration driven by tectonic deformation. This was confirmed by post-2018 Palu earthquake observations, which revealed tectonic deformation causing significant changes in river pathways, slope failures, and rapid deposition of coarse material in structural depressions such as Petobo and Balaroa (Prasetya *et al*., 2019).

Overall, the Quaternary alluvial fan systems in Palu represent the outcome of complex interactions between dynamic fluvial processes and active tectonic controls. Repeated depositional cycles, lateral and vertical facies variations, and fan morphology reflect the strong influence of tectonic activity on the evolution of alluvial fan systems.

4.1.2. Quaternary Sediment Facies of Balaroa and Petobo

Based on reinterpretation of borehole data by Hidayat and Moechtar (2000), the regional subsurface model of Palu and its surrounding area shows variations in Quaternary deposits, reflecting interactions between sedimentation processes and active tectonic influence in The Palu Basin. Kinematic studies by Patria and Putra (2020) indicate that The Palu–Koro Fault initially behaved as a normal fault before evolving into a strike-slip fault. The normal faulting phase played a major role in creating sediment accommodation space, thereby controlling Quaternary sedimentation patterns across the basin.

Balaroa

The Balaroa area of Palu exhibits Quaternary geodynamics influenced by interactions between active tectonics of The Palu–Koro Fault and fluvial sedimentation processes. The formation of old and young alluvial fans in this region was dominated by coarse to medium-grained sedimentation, concentrated mainly in the proximal and medial zones. Tectonic activity caused sediment remobilization, elevation changes, and redistribution of material, driving the formation of new, smaller-scale alluvial fans compared to surrounding areas such as Petobo (Kiyota *et al*., 2020; Jalil *et al*., 2021).

In the young alluvial fan system of Balaroa, regional distribution still focuses on proximal and medial zones, but locally, three subfans can be distinguished, each with different sedimentation characteristics. Sedimentation is dominated by Gms facies (gravel, massive, matrix-supported) resulting from high-energy debris flows, commonly found in proximal to medial fan zones (Walker, 1979; Blair and McPherson, 1994). These units are interbedded with well-sorted, planar-laminated sand facies (Sp), interpreted as shallow unconfined traction flows (sheetfloods) formed on active fan

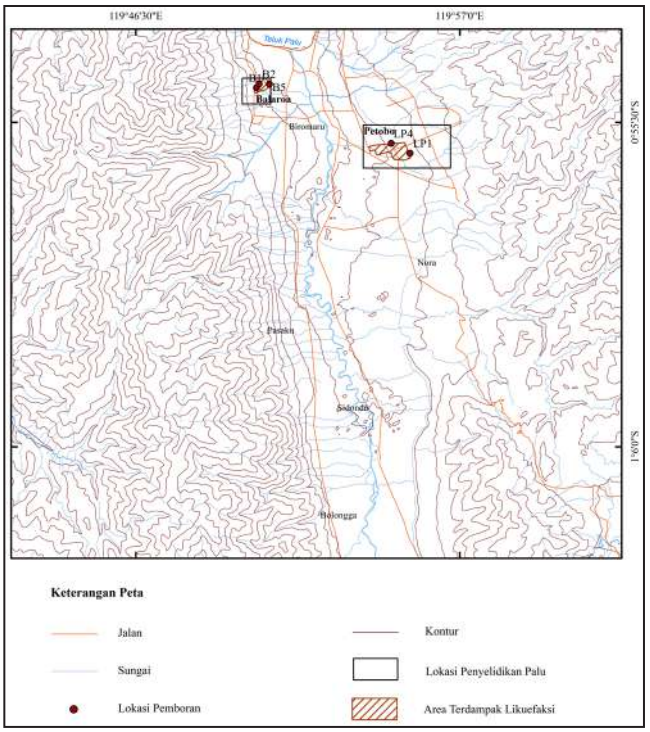

Figure 4.1.4. Borehole locations for Quaternary sediment facies analysis in Balaroa and Petobo, Palu.

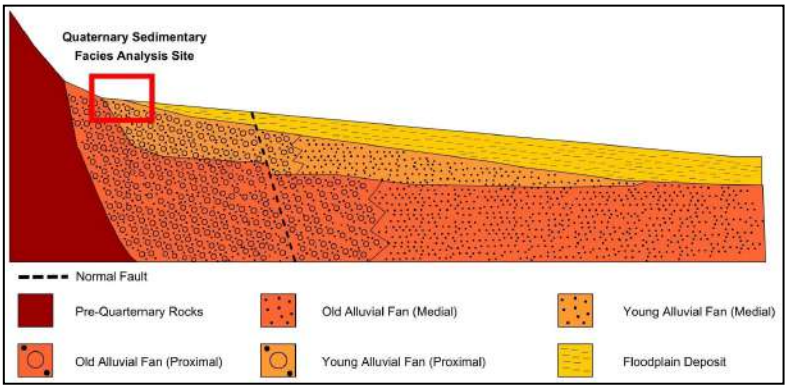

Figure 4.1.5. Quaternary depositional model of the Balaroa area and its surrounding area.

surfaces under steep slopes and high tropical rainfall conditions. The presence of sheetfloods reflects intermittent depositional patterns alternating with debris-flow episodes on the fan surface.

Facies analysis from boreholes B-1, B-2, and B-5 in Balaroa indicates a recurring alluvial fan system, consisting of vertically stacked coarse Gmm (gravel, matrix-supported) facies interbedded with finer FL (fine laminated) facies. This reflects the interaction between high-energy sedimentation processes and quieter depositional phases, as illustrated in Figure 5. Facies classifica-

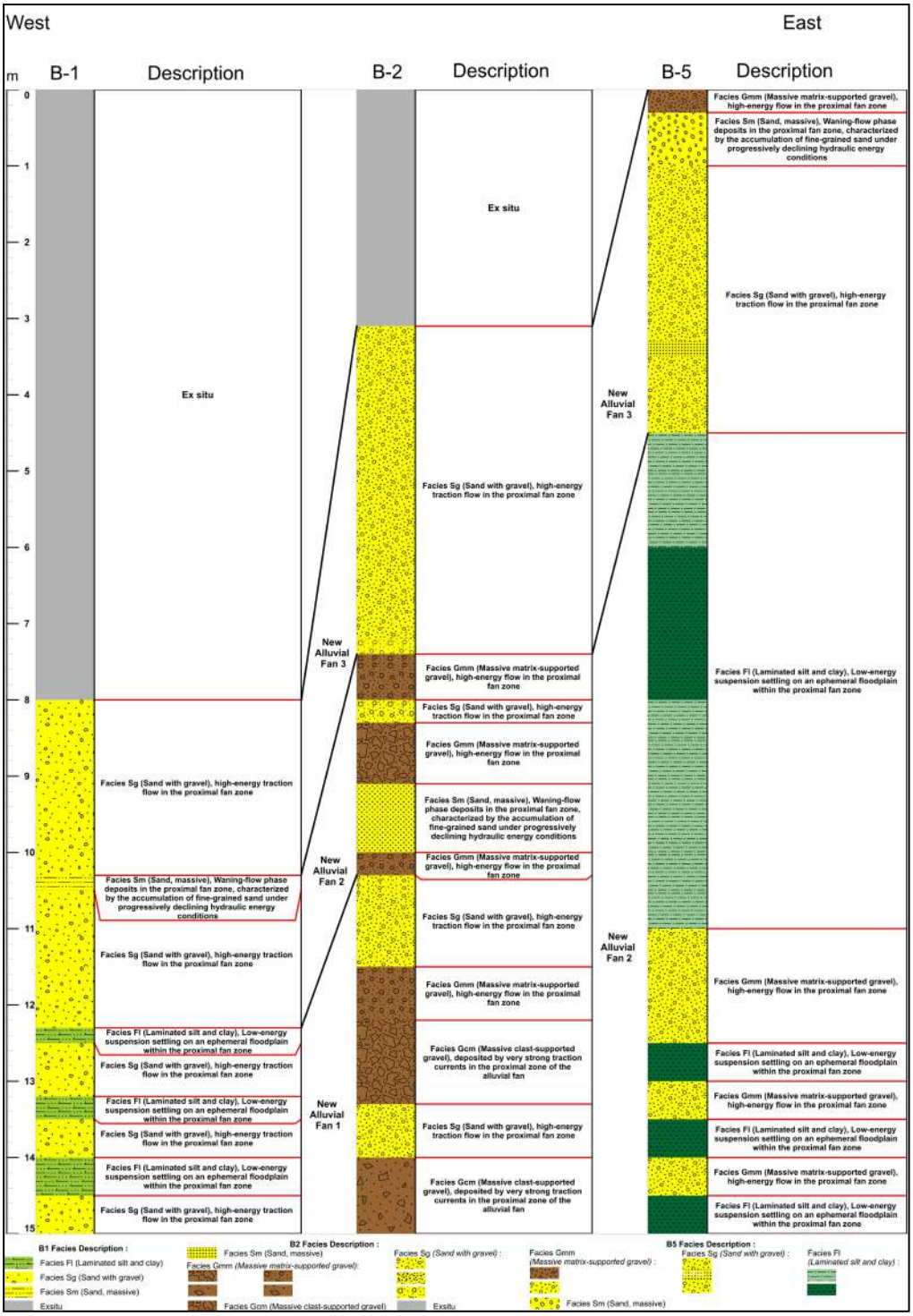

Figure 4.1.6. Quaternary sediment facies analysis of the Balaroa area.

tion follows Blair and McPherson (1994), Walker (1979), and Nichols (2009).

The oldest unit, New Alluvial Fan 1, is recorded at depths of 12.3–15 m (B-1) and 10.5–15 m (B-2), dominated by Gmg facies consisting of cobbles to boulders with massive structures and poor sorting. These deposits represent the product of high-energy, laterally extensive flows carrying coarse sediment loads (debris-laden sheetfloods), typical of proximal fan systems (Walker, 1979; Blair and McPherson, 1994). This unit was not identified in B-5, possibly because the site was beyond the reach of the main flow path during this depositional phase, or because it was eroded by younger fan activity.

In B-1, repetitions of FL (fine laminated) and SG (sandy gravel) facies indicate a sheetflood system with fluctuating energy, marked by deposition of coarse sand from traction currents followed by waning-flow phases producing fine laminations. In contrast, B-2 is dominated by Gmm (gravel, matrix-supported) and SG facies with clast sizes ranging from pebbles to boulders, representing high-energy, dense flows that rapidly deposit sediments in the proximal zone. These differences reflect lateral variations within a single stratigraphic unit, influenced by differences in sediment supply, source distance, and possible structural or paleotopographic constraints directing active flow pathways (Blair and McPherson, 1994; Nichols, 2009; Miall, 1996).

Overlying this, New Alluvial Fan 2 comprises a combination of Gmm (massive matrix-supported gravel), FL (fine laminated), SG (sand with gravel), and Sm (massive sand) facies, dominated by very coarse sand to cobble deposits with poor sorting, interbedded with fine sediments. This interval is recorded at depths of 10.3–12.3 m (B-1), 7.2–10.5 m (B-2), and 10–15 m (B-5). Thin interbeds of well-structured fine sand (Sm) and thin silt (Fl) appear at depths of 9.1–9.5 m and 10.4–10.5 m (B-2), and 12.5–13 m and 14.5–15 m (B-5), reflecting short-lived reductions in flow energy when the depositional system weakened or shifted. Although still within the proximal fan domain, this unit reflects more fluctuating hydrodynamic conditions.

The youngest unit, New Alluvial Fan 3, is recorded in the upper borehole intervals: 4.2–10.3 m (B-1), 3.1–7.2 m (B-2), and 0–4.5 m (B-5). Its main facies is SG (sand with gravel), consisting of coarse sand to unstructured gravel with subangular to subrounded grains and poor sorting. These deposits are interpreted as products of high-energy sheetfloods that spread widely across the proximal fan zone. Thickness differences among the boreholes indicate lateral migration of active flow paths.

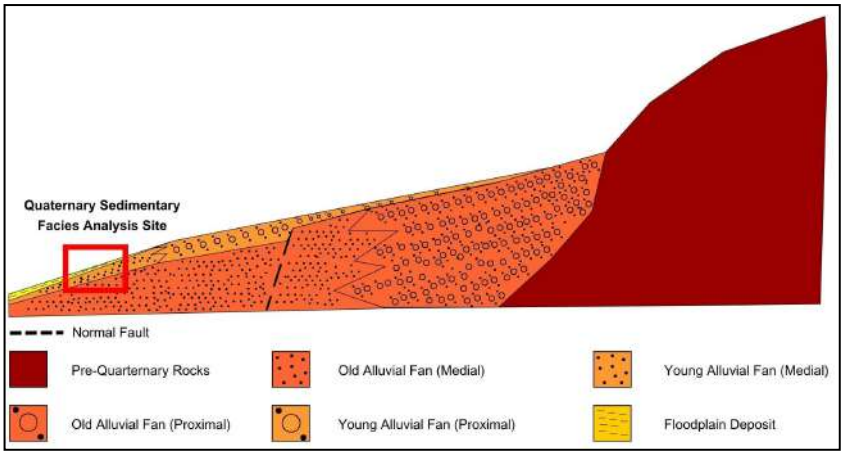

Figure 4.1.7. Quaternary depositional model of the Petobo area and its surrounding area.

This stratigraphic correlation also emphasizes the relationship between sediment facies and liquefaction susceptibility. Intervals with low SPT values (<10), which indicate high liquefaction potential, are consistently associated with fine-grained floodplain facies (Fl–Sm). Depth ranges of 9.5–11 m (B-1), 3.5–4 m (B-2), and particularly 1.5–10 m (B-5) represent fine-textured, well-sorted, and highly porous zones. These deposits are prone to strength loss when saturated and subjected to seismic shaking. The thickening of floodplain deposits in B-5 indicates more intense fine-sediment accumulation at this location, making it one of the most liquefaction-prone zones among the three analyzed boreholes.

Petobo

The Petobo area shows a Quaternary alluvial fan system that developed under the combined influence of active fluvial processes and tectonic activity. This system includes old and young alluvial fans, dominated by coarse to medium-grained sedimentation. Tectonic disturbances deformed the old fan, causing remobilization and redistribution of material. This led to renewed fan formation with more complex and irregular sedimentation patterns.

The young alluvial fan in Petobo is subdivided into three subfans showing lateral facies variations from east to west. Internal variations reflect interactions between tectonic activity and local sedimentation processes.

The sediments are dominated by Sm facies (massive sand) and Fl facies (fine laminated silt), with no evidence of sheetfloods. These facies represent deposition from low-energy fluvial flows and overbank flooding in distal fan or floodplain environments, formed under flat topographic conditions and poorly developed channel systems (Miall, 2006). This indicates that Petobo is most likely located in the downstream portion of the fan system, no longer controlled by the main fan depositional processes.

Stratigraphic and facies analysis from two boreholes, LP-1 (east) and LP-4 (west), as shown in Figure 4.1.8, demonstrates an alluvial fan system composed of several depositional segments that developed progressively through the interaction of variable sediment supply and local tectonic activity. The vertical sequence of the three identified fan units—New Alluvial Fan 1 (oldest), New Alluvial Fan 2, and New Alluvial Fan 3 (youngest)—exhibits repetitive sedimentation patterns reflecting episodic reactivation of the fan surface. This is marked by stacks of coarse deposits overlying fine-grained units beneath them. Overall, this arrangement indicates a discontinuous evolution of the alluvial fan, reflecting the influence of deformation and shifting flow pathways over time

The oldest unit, New Alluvial Fan 1, is recorded at depths greater than 11 m in LP-1 and greater than 12 m in LP-4. The dominant facies is Gmm (massive matrix-supported gravel), composed of gravel and cobbles with massive structures and minor sand as matrix. Coarse-grain size, poor sorting, and the absence of internal structures indicate depositional mechanisms dominated by high-energy surface flows in the medial zone of the fan. At the top of this unit, several very fine sand interbeds are identified in LP-4, marking short pauses in the flow system that allowed suspension deposition under waning energy conditions.

New Alluvial Fan 2, directly overlying Fan 1, displays more complex and heterogeneous facies variations, reflecting changing depositional dynamics within an active fan system. This unit comprises a combination of coarse sand to gravel (Gmm facies) and interbeds of well-sorted fine to very fine sand (Sm facies, massive sand). Laterally, the medial fan zone is marked by Gmm deposits dominating LP-1, characterized by coarse textures, massive structures, and poor sorting. These facies were formed by unconfined surface flows transporting coarse loads under medium- to high-energy conditions, resulting in rapid deposition in the central part of the fan.

The youngest unit, New Alluvial Fan 3, is found at 0–6 m in LP-1 and 0–7 m in LP-4. In LP-1, this reflects a medial alluvial fan environment dominated by medium- to high-energy

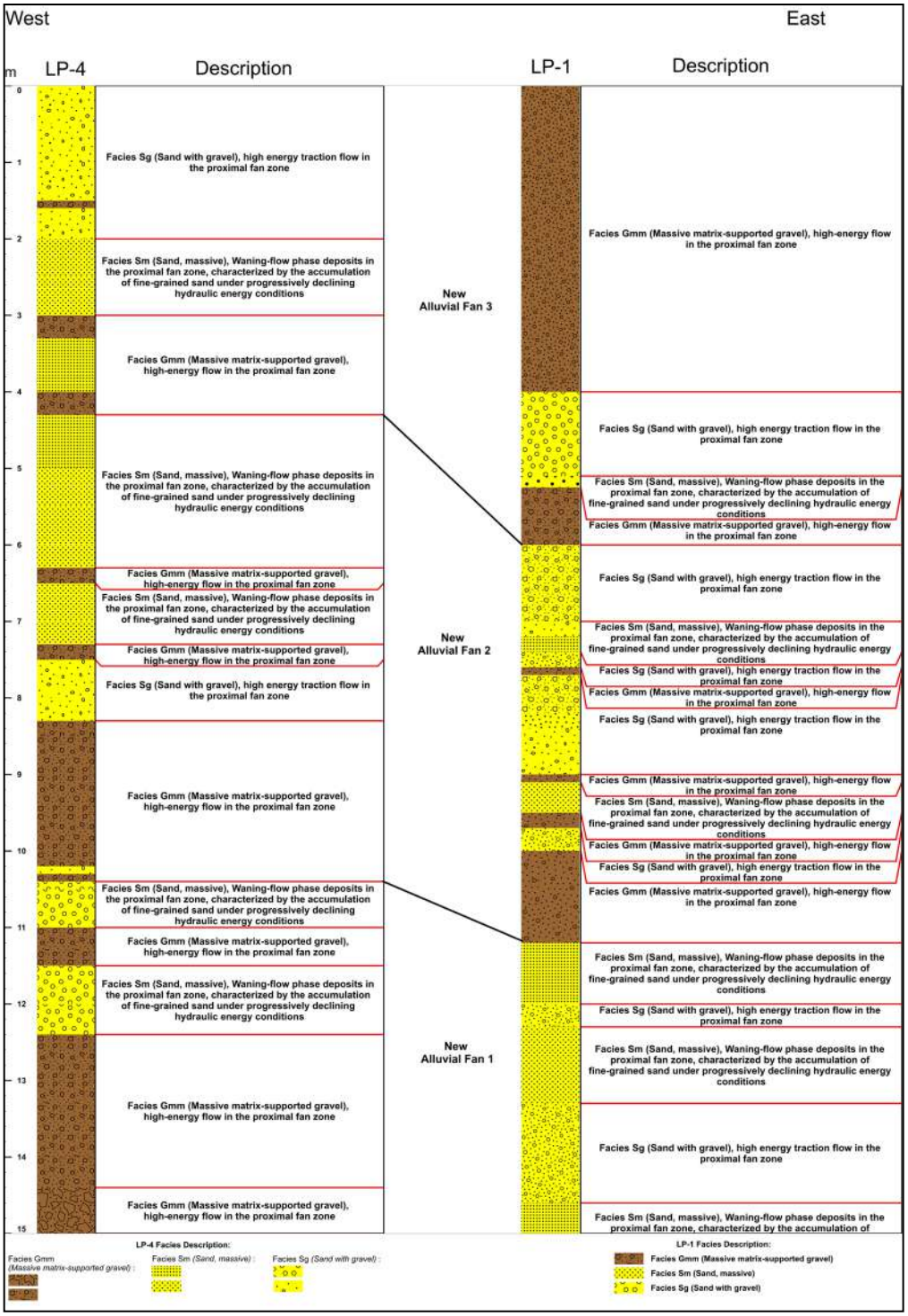

Figure 4.1.8. Quaternary sediment facies analysis of the Petobo area.

sedimentation processes. The presence of Gmm facies (massive matrix-supported gravel) at 0–4 m and 5.25–6 m indicates deposition from mass flows rapidly transporting gravel–cobble material within a sandy matrix. These intervals alternate with Sg facies (sand with gravel) and Sm facies (sand, massive), representing medium-energy traction flows and homogeneous sand deposition due to sudden energy loss, respectively. The repeated alternation between high- and medium-energy facies reflects an avulsing braided channel system within an active alluvial fan, with rapid fluctuations in flow energy and sediment supply driven by upstream hydrological dynamics.

Borehole LP-4 records facies associations typical of medial alluvial fans, dominated by traction currents with occasional mass flows. The Sg facies at 0–2 m represents transport of mixed sand and gravel by medium- to high-energy traction flows, characterizing an active braided-channel system. Overlying this, the Sm facies at 2–3 m indicates homogeneous sand deposition during sudden energy reduction, typical of waning-flow phases in traction systems. The 3–4.3 m interval consists of Gmm facies representing high-energy mass-flow deposits, with poorly sorted clasts in a sandy matrix, indicating rapid deposition from debris flows.

Well-sorted fine to very fine sand intervals identified in LP-4—particularly at 2.5–5 m, 6–7 m, and 11–12 m—were deposited under waning-flow conditions during phases of reduced flow energy. These facies are known to act as pore-water reservoirs susceptible to increased pore pressure during seismic shaking, and therefore have high liquefaction potential (Seed and Idriss, 1971; Blair and McPherson, 1994). In contrast, LP-1, dominated by coarse lithologies with massive structures and minimal fine fractions, tends to have lower liquefaction susceptibility.

4.2. Groundwater Aspects of Liquefaction in Palu 2018

The disaster event of the Mw 7.5 earthquake that shook Palu City, Donggala, and surrounding areas on September 28, 2018, left deep wounds, not only socially but also for geotechnical and geological disaster studies. This event, followed by tsunami and liquefaction, triggered large-scale sustained mudflows in areas such as Balaroa, Petobo, and Jono Oge (Jalil *et al*., 2021; Valkaniotis *et al*., 2018; Mason *et al*., 2019). Liquefaction is the loss of soil strength due to an increase in pore water pressure and a decrease in the effective stress of the soil layer arising from cyclic dynamic loading (Kusuma, 2020), resulting in the process of transforming water-saturated sandy soil into a liquid state (Seed and Idriss, 1973). This earthquake shaking resulted in subsidence, lateral spreading, and very sustained mass soil movement that swallowed thousands of buildings and casualties.

Although the basic mechanism of liquefaction involves the interaction between loose-grained soils (such as sand and silt) that are water-saturated and experience seismic shaking, the event in Palu also presented extraordinary characteristics requiring in-depth study. The level of destruction, the area affected, and the magnitude of lateral soil movement far exceeded predictions of conventional liquefaction models. This is where the hydrogeological aspect, or groundwater dynamics, emerges as a key factor that cannot be ignored in comprehensively understanding the liquefaction phenomenon in Palu.

Areas that experienced severe liquefaction in Palu are generally located on young alluvial plains formed by river and lake deposits. These deposits are dominated by fine to coarse-grained material (silt, sand, gravel) arranged complexly and in layers, forming a heterogeneous aquifer system. Relatively shallow groundwater levels are the characteristic of this area, especially during the rainy season or in irrigated areas. The interaction between active geological structures (especially The Palu-Koro Fault), the composition and stratigraphy of imperfectly consolidated sediments, and the presence and behaviour of groundwater within these layers create highly vulnerable conditions.

An in-depth understanding of the role of groundwater in the Palu liquefaction is not only important for scientifically reconstructing the disaster, but is more crucial for refining future liquefaction hazard prediction models. Hydrogeological factors, which often receive less proportional attention in conventional seismic hazard analysis, proved to be the main determinant of the scale and impact of the disaster in Palu. By comparing liquefaction from various locations around the world and revealing the specific characteristics of groundwater from the perspective of the role of confined or semiconfined aquifers in this region, the groundwater aspect of liquefaction aims to provide a stronger foundation for more effective liquefaction disaster mitigation efforts in Palu and in regions with similar hydrogeological characteristics in Indonesia and the world.

4.2.1. The Role of Groundwater in Liquefaction

Watkinson and Hall (2019) identified that communal irrigation systems increase groundwater saturation in loose-grained quaternary alluvial deposits. Irrigation water infiltration decreases the effective stress of the soil and increases susceptibility to liquefaction during seismic shaking. Spatial analysis using Principal Component Analysis (PCA) including parameters of displacement, slope, vegetation, epicentre, surface rupture, canal, and irrigation works showed a strong correlation between the density of irrigation infrastructure (main canals, branches, and distribution points) and the magnitude of ground displacement (>1 km). Landslides were limited to irrigated areas with slopes ≤1.5°; canals functioned as detachment zones. The aforementioned study was located in the eastern wing part of the Palu basin, which is different from Balaroa.

The 7.5 magnitude earthquake in Palu triggered liquefaction on September 28, 2018. The results of Factor of Safety (FS) analysis with values below the critical limit (FS=1) indicate that earthquakes with magnitudes of 7.5, 6.4, 6.2, and 6.1 in Balaroa, Petobo, and Jono Oge triggered liquefaction at those locations (Triyono *et al*., 2024). The areas most severely affected by liquefaction were at the boundary between the unconfined aquifer system and the confined aquifer system (Setiawan *et al*., 2018). The roughly similar earthquake magnitudes between Christchurch City in 2010 and 2011 and Palu City in 2018, the close epicentre locations, and both cities being located above confined aquifer systems, suggest the role of the confined aquifer system in the Palu liquefaction (Widodo *et al*., 2022).

Theoretically, under certain geological and hydrogeological conditions, ground movement during liquefaction generally occurs with a delay of seconds. Unlike Palu, which required a delay of up to minutes. Several studies have observed the role of confined aquifers causing liquefaction with sustained ground movement and severe impacts in Palu in 2018. Hydrogeologically, this liquefaction is very typical, so it can be designated as Palu-type liquefaction. The role of the confined aquifer will be reviewed based on changes in groundwater levels in wells accessing aquifers deeper than 30 m and groundwater isotopes.

4.2.2. Hydrogeology and Hydrostratigraphy of the Palu Basin

The 2018 Palu liquefaction became interesting due to the sustained ground movement following groundwater flow patterns. Kiyota *et al*. (2025) investigated the triggering mechanism of long-runout flow landslides resulting from the 2018 Sulawesi Earthquake through a review of hydrogeology and groundwater dynamics. The soil layer structure in landslide areas, such as Petobo, Balaroa, and Jono-Oge, shows the presence of sandy gravel aquifers at depths of >20 m receiving groundwater flow from upstream areas. This aquifer is covered by a low-permeability sandy silt layer, creating confined groundwater pressure (40–60 kPa above hydrostatic pressure) before the earthquake. Groundwater flow simulation with MODFLOW-NWT confirmed that this high pressure primarily originates from groundwater supply through the gravel aquifer from upstream, not from surface irrigation channels, whose influence is considered minimal. Signifi-

cant liquefaction in the sandy silt layer (SPT-N 10-20) occurred due to a combination of confined groundwater pressure and earthquake shaking (PGA 281−471 gal). This process increased the permeability of the silt layer, triggering the flow of confined groundwater to the surface in large volume and long duration. The rising water turned the surface layer into mud, and triggered ground movement of up to hundreds of meters on slopes of <5 %. The study results emphasize the importance of monitoring groundwater pressure in aquifers and managing surface water infiltration in upstream areas to mitigate similar risks. Widodo *et al*. (2022) deepened the liquefaction mechanism with a focus on the role of the confined aquifer in large-scale groundwater expulsion. The earthquake triggered an increase in pore pressure and permeability in thin confining layers, allowing water transfer from the confined aquifer to the unconfined aquifer above it. Numerical simulation using pore pressure dissipation and permeability increase models showed that a combination of high hydraulic pressure (HHR= 1.4) and permeability ratio (EPR = 4) produces water flow (GE flux) of up to 27 l/s/m². Stable isotope data ($\delta^{18}O$ and $\delta^{2}H$) confirm the water source from deep aquifers through new springs post-earthquake, which worsened sustained mudflow and ponding. Referring to Santosa *et al*. (2021), the hydrostratigraphy of the liquefaction-affected area in Palu post the 2018 earthquake consists of four main layers: (1) an unconfined aquifer (alluvium and coastal deposits/Qa) with a thickness of 17.77−72.48 m, located at an elevation of 341 m above sea level (asl. to -2.29 m asl, acting as a porous layer storing water; (2) an upper aquitard (Sulawesi Molasse Sarasin and Sarasin/QTms) with a thickness of 0.12−0.61 m, functioning as a relatively impermeable layer; (3) a semiconfined aquifer (QTms) with a thickness of 20.58 −86.51 m; and (4) a lower aquitard (granite, Tinombo Formation, metamorphic rocks, and Latimojong Formation) which is impermeable. In liquefaction areas like Balaroa, the rupture of the confined aquifer caused an increase in groundwater pressure in the upper layer, triggering liquefaction. While in Petobo, no aquifer damage occurred, so liquefaction did not appear. This hydrostratigraphic structure, especially the presence of rupture-prone confined aquifers and post-earthquake hydraulic connection, is a key factor in the escalation of liquefaction in certain areas. A study by Wardhana *et al.* (2024) identified the subsurface structure causing liquefaction in Palu post the 2018 earthquake through gravity anomaly analysis. Bouguer mapping results show low anomalies (-2–10 mgal) in Petobo and medium anomalies (19.5–34.5 mgal) in Balaroa, indicating water-saturated alluvial sediment basins prone to liquefaction. Residual analysis using the polynomial method revealed graben structures bounded by normal faults (west – east in Balaroa) and strike-slip faults (Petobo), controlling the accumulation of groundwater in saturated sand-clay layers. This basin acts as a local aquifer with high pore pressure due to water saturation, which reduces soil shear strength during an earthquake. Low gravity anomalies correlate with water-saturated zones, while high-low anomaly contrasts indicate the presence of secondary faults that worsen groundwater flow dynamics. The Palu-Koro Fault structure and its derivatives create groundwater migration pathways, increasing liquefaction risk in alluvial areas. This study confirms that the combination of hydrogeological conditions (water saturation, basin structure) and local tectonic activity are key factors in liquefaction vulnerability, so gravity anomaly mapping can be an effective tool for identifying risk zones based on groundwater characteristics. The hydrogeology of the Palu basin becomes complex with the presence of active structures or tectonics indicated by the Palu-Koro Fault.This fault splits the western part of Palu, contributing to the formation of a fractured media hydrogeological system where deep groundwater flows. The relationship between morphology and groundwater conditions in The Palu Groundwater Basin, including in the alluvial plain groundwater mandala, refers to Ruchiyat and Denny (1989) with the following characteristics:

- Unconfined groundwater level less than 7.5 m from the local ground surface;
- Semiconfined to confined groundwater is likely found at depths greater than 36 m from the local ground surface;
- Springs generally have a discharge of less than 5 l/sec, except in the Wani area where discharge reaches 25 l/sec.

The groundwater flow pattern, referring to Suryaman *et al.* (1995), is controlled by the local topographic shape, generally flowing from hilly areas towards river valleys. Groundwater in aquifers located deeper than 30 m is generally confined or semiconfined. Piezometric levels are generally from 8 m below ground level (bgl.) to 6 m above ground level (agl.), which on average are higher than the water table of the unconfined aquifer, causing a tendency for upward flow from the deeper confined aquifer. The main factor of the 2018 Palu liquefaction in the confined aquifer, based on the conceptual model of the hydrogeological cross-section in Balaroa and Petobo, lies in old alluvial fan deposits starting at depths of 55 m in Balaroa and 52 m in Petobo (Widodo *et al*., 2022).

The hydrogeological conditions at the time of liquefaction can be reviewed from the conditions of the aeration zone and the confined aquifer. A confined aquifer with high hydrostatic pressure will create an energy reserve that is released during an earthquake (Bradley *et al*., 2019). This condition is created by impermeable layers such as clay or cap rock that hinder drainage and prolong the duration of high pore pressure. The aeration zone (unsaturated zone) above the water table can worsen liquefaction through vertical cracks caused by pressure from the confined aquifer, forming channels for the flow of liquefied material (Sassa and Takagawa, 2018), and degradation of cohesion as pressurized water fills the bonds of unsaturated soil particles (Fredlund and Rahardjo, 1993). Groundwater quality has an influence when Total Dissolved Solids (TDS) values are high, *i.e.* more than 500 mg/l, which can reduce soil shear strength through dispersion of clay particles due to Na+ and Cl- ions that disrupt soil structure (Kiyota *et al*., 2019), and reduction of cohesion through increased negative charge of soil particles lowering shear strength (Xenaki and Athanasopoulos, 2003).

The groundwater system in Palu is controlled by several main factors, namely geological conditions as the pathway for groundwater flow and climatic conditions as the water source that fulfills the hydrological cycle flowing in The Palu Groundwater Basin (CAT Palu). Geological conditions become very dynamic structurally and tectonically due to the presence of The Palu-Koro Fault path in the western part, forming a basin valley filled with Quaternary alluvial deposits as the main aquifer. The fractured media hydrogeology typical of tectonic areas is active, with several springs found with discharges greater than 10 l/sec, some of which have hot temperatures.

Palu Basin Groundwater System

Groundwater in the Palu basin follows the local hydrological cycle influenced by climate, including type Am (tropical monsoon climate) according to the Koppen-Geiger system, which has distinct wet (November−April) and dry (May-October) seasons. Average annual rainfall ranges from 800–1,200 mm. Interannual and seasonal rainfall variability directly affects the magnitude of groundwater recharge. Viewed from rainwater isotope data through the local meteoric water line (LMWL) of the Palu area and the Indonesian LMWL with the equation LMWL $\delta^2H=7.298\delta^{18}O+3.506$, it is still lower compared to The Global Meteoric Water Line (GMWL). This reflects the influence of intensive evaporation processes in a humid tropical climate, visually seen from the clockwise shift of the LMWL regression line compared to the GMWL in Figure 4.2.1 (Suwarman *et al*., 2024).

Isotope data from springs, dug wells, and boreholes at points of hydrogeological interest from the 2024 Palu CAT groundwater conservation activity and a special study in 2025 show that springs (MA) are concentrated near the LMWL with relatively high $\delta^{18}O$ values (-7.5 ‰ to -5.0 ‰), indicating origin from local rainfall recharge at low eleva-

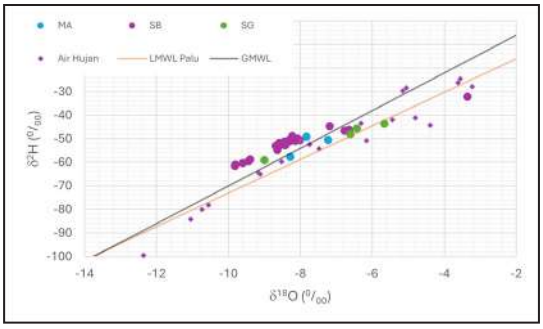

Figure 4.2.1. The black GMWL line is higher than the intersection point compared to the red Palu LMWL line, indicating the condition of evaporation below clouds.

tion with a short hydrological cycle. Conversely, boreholes (SB) show the lowest isotope values ($\delta^{18}O$: -9.0 ‰ to -6.5 ‰; $\delta^{2}H$: -80 ‰ to -50 ‰), indicating origin from deep aquifers or recharge in mountainous zones with long residence times (>100 years). Meanwhile, dug wells (SG) have a wide distribution with some samples deviating below the LMWL due to the influence of evaporation and surface water contamination (Clark, 2015). The low isotope values in dug wells and shallow monitoring wells in some locations indicate a contribution from the confined groundwater flow system (deep groundwater flow) flowing vertically towards the unconfined aquifer system (shallow groundwater flow) through an inter-aquifer transfer mechanism (leaky aquifer).

Groundwater isotope data specifically for the affected areas in Balaroa, Petobo, and Jono Oge, supplemented with references from Widodo *et al.* (2022), are presented in Table 4.2.1. Their distribution is shown in Figure 4.2.2, covering the affected areas and their surroundings. In Figure 4.2.3, it can be seen that groundwater in Balaroa has the lowest isotope values compared to Petobo. This shows different groundwater flow origins; Balaroa groundwater flow direction is from southwest to northeast (Figure 4.2.4), and Petobo tends to have a flow direction from east to west (Figure 4.2.5). Meanwhile, in Jono Oge, mixing was detected in the shallow aquifer within the unconfined aquifer in 2021.

The Mw 7.5 earthquake induced significant changes in the aquifer system. Post-earthquake isotope analysis revealed abnormal mixing between shallow and deep aquifers. Borehole (SB) samples showed a compositional shift closer to spring (MA)/dug well (SG) values. For example, $\delta^{18}O$ -9 ‰ appeared in shallow wells, proving the occurrence of vertical flow through fault fractures activated during the earthquake. This phenomenon disrupts the hydrological isolation of deep aquifers and promotes the migration of old water from confined aquifers to shallow zones (Figure 4.2.3 and Figure 4.2.5). On the other hand, dug wells experienced an isotope shift to the right below the LMWL, reflecting increased surface water contamination due to damaged sanitation infrastructure. A similar pattern was observed in global fault zones like San Andreas (USA) where earthquakes caused deep water to emerge in surface springs.

A hydrogeological study by the LIPI Geotechnology Research Centre Team (2019) revealed that the groundwater level in liquefaction-affected areas ranged between 1.5−2.5 m below the surface. The combination of high rainfall (1,800 −2,500 mm/year) and flat topography caused significant groundwater accumulation, increasing soil saturation to >90 %. Natural drainage systems hindered by sedimentation worsened water retention. The Palu Basin has an annual recharge rate of 500–700 mm/year from rainfall and river flow. However, confined aquifers have high water availability with transmissivity values of 50–100 m^2/day and minimal seasonal fluctuation due to impermeable cover layers (Bradley *et al*., 2019).

Research by Patriaman *et al*. (2021) analyzed liquefaction potential in Palu Bay post the 2018 earthquake, focusing on hydrogeological and groundwater conditions. This area is dominated by noncohesive soils (sand, gravel, and silt) prone to liquefaction, especially in the western and southern parts adjacent to The Palu-Koro Fault. The shallow groundwater level (0.09–4.48 m below surface) increases water saturation in soil layers, and reduces shear strength during earthquakes. Analysis using Standard Penetra-

Tabel 4.2.1. Data Isotop Air Tanah di Sekitar Daerah Terdampak

LOKASI	BT	LS	$d^{18}O$ (‰)	$d^{2}H$ (‰)	REFERENSI
Balaroa flowslide	119,8438	-0.9039	-9,45	-58,62	Widodo dkk. 2022
Jono Oge-Deep	119,9165	-0,9746	-9,51	-57,78	Widodo dkk. 2022
Jono Oge-Shallow	119,9174	-0,9766	-8,76	-54,68	Widodo dkk. 2022
BPN Office Palu	119,8764	-0,8881	-9,09	-54,69	Widodo dkk. 2022
Birobuli	119,9010	-0,9324	-9,37	-55,73	Widodo dkk. 2022
SB-3 Mesjid BTN Kawatuna	119,9325	-0,9178	-8,60	-53,33	Badan Geologi 2024
MA-4 MA-Gawalise	119,8420	-0,9154	-9,44	-59,58	Badan Geologi 2024
SB-12 Kolam Renang CAFIT	119,8477	-0,9154	-9,81	-61,07	Badan Geologi 2024
SP-18 RS Anutopura	119,8497	-0,8999	-8,64	-54,89	Badan Geologi 2024
SB-20 Hotel Sutan Raja	119,8978	-0,9185	-8,30	-51,03	Badan Geologi 2024
SB-33 Pak Iwan	119,8890	-0,9326	-8,69	-53,00	Badan Geologi 2024
SP-P1 Jl. PDAM, Duyu	119,8424	-0,9137	-9,00	-59,10	Badan Geologi 2025
MA-P2 Balaroa top flowside	119,8406	-0,9065	-8,28	-57,75	Badan Geologi 2025
SG-P4 Petobo flowside	119,9148	-0,9404	-6,61	-48,00	Badan Geologi 2025
SP-P5 Petobo, Jl. Tondei	119,9156	-0,9429	-6,65	-46,21	Badan Geologi 2025
SP-P6 Petobo, Jl. Tondei	119,9159	-0,9431	-6,77	-46,67	Badan Geologi 2025
MA-P7 Ngatabaru	119,9597	-0,9216	-7,23	-50,61	Badan Geologi 2025
MA-P8 Petobo flowside	119,9189	-0,9398	-6,67	-46,79	Badan Geologi 2025
SG-P9 Petobo flowside	119,9183	-0,9379	-6,43	-45,68	Badan Geologi 2025
SG-P10 Jono Oge	119,9178	-0,9825	-5,67	-43,62	Badan Geologi 2025

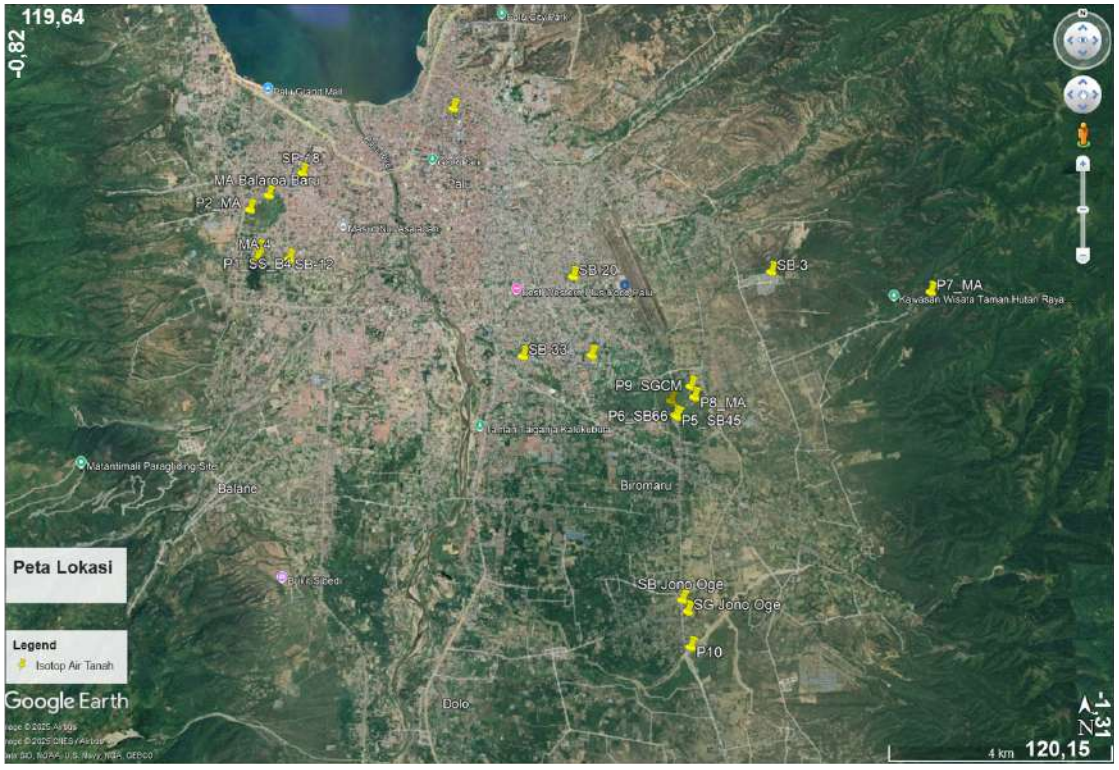

Figure 4.2.2. Distribution of groundwater isotope data collection points.

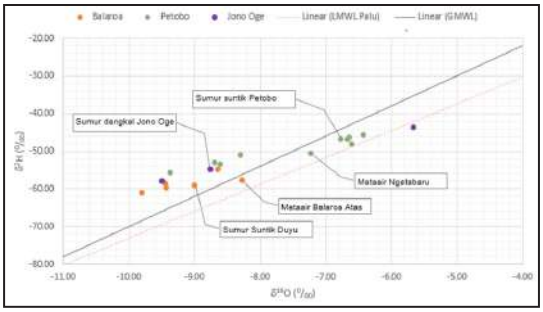

Figure 4.2.3. Groundwater in the Balaroa area tends to have lower isotope values compared to Petobo, with a distribution pattern of groundwater from deep confined aquifers to shallow unconfined aquifers from left to right.

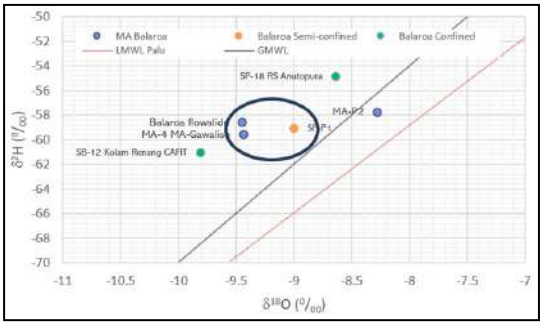

Figure 4.2.4. Mixed zone in Balaroa indicated by the presence of groundwater from the confined aquifer.

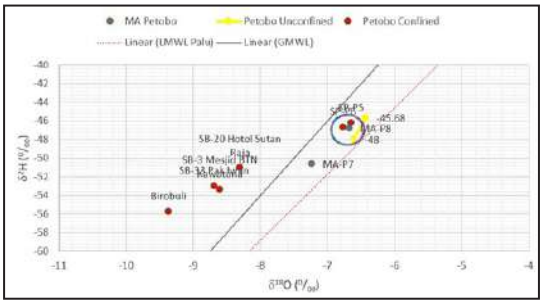

Figure 4.2.5. Mixed zone of groundwater from the confined aquifer in Petobo. (Note: Figure number seems inconsistent, likely should be 4.2.5 based on context).

tion Test (SPT) data and the Seed-Idriss method showed that zones with loose sandy soil and shallow groundwater (<2.5 m) have a low Safety Factor (FS) (<1) and a "very high" Liquefaction Potential Index (LPI) (LPI >15). This condition is worsened by the tectonic activity of the Palu-Koro Fault which triggers dynamic pressure and groundwater movement. Conversely, the eastern part of Palu Bay with deeper groundwater (>2.5 m) and clay content shows "very low" liquefaction risk. This study confirms that the interaction between basin morphology, groundwater depth, and active geological structure are key factors in liquefaction vulnerability. Risk mitigation in hazardous zones (west and south) needs to prioritize soil stabilization and drainage management to reduce water saturation in surface layers.

Research by Tohari *et al.* (2021) examined the hydrogeological factors causing liquefaction in Balaroa and Petobo after the 2018 Palu earthquake using resistivity methods. The results showed that liquefied soil layers have low resistivity (<50 Ωm), indicating high water saturation in alluvial sediments (sand-clay) trapped in subsurface basins. This basin morphology is formed due to Palu-Koro Fault activity and becomes a shallow aquifer zone (<10 m) that triggers groundwater accumulation, and increases pore pressure. Resistivity anomalies also revealed a gentle slope boundary between water-saturated (liquefiable) layers and dense layers (alluvial fan), which accelerates soil mass flow during earthquakes. Graben structures due to normal faults create groundwater flow pathways that worsen layer saturation. In Petobo, steeper boundary slopes caused more extensive liquefaction flow compared to Balaroa. This study confirms the critical role of hydrogeological conditions (basins, water saturation, and pore pressure) in liquefaction vulnerability, and the need to integrate aquifer mapping and subsurface structure for risk mitigation in active seismic regions.

The studies and research mentioned above affirm that liquefaction in Palu is a synergy between natural factors (confined aquifer, alluvial geological conditions) and anthropogenic factors (irrigation). The irrigation system not only increases shallow groundwater saturation, but also interacts with deep aquifer dynamics through hy-

draulic changes. The practical implication is that liquefaction risk evaluation in seismic areas needs to expand coverage to depths of >30 m, including analysis of confined aquifers, hydraulic pressure, and confining layer thickness. Mitigation can be optimized by redesigning irrigation systems (*e.g.* tiered channels to reduce groundwater level fluctuations) and integrative monitoring of deep groundwater response during spatial planning. These findings emphasize the importance of a multidisciplinary approach in understanding complex geohydrological disasters.

Hydrogeological Characteristics of Severely Affected Areas

Petobo and Jono Oge are located in the southern part of the basin dominated by lacustrine and fluvio-deltaic deposits rich in alternating thin silt and fine sand layers. Extensive traditional irrigation systems cause chronically very shallow groundwater levels (often < 2m). The presence of continuous clay/silt layers near the surface creates semiconfined conditions in the saturated sand layers below and hinders pore water pressure dissipation. Balaroa is located closer to the city centre and The Palu-Koro Fault. Stratigraphy shows river alluvial (fluvial) deposits with lenses of sand and gravel in a silt matrix. The groundwater level is also relatively shallow. Direct proximity to the main fault zone increases shaking intensity. One key factor that worsened and expanded the impact of liquefaction in areas like Balaroa, Petobo, and Jono Oge is the presence of confined aquifers in the subsurface geological system. This section discusses the critical role of confined aquifers in the liquefaction mechanism that occurred in Palu. The areas severely affected by liquefaction along The Palu Basin are elongated depressions filled with young Quaternary deposits characterized by alluvial material and layered formations with different permeabilities. Alluvial material consists of sand, silt, gravel, and clay deposits laid down by rivers and alluvial processes. Layered formations with subsurface stratigraphy show layers with different permeabilities consisting of aquifers and aquitards/ aquicludes. Aquifers are composed of water-saturated sand and gravel, thick, and highly permeable. Aquitards/aquicludes are low-permeability silt or clay layers that cover the aquifer at the top, forming a barrier layer, and often also bound it at the bottom. This condition causes water in the aquifer to be under higher hydrostatic pressure than if the aquifer were unconfined. Strong earthquakes produce cyclic shear stress on water-saturated soil. Under normal conditions, increased pore water pressure due to shaking will dissipate gradually. However, the presence of a confined aquifer has the potential to trigger a much more dangerous liquefaction mechanism, namely:

1. Very high increase in pore water pressure. Earthquake shaking causes saturated soil particles (especially sand) to compact, suddenly increasing the pressure of the water filling the pore voids (pore water pressure) within the sand layer of the aquifer.
2. Hindered dissipation mechanism by the confining layer (aquitard-aquiclude). The impermeable clay/silt layer above the confined aquifer acts as a very effective barrier (seal). This layer hinders/blocks upward water flow to release the high pore pressure formed suddenly in the underlying sand aquifer.
3. Pressure accumulation and loss of shear strength. This trapped pore water pressure, which cannot dissipate quickly, continues to accumulate until it reaches a value equal to or exceeding the vertical effective stress ($\sigma'v$) compressing the sand layer. When the ratio of pore water pressure to effective stress (ru) approaches, the effective stress approaches zero. At this point, the sand loses almost all its shear strength and behaves like a viscous fluid. This is the essence of liquefaction.
4. Lateral flow and sand boil mechanism. The liquefied material (sand-water) within the high-pressure confined aquifer seeks an outlet. This very large pressure impacts:
   - Causing the fragile overburden layer to uplift and crack.
   - Triggering very strong eruptions of liquefied material (sand boils, mud volcanoes) through these cracks to the surface.

- Moving the liquefied mass laterally in large volumes underground, following the topographic slope. It is this sustained lateral flow that causes ground flow and the shifting of buildings and infrastructure over hundreds of meters, as happened in Petobo and Balaroa.

The specific impacts on the Palu liquefaction are as follows:

- Scale and speed: High pore water pressure in the confined aquifer allows liquefaction to occur with very large volume and high speed, far exceeding ordinary liquefaction events.
- Wide reach: Caused by the lateral flow of liquefied material driven by confined aquifer pressure, able to cover very wide areas.
- Extreme surface deformation: Occurrence of ground surface subsidence, ground cracking, and sustained horizontal ground movement that destroyed entire settlements.
- Relatively long duration of water and sand eruptions (sand boils), continuing for days after the earthquake, indicating the still high pore water pressure in the confined aquifer system that had not been fully released.

The presence of a confined aquifer beneath an impermeable cover layer is a key geohydrological factor that explains why the liquefaction in Palu in 2018 reached an extraordinarily destructive scale and intensity. The impermeable cover layer acts as a lid preventing the release of excess pore water pressure generated by earthquake shaking within the underlying saturated sand layer. It is this accumulation of very high pore pressure that causes the soil to lose its shear strength en masse, and drives lateral flow and surface eruptions of liquefied material with tremendous force. Detailed understanding of the existence, depth, thickness, and hydraulic properties of confined aquifers and their cover layers becomes an essential component in liquefaction vulnerability assessment and disaster mitigation planning in areas with similar geological settings, especially along active faults like Palu-Koro.

Changes in Groundwater Flow Patterns

Measurements of the water table of unconfined aquifers and the piezometric surface of confined aquifers have been conducted by The Geological Agency through activities assessing the potential of the Palu groundwater basin in 1989 and 1995 (Figure 4.2.6). Hydrogeological observation objects include springs, dug wells, and boreholes. Typical wells in the Palu area are driven wells consisting of 1.5 inch iron pipes. Driven wells in the Balaroa area with a depth of 9 m produce artesian flow with a discharge of about 0.5 l/sec. Meanwhile, in the Petobo area, depths reach 50–60 m. Based on the 1995 and 2024 water table contours, shifts can be seen in some segments, including the affected areas (Figure 4.2.7). The affected areas fall within the medium–high groundwater potential category with aquifer transmissivity of 10–500 m per day. The unconfined water table is generally 5–50 m below the ground surface, the confined piezometric surface is positive 3 m above ground level to 5 m below ground level. The condition of the positive water table in the central to northern part of Palu City forms an arch whose boundary is at the base or foot of the affected area.

The lateral shift of the water table in Petobo reaches 1 km for the water table at 60 m above sea level. The central part of the affected Petobo area experienced a drop of 12 m from a water table depth of 60 m asl. in 1995 to 48 m asl. in 2024. Generally, in the affected areas, the 2024 water table has shifted towards the outside of the basin compared to 1995, meaning that the water table has dropped. Based on this, it appears that the occurrence of the earthquake followed by liquefaction caused an increase in pressure head in the confined aquifer, which primarily occurred in locations directly affected by liquefaction.

4.2.3. Comparative Analysis of Liquefaction

A global comparative analysis of the liquefaction that occurred in Palu can be compared with the 2011 Christchurch Earthquake in New Zealand and the 1964 Niigata Earthquake in Japan

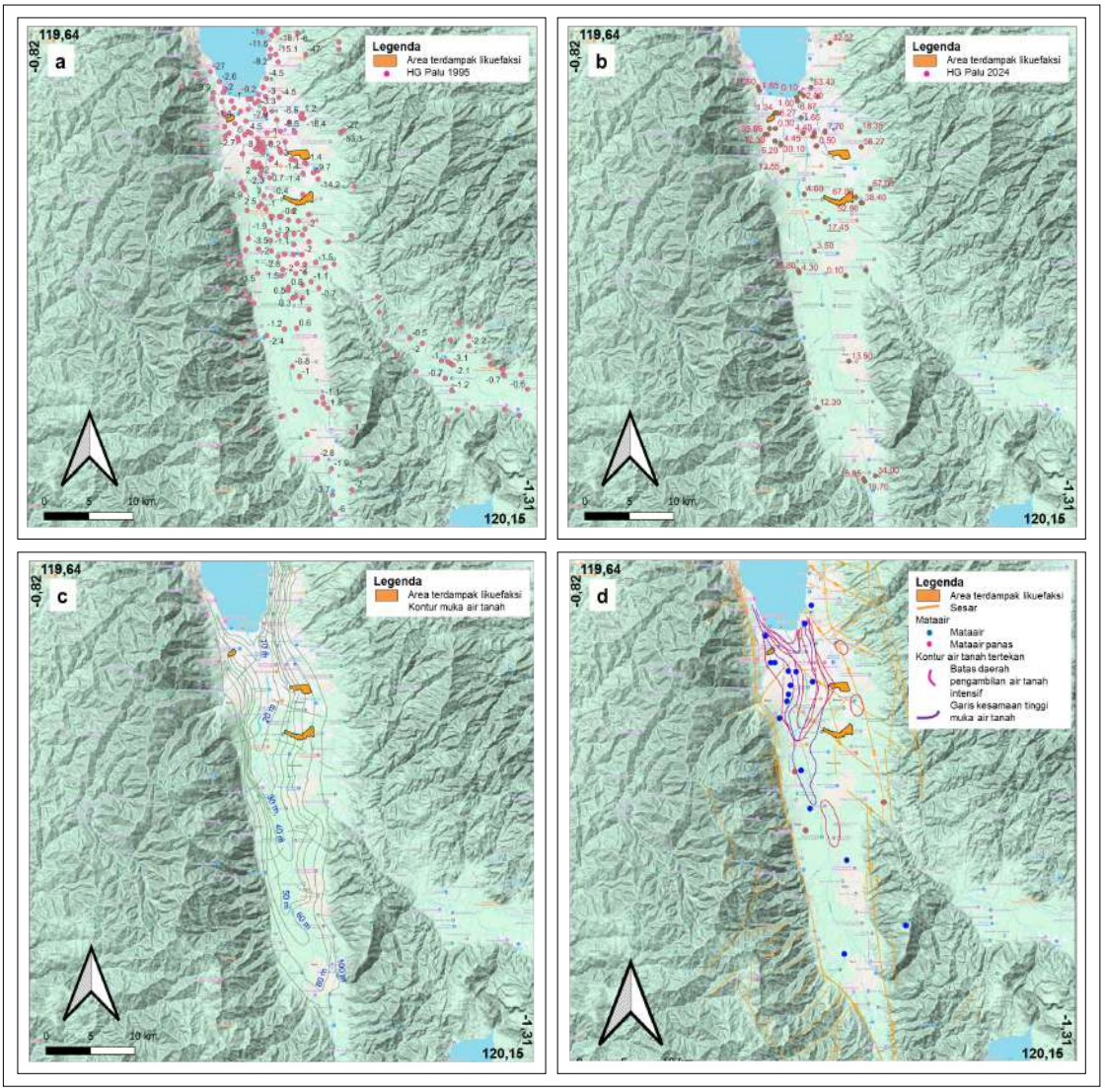

Figure 4.2.6. (a) Collection of hydrogeological points of interest in 1995, (b) Palu water table 2024, (c) water table contour lines, and (d) spring distribution with structure.

(Table 4.2.2). This comparative analysis can be reviewed from the hydrogeological conditions and mechanisms, namely confined aquifer conditions and the aeration zone.

The hydrogeological conditions in Palu involve high-pressure confined aquifers beneath impermeable clay layers, a thin aeration zone with low permeability value K=10^{-6} m/sec (Watkinson and Hall, 2021). The mechanism involves hydraulic fracturing in the aeration zone triggering massive lateral flow (Jalil *et al*., 2020), resulting in 68,451 houses destroyed and 3,354 fatalities (BNPB, 2018). The hydrogeological conditions of the Christchurch earthquake involve shallow confined aquifers with moderate pressure, a thick aeration zone with high permeability up to 10^{-4}

m/sec (Green *et al*., 2014), with a mechanism where pressure is partially dissipated through the aeration zone producing slow flow.

The hydrogeological conditions of the Niigata Earthquake involve water-saturated sand aquifers with a shallow water table and a mechanism of conventional liquefaction with building subsidence without massive lateral flow (Ishihara, 1993). The 1989 Loma Prieta liquefaction in the United States has similarities with Palu 2018 viewed from anthropogenic factors with the construction of irrigation in Palu and reclamation in Loma Prieta which worsened the impact.

4.3. "Palu Type" Liquefaction from Engineering Geology Aspect

One of the effects of the September 28th, 2018, earthquake was liquefaction, which caused flow landslides. Several locations that experienced by flow landslides were Balaroa, Petobo, Jono Oge,

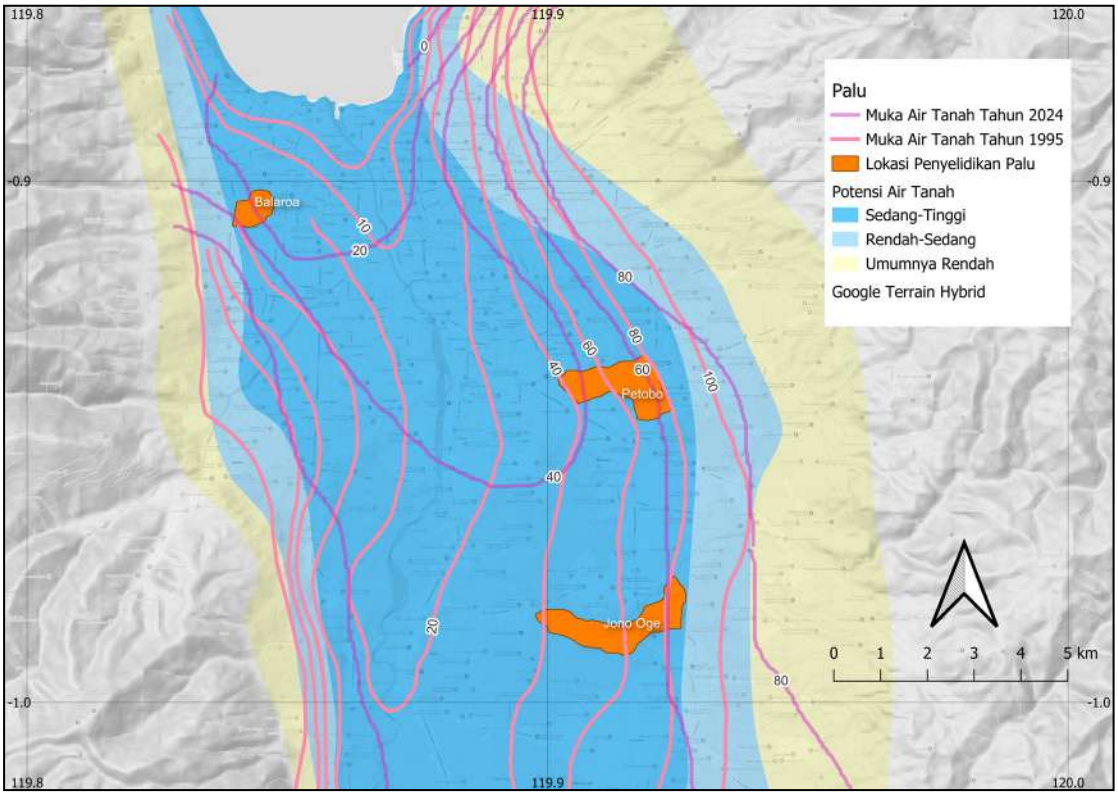

Figure 4.2.7. Shift in water table contours; pink colour represents the 1995 water table and purple the 2024 water table.

Table 4.2.2. Liquefaction Comparison

Parameter	Palu (2018)	Christchurch (2011)	Niigata (1964)
Aquifer Pressure (kPa)	150-200	100-120	50-80
Aeration Zone Thickness (m)	2-5	5-10	1-2
Flow Velocity (m/sec)	2-3	0,5	0,1-0,3
Damage Type	Massive lateral flow	Local subsidence	Structural subsidence

Lolu, Sidondo, and Sibalaya. This phenomenon causes severe damage to land surface and civil structures, and numerous casualties.

Several researchers have published the factors causing this phenomenon, which in general summarize the causes due to the strong shaking effect, relatively gentle slope gradient, sandy soil lithology with relatively low N-SPT values, shallow groundwater levels with high pore water pressure due to the presence of an impermeable layer. Specifically, the case at the Balaroa location is controlled by fault movement (Yoshida *et al*. 2020; Jalil *et al*., 2021) while at the Petobo and Jono Oge locations there is a contribution of water pressure originating from the Gumbasa water channel (Bradley *et al*., 2019; Watkinson, 2019; Cummins, 2019; Jalil *et al*., 2021), but other opinions state that this irrigation channel has little effect on the Kiyota (2025) landslide mechanism and the Gumbasa irrigation channel is not the main factor but rather a supporting factor for the liquefaction process (Widodo *et al.,* 2022).

Several hypotheses of liquefaction mechanisms that trigger landslides have been studied by several researchers, including the mechanisms of cracks and confined aquifers (Buana, 2018), the mechanism of hydraulic contribution of unconfined aquifers and semi-confined/confined aquifers (Widodo *et al*., 2019) then continue for detail studied in 2022 (Widodo *et al*., 2022), the mechanism of anthropogenic hazards from irrigation channels (Watkinson and Hall, 2019), the water film mechanism (Kokusho *et al*., 2025), the mechanism of water interlayer formation and groundwater inflow from confined aquifers (Kiyota *et al*., 2025).

The causal factors and mechanisms of liquefaction as described in the previous paragraph have partially answered the liquefaction phenomenon that triggers landslide movements

Liquefaction triggering landslides in the western (Balaroa) and eastern (Petobo, Jono Oge, Lolu, Sidondo, and Sibalaya) areas is an interesting phenomenon, because the western part is associated with a fault, and the eastern part is associated with the Gumbasa irrigation canal. It is suspected that the irrigation canal controls the liquefaction that triggers the flow landslides, but it does not occur in the western part of The Palu Valley. Conversely, the western part of The Palu Valley, which is suspected to be strongly controlled by the fault, experiences liquefaction, and the same phenomenon also occurs in the eastern part of The Palu Valley where there is no fault. Information on similar events around the world is still limited to answer this phenomenon and whether this phenomenon is a phenomenon with unique characteristics of the "Palu Type" remains a mystery.

Rapid Assesment Map After The Earthquake of September 28th, 2018

One of the Geological Agency teams conducted a rapid mapping of surface land damage on the sixth day, namely October 3rd, 2018 to October 17th, 2018. The aim of mapping is an inventory of damage due to the effects of shocks on surface land, especially in The Palu Valley where many casualties and damage to building infrastructure occurred. The inventory uses a qualitative descriptive mapping method with a grid size of 250 m x 250 m. The assessment criteria (Table 4.3.1) use modifications from Ballegooy *et al.* (2012) based on the criteria for liquefaction events, cracks, vertical and horizontal deformation and undulation as in Table 4.3.1. The assessment class is divided into three parts, namely low, medium, and high, while for tsunamis it is a separate assessment class as in Figure 4.3.1.

The results of rapid mapping (Figure 4.3.1) show that significant surface land damage due to the effects of the earthquake shocks of September 28, 2018 is along the slope break area or changes in the morphology of the alluvial fan towards the alluvial plain as in Figure 4.3.2. Generally, the alluvial plain section experienced relatively minor surface land damage and this represents most of the conditions in The Palu Valley.

Earthquake-induced ground cracking data from rapid mapping (Figure 4.3.3) shows two distinctive phenomena. The first is ground cracking, part of The Palu Koro Fault, which is compressive

Tablee 4.3.1. Rapid Assessment of The Earthquake Shock Effects to Surface Land Damage in The Palu Valley on September 28th, 2018

CLASS	CRITERIA	EVALUATION
LOW (GREEN)	1. Liquefaction does not occur or may locally (liquefaction occurs in less than 5 % of observation locations) 2. Ground cracks less than 1 cm 3. Vertical displacement does not occur 4. Lateral displacement does not occur 5. Ground undulating does not occur	Surface land damage is relatively safe, but it can still damage buildings due to wave amplification
MEDIUM (YELLOW)	1. Liquefaction can occur locally (approximately 5% – 25 % of observation locations experienced liquefaction) 2. Ground cracks less than 5 cm 3. Vertical displacement is less than 10 cm 4. Lateral displacement less than 5 cm 5. Ground undulating may occur	Surface soil damage can occur due to the presence of ground cracks (surface rupture), which may be accompanied by localized liquefaction. Lateral and vertical deformation may occur on a small scale.
HIGH (RED)	1. Liquefaction can occur extensively (more than 25 % of the observation location experiences liquefaction) 2. Ground cracks more than 5 cm 3. Vertical displacement is more than 10 cm 4. Lateral displacement does not occur 5. Ground undulating may occur extensively	Surface soil damage is controlled by surface rupture, which can be accompanied by liquefaction, horizontal and vertical deformation, and can trigger landslides on gentle slopes (generally <15 %). The impact of soil damage is generally relatively
(BLACK)	Tsunami	Land damage caused by tsunami

Figure 4.3.1. Examples of ground surface damage in each class and damage due to tsunami (Source: Buana and Supartoyo).

and partly tension-type, in the western part of The Palu Valley and it has north-south direction. The second is ground cracking, predominantly tension-type, in the eastern part of The Palu Valley, which tends to north-south direction and follows the topographic contours. The liquefaction that triggered the flow ground motion occurred in the ground crack pattern zone. This suggests a relationship between the formation of ground cracks and the liquefaction that triggered the flow ground motion.

Flow landslides at Palu are a phenomenon initiated by liquefaction due to the effects of earthquake shaking on 28th September 2018. This paper will focus on three locations: Balaroa, Petobo, and Jono Oge, which experienced massive damage. The analysis utilizes data from The Geological Agency (Badan Geologi), JICA (2019), and data from previous scientific publications.

4.3..1. Balaroa

4.3.1.1. Geology of the Affected Area at Balaroa

Balaroa is part of an alluvial fan system with a debris-flow dominated fan type or type I alluvial fans as in Figure 4.3.4 (Blair dan McPherson, 1994). The character reflects a high-energy, short-term depositional mechanism controlled by a debris flow that it is common in the proximal to medial parts of the alluvial fan system.

The crown outcrop of the Balaroa flow landslide (outcrop height between 4 m–7 m) is granite debris and genetically, the architectural elements are sediment gravity flow and gravels lithofacies according to Miall (2006) classification that it has the Gmm facies (matrix-supported, massive gravel), as in Figure 4.3.5. Miall (2006) says that the Gmm facies is part of the matrix-supported gravel which has a matrix in the form of sand, silt and mud and rock fragments and poorly sorted matrix.

The liquefaction that trigger flow landslide occurred in the alluvial fan in Balaroa at a depth of less than 15 m based on field observations, qualitatively. Balaroa alluvial fan is relatively deep, and the liquefaction that trigger flow landslide is relatively shallow. Reconstruction of a shallow alluvial fan undergoing liquefaction is a way to identify its shape dimensions. In this case, the reconstruction of a shallow alluvial fan (less than 30 m) uses a combination of outcrop data, lithology data, and N-SPT from JICA (2019) and Dwianca *et al*. (2020), Vs30 values (Triyono *et al*., 2024), and gravity values (Wardhana *et al*., 2024). The horizontal reconstruction results (Figure 4.3.6) show two alluvial fan shapes that tend to have a lobate shape . The lobate shape in the upper alluvial fan (KBA) is narrower, and is estimated to be younger than the lower alluvial fan (KBB). Vertically, shallow alluvial fans (up to 30 m depth) in the affected area are divided into four Groups with codes from oldest to youngest in sequence, namely KB-1, KB-2, KB-3, and KB-4.

The KBA alluvial fan is the youngest fan with Gmm and Gmg facies (massive and clast matrix-supported gravels). The KBA fan is estimated to be up to 15 m thick, and its lithology originates from debris flows. The lithology consists of granite fragments to gravel-sized boulders and the dominant matrix is fine to coarse sand and silt. The KBA fan is characterized by the contact of fragments with the sand-silt matrix being more dominant than the contact between rock fragments and some rock fragments are very few (Figure 4.3.7). The density value from the standard penetration test is relatively low (N-SPT less than 10). The low N-SPT value from BH-01 data at a depth of 2 m (Dwianca *et al*., 2020) when projected onto the crown outcrop will have a layer containing a lot of silt-sand and relatively few rock fragments (Figure 4.3.7).

The KBB alluvial fan is older than the KBA and it may be part of a debris flow containing granite rock fragments. The KBB fan has a thickness of up to 30 m based on available data and may be deeper. Drilling data only indicates grain size and does not clearly depict the contact between fragments. The determination of the KBB alluvial fan uses an analogy concept by utilizing outcrops in the upstream part of the affected area as the source material. Based on the

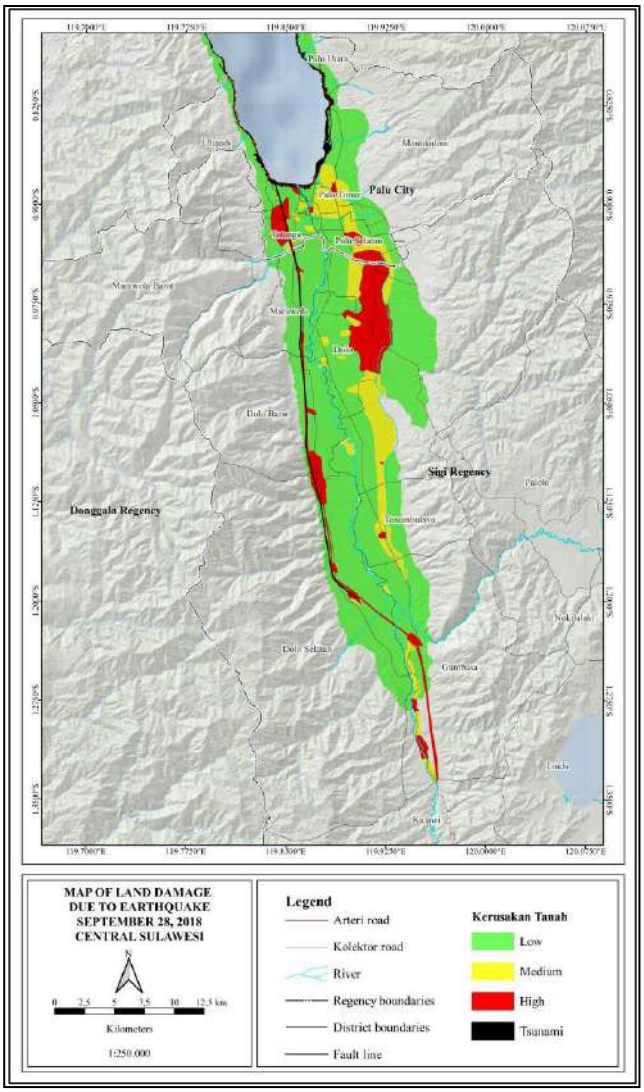

Figure 4.3.2. Ground surface damage map due to the earthquake of September 28th, 2018.

outcrops (Figure 4.3.8), the KBB in the affected area may part of the Gcm (clast-supported, massive gravels) and Gci (clast-supported gravels) facies. According to Miall (2006), the Gcm facies reflects a thick, pseudo-plastic debris flow from either laminar or turbulent flow. The Gci facies can reflect two conditions: a high-strength debris flow with abundant rock fragments or a low-strength debris flow with an inertial bed load in laminar or turbulent flow.

The KBB has a dominant contact between rock fragments rather than contact between rock fragments and the matrix. Standard penetration test data shows very high N-SPT values or very dense densities in the Gci facies, while the Gcm facies tends to have a range of N-SPT values that reflect densities ranging from medium to very dense.

Based on the results of mineralogical tests with x-ray diffraction (Figure 4.3.9), KBA has a

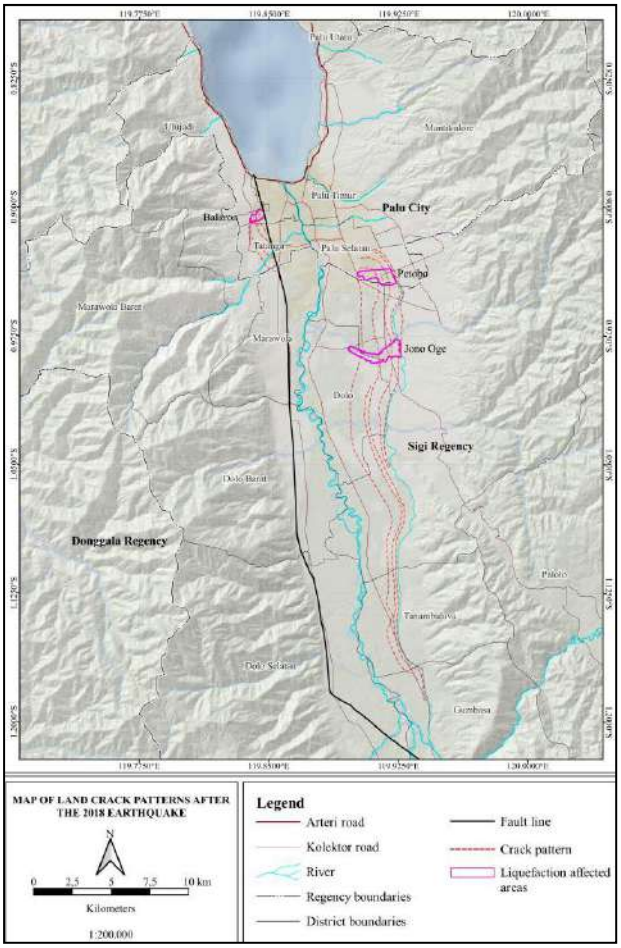

Figure 4.3.3. Ground crack patterns map after the 2018 earthquake.

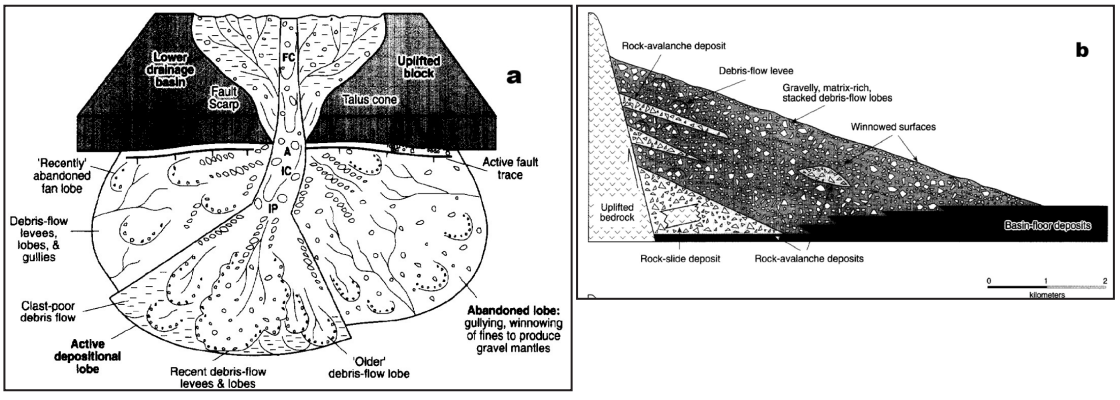

Figure 4.3.4. (a) Alluvial fan type I with sediment gravity flow of main process and (b) vertical cross-section of type I according to Blair and McPherson (1994) at Balaroa.

Figure 4.3.5. Lithological outcrop at the crown of the Balaroa landslide (Source: Buana, 2018).

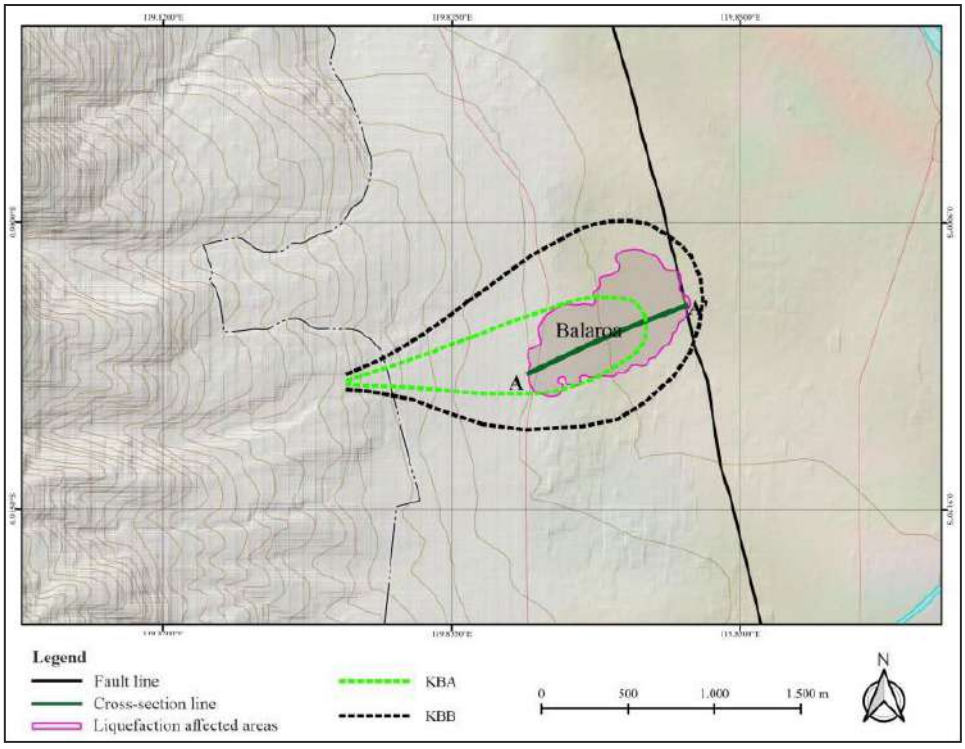

Figure 4.3.6. Reconstruction of the alluvial fan of the affected area in Balaroa.

Figure 4.3.7. Silty sand layer with relatively few fragments as part of the Gmm facies (Source: Buana, 2018).

Figure 4.3.8. Outcrop of the upstream part of the Balaroa impacted area which is analogous to the lithology of the KB-2 alluvial fan (Source: Buana, 2018).

more dominant amount of feldspar (38 %) than quartz (29 %) while KBB has a greater amount of quartz (37 %) than feldspar (15 %). Clay minerals in small amounts (2 % – 3 %) in KBA and KBB have montmorillonite and kaolinite except for the illite type which is only found in KBB. The difference between KBA and other KBB is the presence of minerals originating from ultrabasic (celadonite and pentlandite around 3 %) and calcite (5 %) in KBB, although in small amounts however it was not found in KBA. Based on the data, KBA and KBB are estimated to originate from the same dominant source, except at certain times it came from different sources. However, this condition is not explained in detail in this study.

Based on outcrop data on the Balaroa crown, borehole data and standard penetration test data

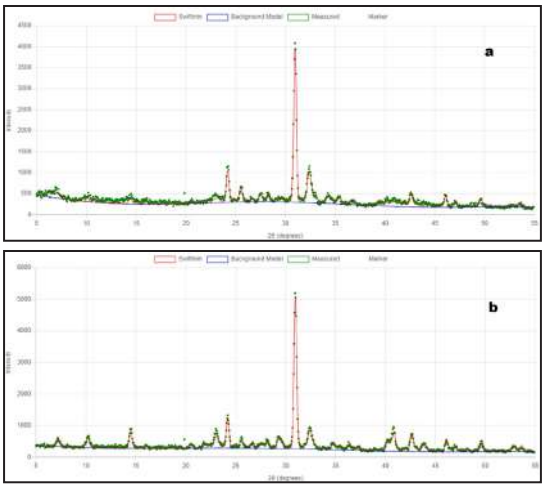

Figure 4.3.9. (a) X-ray diffraction test results pattern of KBA alluvial fan and (b) KBB alluvial fan.

in Dwianca (2020), and JICA (2019), electrical resistivity tomography from The Geological Agency in October 2018, Aswad *et al*. (2019), Tohari *et al*. (2021), visualization of subsurface geological conditions up to 30 m below ground level based on a geological profile cross-section in a relative west–east direction as in Figure 4.3.10.

The KBB alluvial fan consists of two phases of alluvial fan formation KB-1 and KB-2. The KB-1 subgroup consists of granite rock fragments up to the size of gravel boulders that are abundant compared to the KB-2 subgroup. The KB-2 subgroup has almost the same character as KB-1. The difference is in the amount of medium–coarse sand that it has medium to dense density and more abundant than the KB 2 subgroup that it has dense to very dense sand density. KB-1 is estimate as Gci facies, while KB-2 is a Gcm facies according to the Miall (2006) classification.

The KBA alluvial fan consists of two phases, namely the KB-3 and KB-4 subgroups. KB-3 consists of silt, clay with a mixture of sand, stiff to hard consistency. KB-4 consists of a lithology that mixture of abundant sand–silt with low density mixed with granite rock fragments up to boulders. KB-3 is estimated as Gmm facies while KB-4 is a Gmg facies according to the Miall (2006) clas-

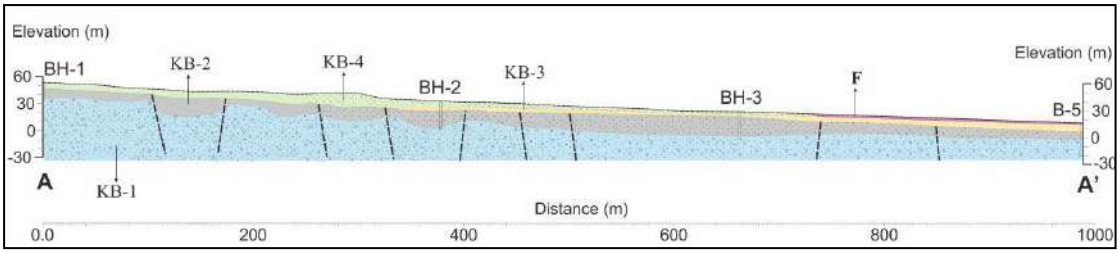

Figure 4.3.10. Cross-section of the geological profile of the Balaroa liquefaction affected area from west to east.

sification. The F symbol is fluvial consisting of low to medium density silt sand which is the result of fluvial processes, and it does not include debris flow deposits such in the KBA and KBB groups. It is estimate as Fsm facies with an environment towards swamps.

The interpretation of the cracks (Figure 4.3.10) is derived from the electrical resistivity topography, which has relatively contrasting resistivity values. The cracks generally have values of less than 60 ohm m, and they may continue to a depth of more than 40 m. These continuous cracks have relatively low resistivity values and indicate the possibility of the cracks being filled with fluid (water). Based on observations of cracks on the ground surface, the interpretation of the cracks (Figure 4.3.10) is related to the ground cracks that occurred on September 28th, 2018 (Figure 4.3.3). The post-earthquake crack pattern (Figure 4.3.2) depicts a negative flower structure pattern. The downstream surface rupture is part of The Palu Koro Fault system. Natawidjaja *et al*. (2021) conducted research in Palu Bay, and one important point was the identification of negative flower structures along the main fault in the western part of Palu Bay, which become shallower or disappear as they move towards the coast. Wu *et al*. (2021) create a model that show the Balaroa impact area as part of a negative flower structure.

The affected area of Balaroa liquefaction may part of a negative flower structure (Figure 4.3.5) that existed before the September 28th, 2018 earthquake. The ground cracks in the Balaroa liquefaction-affected area may result from the reactivation of ancient buried cracks.

Data that support the interpretation is the swamp environment in downstream of the affected area lies along the September 28th, 2018 surface rupture. The results of the Geological Agency carbon dating test on the swamp environment in downstream of the affected area at a relatively shallow depth (2.3 m) and the age approximately 805 ± 185 BP. The swamp environment that stretches in the same direction of the surface rupture may a local basin (sag ponds), and part of ancient fault. It indicates that there was earthquake activity that triggered the fault in the past and the possibility of cracks might forming as part of a negative flower structure pattern in the KBB alluvial fan group. Then the KBA alluvial fan deposits covered the KBB alluvial fan.

The confined groundwater conditions around the affected area in Balaroa have been inventoried by the Geological Agency in Ruchijat *et al*. (1989) and updated by Suryaman *et al*. (1995). Suryaman *et al*. (1995) identified a confined water zone (Figure 4.3.11) and overlapped it on downstream of the liquefaction-affected area that triggered the flow slide, such as in Balaroa, Petobo, and Jono Oge. It indicates that before the liquefaction event that triggered the flow slide, the water pressure conditions around the toe area had relatively high pressure from a confined aquifer. Widodo (2019) concludes that the aquifer system is semiconfined/confined. have contributed to worsening liquefaction and landslide in Petobo, Jono Oge, and Balaroa. The contribution is a connection hydraulics between the unconfined aquifer system and semiconfined/

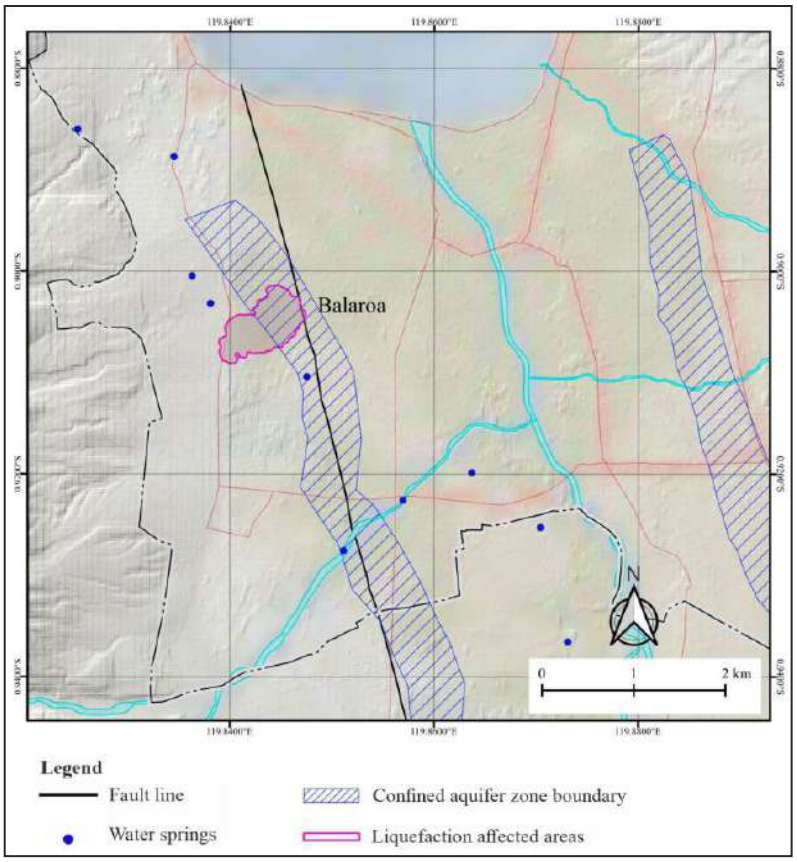

Figure 4.3.11. Confined aquifer surrounding Balaroa (Suryaman, 1995).

confined aquifer system to dissipate the confined aquifer system and trigger groundwater flow massive from confined aquifer system to unconfined aquifer system. The confined aquifer in Balaroa lies at a depth more than 55 m (Widodo, 2022).

Isotope values in dug well and borehole in several locations in Balaroa have low values (approximately -9 ‰). The value indicates the contribution of a confined groundwater flow system (deep groundwater flow) that flows vertically to the unconfined aquifer system (shallow groundwater flow) through an inter-aquifer transfer mechanism (leaky aquifer). Widodo (2022) says that stable isotope data ($\delta^{18}O$ and $\delta^{2}H$) confirm the water source from the deep aquifer through new springs after the earthquake.

4.3.1.2. Liquefaction Safety Factors in The Balaroa Affected Area

The sediment deposition process in Balaroa is a debris flow that forms an alluvial fan, as explained in the previous paragraph. The liquefaction that triggers landslides in Balaroa is related to the geological history of sediment deposition and engineering properties values, generally. Safety factor of liquefaction can determine the condition of the lithology strength against liquefaction that directly begins with earthquake shaking. Data from standard penetration tests, cone penetration tests, and other soil density tests were not 18th, 2018. The assumption is post-earthquake standard penetration test values have the same values as before the earthquake. Data that used in the analysis are boreholes and standard penetration tests

from Dwianca *et al*. (2020) for locations BH-01, BH-02, BH-03, and JICA (2019) for location B-5.

The back analysis uses the cyclic stress concept (Seed and Idriss, 1971) and the calculation procedure uses the guidelines from Youd and Idriss (2001). The peak ground acceleration of Balaroa on September 28th, 2018, was 281 gal in the east-west direction, 203 gal in the north-south direction, and 335 gal in the vertical direction (Dwianca *et al*., 2020). The analysis uses 335 gal of peak ground acceleration value. The calculation results indicate that liquefaction is likely to occur (safety factor less than 1) in several lithological layers in red colour (Figure 4.3.12a). The layers that prone to liquefy are in the KB-3 and KB-2 subgroups.

Flow liquefaction is part of contractive soil, and according to Robertson (2017) flow liquefaction can occur in almost saturated or saturated contractive soils such as in very loose sand, silt or sensitive clay. Fear and Robertson (1995) have made a boundary line between contractive and dilative soils by connecting the value of N1 (60) with overburden effective stress. Scot and Olson (2003) evaluated several boundary lines and provided recommendations for using boundary lines according to Fear and Robertson (1995) to distinguish contractive and dilative soil properties in a practical field approach. Based on Fear and Robertson (1995), Balaroa up to a depth of 20 m? shows contractive in the upstream (BH-1 and BH-2) and toward downstream (BH-3 and B-5) tends to be dilative, relatively (Figure 4.3.12b).

Iwasaki *et al.* (1981) propose a liquefaction potential index to assess the level of liquefaction. The liquefaction potential index is divided into four classes, *i.e.* very low (PL = 0), low (0<PL < 5), rather high (5<PL < 15), and very high low (PL > 15). BH-02 is very high, while the others are rather high (Figure 4.3.13). If a simulation of the

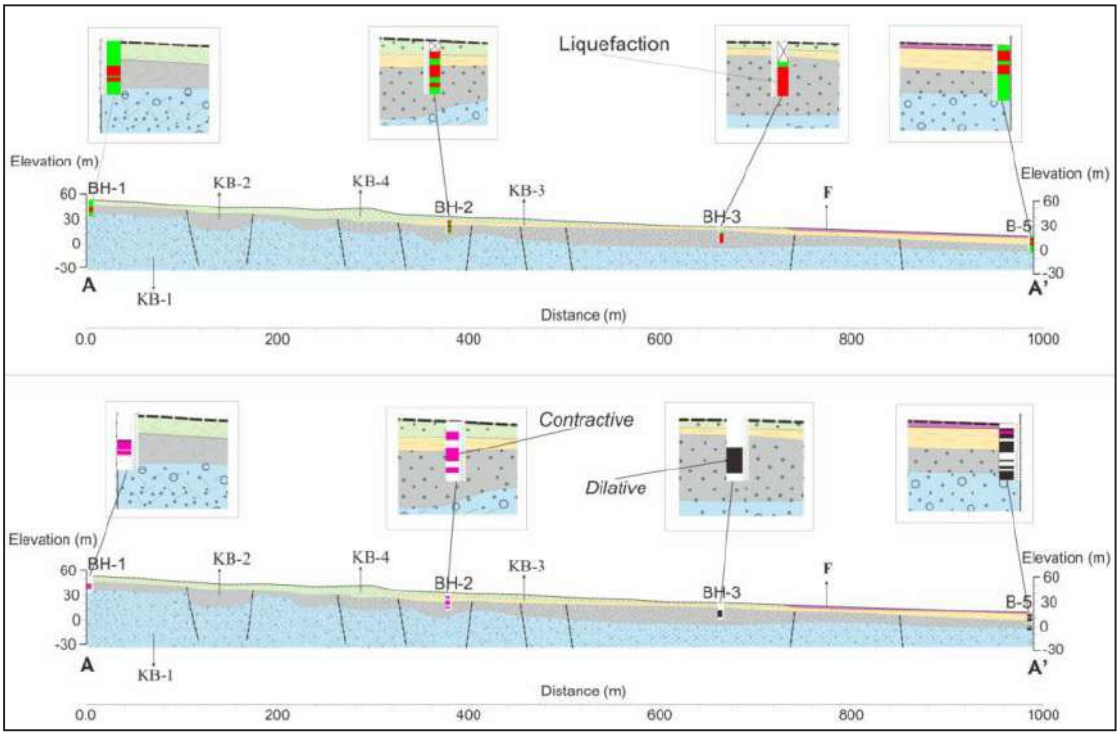

Figure 4.3.12. (a) Reconstruction of lithology that prone to liquefy (red) and (b) reconstruction of contractive (purple) and dilative (black) behaviour at Balaroa.

critical point of liquefaction is carried out, BH-02 is the weakest point of liquefaction compared to the other points and only requires 0.1g to initiate liquefaction (Figure 4.3.14).

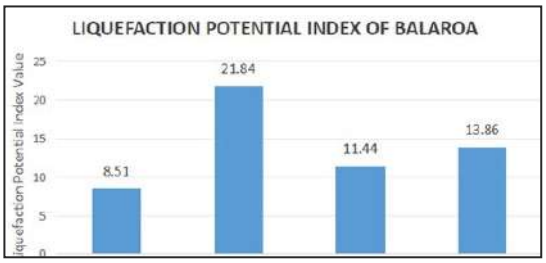

Figure 4.3.13. Liquefaction potential index of BH-01, BH-02, BH-03, and B-5 at Balaroa.

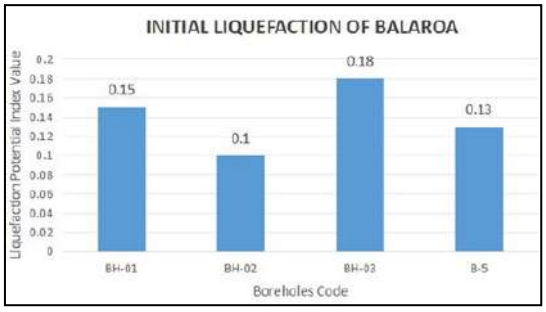

Figure 4.3.14. Initial liquefaction of BH-01, BH-02, BH-03, and B-5 at Balaroa.

4.3.1.3. Identification of Weak Layers Susceptible to Liquefaction That Trigger Landslides in Balaroa

The weakening of the N value from the standard penetration test results lies in the alluvial fan subgroup KB-3 (N<10) of the Gmm facies and KB-2 which has N between 10 to 22 of the Gmg facies. Based on sediment flow classification, Schultz (1984) propose four types of flow regimes (Figure 4.3.15). Alluvial fan KB-3 has type I (plastic debris flow) and KB-4 has type III (pseudoplastic debris flow). KB-1 has type IV (pseudoplastic debris flow inertial bedloads), while KB-2 has type III. The Gmm and Gmg facies according to Miall (2006) classification are equivalent to the Dmm and Dmg facies which are respectively included in type I and type III according to Schultz (1984). Type I describes a large flow and high yield strength in slurry deposits (sediments are a mixture of solids and liquids such as mud or paste). Type I shows an increasing fine fraction due to the laminar flow process. Type III characterizes a relatively high increase in water content from laminar or turbulent flow, a low yield point, so that it deposits more coarse fractions and rock fragments. Type IV is like type III except that there is a collision process of rock fragments.

Based on borehole data and standard penetration tests of locations B-1 (JICA, 2019) and BH-1 (Dwianca, 2020) and crown outcrop data (Figure 4.3.5), resistivity data and calculations of safety factors against liquefaction, weak layers that prone to become slip surface (safety factors less than 1) are in the KB-3 subgroup layer (Gmm facies) that it has type I sediment flow type (Figure 4.3.16). Safety factors less than 1 or liquefaction layers are also found in the KB-2 subgroup (Gmg facies) which is positioned below KB-3. Despite having the same matrix supported, KB-2 is not included as a slip surface in the reconstruction, because the N-SPT value is greater than KB-3 (medium to dense density).

Genetically, KB-3 (type I) may the result of evolution from KB-2 (type III) and KB-1 (type IV) due to the reduction in water content during the downstream sedimentation process. According to Schultz (1984), the flow yield point increases and the loss of water during the downstream journey causes the deposition of rock fragments first. Then, the sediment has increasingly fine grains downstream and the evolution change type IV or III to type I. Mineralogical data from XRD tests (Figure 4.3.9) emphasize the evolutionary process, because the alluvial fan system up to a depth of 30 m (KBA and KBB) originates from relatively the same source.

The dominance of feldspar and quartz and a very small amount of clay minerals (2 %-3 %) cause the layer to be noncohesive. Wagner (2013) says that soil strength depends primarily on the contact between grains.

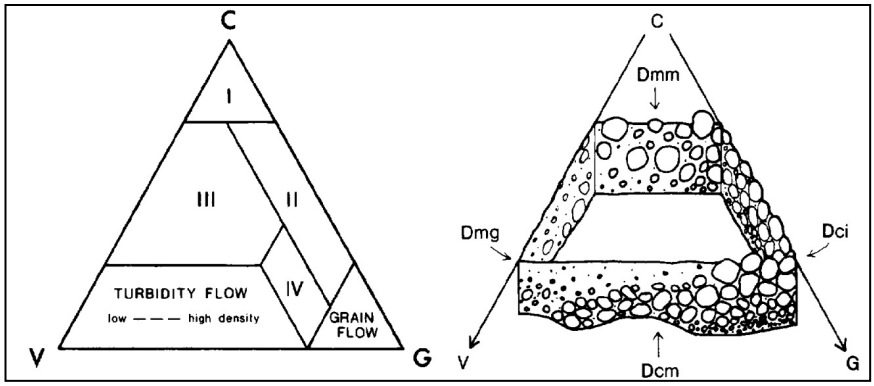

Figure 4.3.15. Conceptual sediment flow classification (Schultz, 1984).

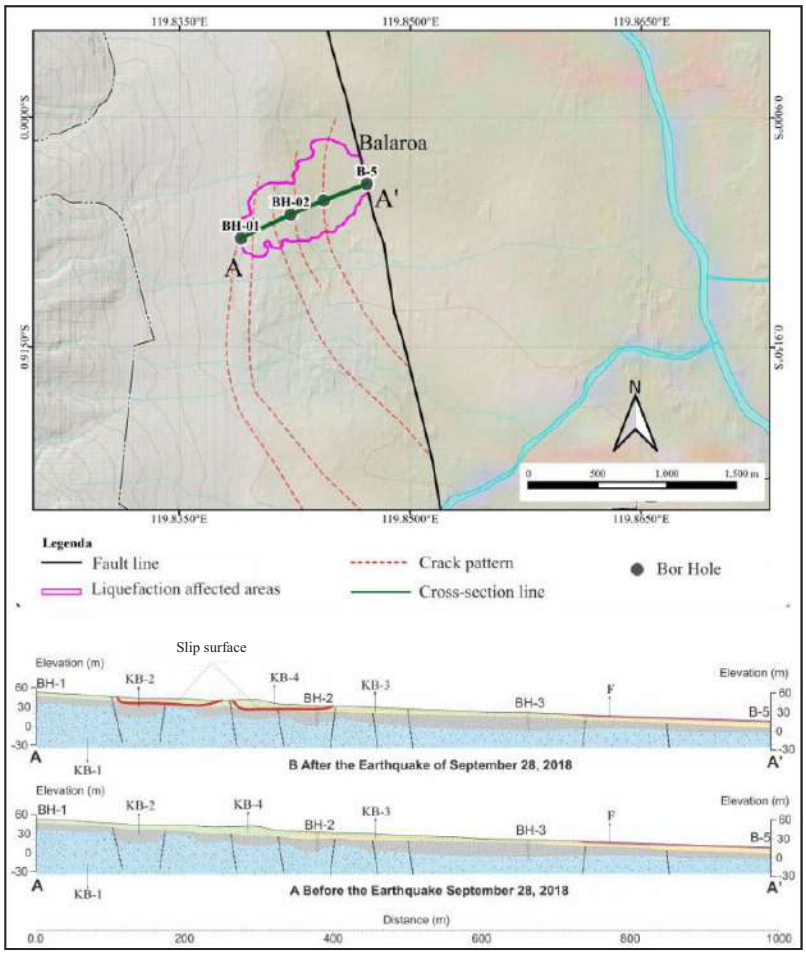

Figure 4.3.16. Reconstruction of the slip surface (red line) based on post-earthquake soil crack and water seepage data, lithology, N-SPT value, resistivity value, and the results of the calculation of the safety factor value against liquefaction.

4.3.1.4. The role of water pressure from confined aquifers in liquefaction that triggers landslide in Balaroa

The liquefaction process requires strong pore water pressure. Different perspectives on the origin of water pressure source have become dynamic discussion topic. Based on observations and geological data recordings of surface damage at Balaroa a week after the earthquake, the liquefaction that trigger the landslides had specific characteristics. Key points observed were major faults, ground cracks, springs, and a dominant matrix-supported layer with a noncohesive silt-sand grain size.

The main fault is located near the downstream of the Balaroa impact area, and ground cracks have formed in an arc-like pattern (Figure 4.3.3). The cracks may part of a relatively deep (over 40 m) negative flower structure based on electrical resistivity tomography test (Figure 4.3.10). Observations on the crown of approximately 7 m showed water seepage in the mixed sand and silt layer (matrix supported) that N-SPT value approximately 8, while projected onto the BH-01 (Dwianca, 2020). Water seepage was not only found in the crown, but also in other locations of the Balaroa landslide.

The impermeable layer that indicating a shallow confined aquifer (less than 30 m) is found from the center of landslide toward the downstream. The results of the JICA (2019) physical properties analysis in the downstream section (Bor B-5), show the dominance of fine fractions (around 60% -80%) have low plasticity, so that this layer is semi-impermeable or a semiconfined aquifer, and the further towards the crown it is likely to be an unconfined aquifer. It shows that stress conditions are not fully undrained. The suspected possibility of the liquefaction process that triggers landslides does not only come from the unconfined aquifer, but water pressure can occur from multilayered confined aquifers. Multilayered confined aquifer is connected to the unconfined aquifer through a fractured medium due to the formation of a negative flower structure.

Interviews with local residents during data collection indicated that there was a time lag of several minutes after the earthquake ceased for flow landslides to occur. Similarly, Mason *et al.* (2021) stated that flow slide are not co-seismic events, but occur several minutes after the earthquake ends. The water film concept, as proposed by Kokusho *et al.* (2025), may occur in shallow, semiconfined aquifers, but the high water pressure from the confined aquifer to the unconfined aquifer through vertical fractures may have a more destructive effect, leading to flow landslides.

In case, the hypothesis of liquefaction occurs not only from excess pore water pressure in the weak layer, but also the contribution of water pressure from the confined aquifer layer that provides relatively large water pressure on the weak layer through the media of cracks that formed during the earthquake process. Buana *et al.* (2018) mentioned that the water pressure process that triggered liquefaction through cracks that formed simultaneously with the ground oscillation process in low-plasticity silt material that was " sand-like ". Ridla *et al*. (2012) conducted experiments on cracks in silt layers related to liquefaction and stated that the cracks in silt layer due to earthquake shocks caused a large settlement at the bottom of the silt layer as a result of the rapid dissipation of excess pore water pressure. Cracks in the silt layer can cause pore water pressure to decrease drastically in the soil layer below the silt layer and will increase drastically in the soil layer above the silt layer. Widodo *et al*. (2019) mentioned the contribution of the connection hydraulics between the unconfined aquifer system and semiconfined/confined aquifer system in order to dissipate the aquifer system under pressure cause groundwater flow massive from confined aquifer system into the unconfined aquifer system.

Data that emphasize the contribution of confined aquifers to the liquefaction process that triggered landslides at Balaroa before the earthquake of September 28, 2018, are similar data of confined aquifers zone that refer to Ruchijat *et al*. (1989), and it was updated by Suryaman *et al.* (1995) in Figure 4.3.10 and electrical resistivity

tomography around Balaroa (Marjiyono, 2013) in Figure 4.3.16. Data after the earthquake are ground crack data, isotope data, eletrical resistivity tomography, and confined aquifer contours (Abdullah *et al*., 2024).

Indications of confined aquifers (black arrows) from electrical resistivity tomography (Figure 4.3.17a) Marjiyono (2013) and the post-earthquake electrical resistivity tomography in the crown section (Figure 4.3.17b) show a combination with tectonic process cracks and possibly have the same pattern up to the Palu valley section. The relatively small resistivity value (less than 60 ohm m) and relatively vertical concentric patterns intersecting with relatively large resistivity values suddenly indicate the role of tectonics that controls the pattern of the confined aquifer zone through vertical cracks. The confined aquifer zone is estimated to reach a depth of more than 40 m.

The contours of confined aquifer around the affected area change in same value contour lines between 1995 and 2024 (Figure 4.3.18). Some contours indicate an increase and decrease groundwater level of confined aquifer. It may due to the cracking process that affected the confined aquifer layer that occurred due to negative flower structure during the earthquake of September 28th, 2018. In the case of the 2008 Wenchuan Earthquake, Shi and Wang (2016) stated that there had been a change in the confined aquifer to a semiconfined one due to the reopening of old vertical cracks. Liao *et al*. (2015) argued that the 2008 Wenchuan Earthquake disrupted the groundwater system by damaging the bonds between the aquitards attached to the confined aquifer through old cracks or the formation of new cracks, thereby changing the permeability and poroelastic properties of the groundwater system.

Geologically, downstream approximately 1 km from the Balaroa affected area, there are swamp deposits that may part of the sagponds from the ancient Palu Koro Fault. The age was approximately 805±185 BP based on carbon dating data from The Geological Agency at a depth of 2.3 m. The results of The Geological Agency carbon dating test at a depth of 27 m and the age

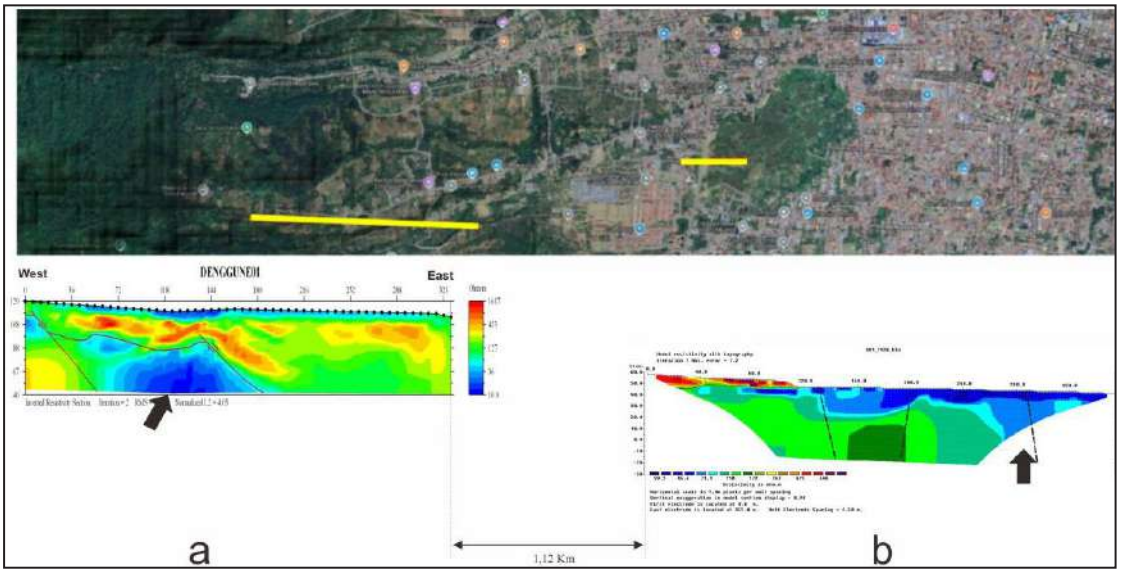

Figure 4.3.17. (a) Interpretation of the electrical resistivity tomography of the upstream part of the affected area (Marjiyono, 2013) and (b) the crown of the Balaroa affected area in 2018 which shows a combination pattern between geological structures and confined aquifer zones (blue colour).

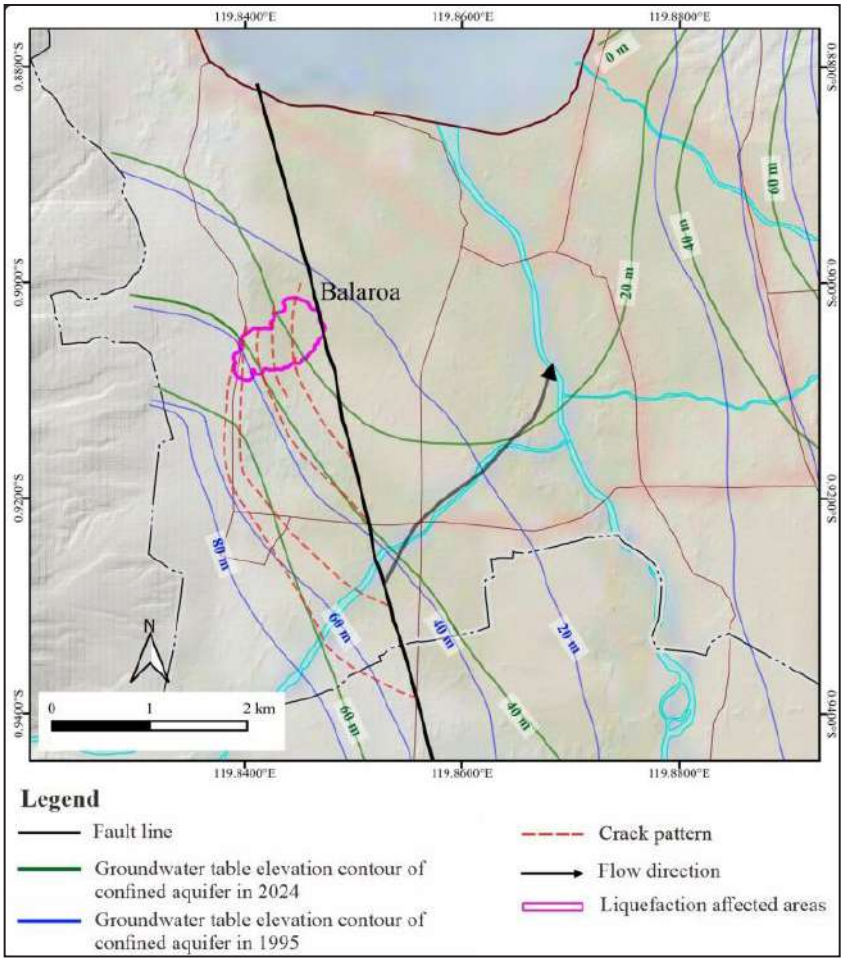

Figure 4.3.18. Groundwater elevation contour changes of confined aquifer before (Suryaman *et al*., 1995) and after the September 28th, 2018 earthquake at Balaroa (Abdullah *et al*., 2024).

was approximately 6306 ± 272 BP that it may equivalent to the alluvial fan of the KB-1 sub-group. It indicates that after the formation of the KBA alluvial fan there was seismic activity that caused the formation of swamp deposits which are estimated to be sagponds that formed by The Palu Koro Fault.

The September 28th, 2018 cracks are part of ancient negative flower structure whose crack section has closed and then reactivation again. According to Shi and Wang (2016), the change from a confined to a semiconfined aquifer is due to an earthquake opening old vertical cracks and will close over time. Observations of isotope data in Balaroa (Abdullah *et al.,* 2024) mention that the borehole (SB) shows the lowest isotope values ($\delta^{18}O$: -9.0 ‰ to -6.5 ‰; $\delta^{2}H$: -80 ‰ to -50‰), and it may come from deep aquifer or recharge in the mountainous zone with a long residual time (>100 years). Widodo (2022) observed isotopes from new springs after the 2018 earthquake at Balaroa, and it shows $\delta^{18}O$ values of -9.45 ‰ and $\delta^{2}H$ of -58.62 ‰.

The nearly identical values between the deep well and the springs indicate that cracks have formed that cut through the confined aquifer and

some have emerged to the surface as new springs. Whether the cracks formed during the September 28th, 2018 earthquake were old, buried cracks or new cracks is a challenge to be studied in detail in the future, because the data is still not well available.

The process of increasing excess pore water pressure that causes liquefaction may occur in the weak layer near the ground surface. Elsewhere, liquefaction induced flow landslide wait from relatively strong water pressure process from a confined aquifer that experienced vertical cracks towards the weak layer within minutes after the earthquake based on information from local residents and Mason *et al*. (2020). Time lag is qualitative information and requires verification and specific study. As a comparison, Wang (2004) mentioned the time required for increased river water discharge due to the process of opening cracks connecting deep aquifers for 15 minutes in the case of the San Siemon earthquake, California in 2003.

4.3.2. Petobo

4.3.2.1. Geology of The Affected Area at Petobo

Based on the Blair and McPherson (1994) classification, Petobo is part of a type II alluvial fan system (Figure 4.3.19). Dominant primary process of type II alluvial fan is the sheetflood process that unrestricted flow of water that carries sediment and spreads in all directions toward the fan slope, because it is not limited by channel walls.

Sheetflood-couplet is a typical character and in general fine grains (laminated sand and gravel) are generally more than coarse grains (gravel and cobble).

The outcrop (Figure 4.3.20) of Petobo crown flow landslide (outcrop height approximately 7 m) is a mixture of granite and metamorphic rock debris. Genetically, it consists of architectural elements of sandy bedforms that it has sand lithofacies and architectural elements of sediment gravity flows that it has gravel lithofacies according to Miall (2006) classification. Traction facies such as Sm (massive sand), Sg (gravelly sand), and Sh (horizontally laminated sand) develop more frequently and thicker than Balaroa site. The vertical transition from Gmg (matrix supported gravel) to Sm and Sh shows the phenomenon of waning flow that describe gradual decrease in flow energy in a single sedimentation event. This process produces a downward grained arrangement pattern (fining upward) with parallel lamination structures or massive sand layers.

Although traction facies are present, the typical characteristics of braided fan systems are not found, such as repeated accumulation of river channel deposits, Sp (Sand planar cross-bedded) and St cross structures (Sand

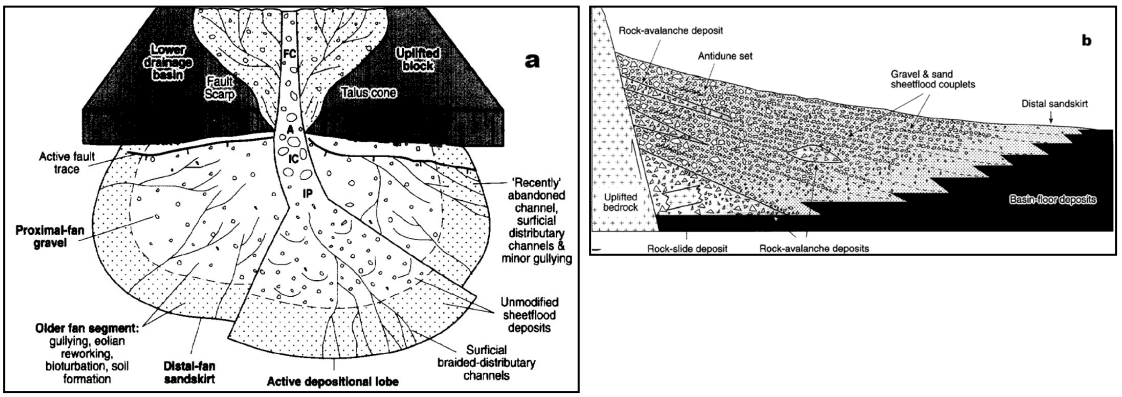

Figure 4.3.19. (a) Type II alluvial fan with the main process of *sheetflood-couplet* and (b) type II vertical cross section according to Blair and McPherson (1994) in Petobo.

Figure 4.3.20. The outcrop of the Petobo landslide crown showing alternating layers of gravel - pebbles (sediment gravity flow products) and sand (sand bedforms products) (Source: Buana, 2018).

trough cross-bedded), changes in river position and fluvial facies arrangement patterns that are interconnected both laterally and vertically. The traction facies present are more in the form of individual layers or limited intercalations, without showing a repeating fluvial depositional pattern. This indicates that the dominant process is sheet flood which in terms of facies shows the characteristics of wa n ning flow due to the weakening of traction energy.

The potential for liquefaction in Petobo in 2012 was predicted by Widyaningrum *et al*. (2012) with a high category and has occurred in 2018. Liquefaction induced landslides lies in the alluvial fan in Petobo at a depth of less than 15 m qualitatively from field observations. Reconstruction of shallow alluvial fans (less than 30 m) using a combination of outcrop data, lithology data and N-SPT from JICA (2019) and Upomo *et al*. (2023), Vs30 values (Triyono *et al*., 2024), and gravity values (Wardhana *et al*., 2024). The results of the reconstruction around the Petobo affected area horizontally (Figure 4.3.21) estimated that there are four alluvial fans covering the affected area to a depth of 30 m. The order of fans from young to old is KPA, KPB, KPC, KPD, KPE. Alluvial fans generally have an arc shape except for the lobate-shaped KPC fan which it may part of a very dominant sediment gravity flow architectural element, while the others tend to be predominantly sand bedform architectural elements.

KPA from outcrop data in the crown, boreholes data BH-1 and BH-4 (Upomo, 2023) consists of facies Sm which has a relatively low N value from standard penetration tests up to 3 m. KPB may consist of facies Gmm from borehole data LP-2 (JICA, 2019) and N value of more than 50. KPC based on outcrop data in the crown, boreholes data BH-1, BH-4, and BH-2 (Upomo, 2023) and LP-4 (JICA, 2019) consists of facies Gmg alternating with facies Sm and Sh. Standard penetration tests tend to provide high N-SPT values (more than 50), while in facies Sm/Sh tends to be relatively low (less than 10). KPD may safe on the Petobo affected area. KPE based on upstream Petobo outcrop data (Figure 4.3.22) and boreholes data BH-1, BH-4, BH-2 and BH-5 (Upomo, 2023); LP-1, LP-2, and LP 4 (JICA, 2019) consist of alternating Gcm facies which are thicker than Sm facies. Standard penetration test on its facies is relatively high with N-SPT value more than 50.

Based on the results of mineralogical tests with x-ray diffraction on alluvial fans that have an influence on the Petobo affected area (KPA, KPB, KPC, KPE), alluvial fans KPA, KPC, and KPE originate from the same material source, but have different deposition time intervals, while KPB may come from different sources. The difference is the average composition of the main minerals of KPA, KPC, KPE for feldspar (43 %) and quartz (24 %) less than KPB which has an average percentage of feldspar (58 %) and quartz (28 %). In addition, KPA, KPC, KPE have magnesiohornblende, barroisite and laumonite minerals that are not found in KPB.

The depiction of the geological profile cross-section in the Petobo affected area (Figure 4.3.23) uses outcrop data and electrical resistivity tomography from the Geological Agency, and electrical resistivity tomography, boreholes data, standard penetration test values of BH-1, BH-4, BH-2, BH-5 (Upomo, 2023). Vertically, the subsurface geological conditions up to a depth of 30 contain three alluvial fan groups and one fluvial environ-

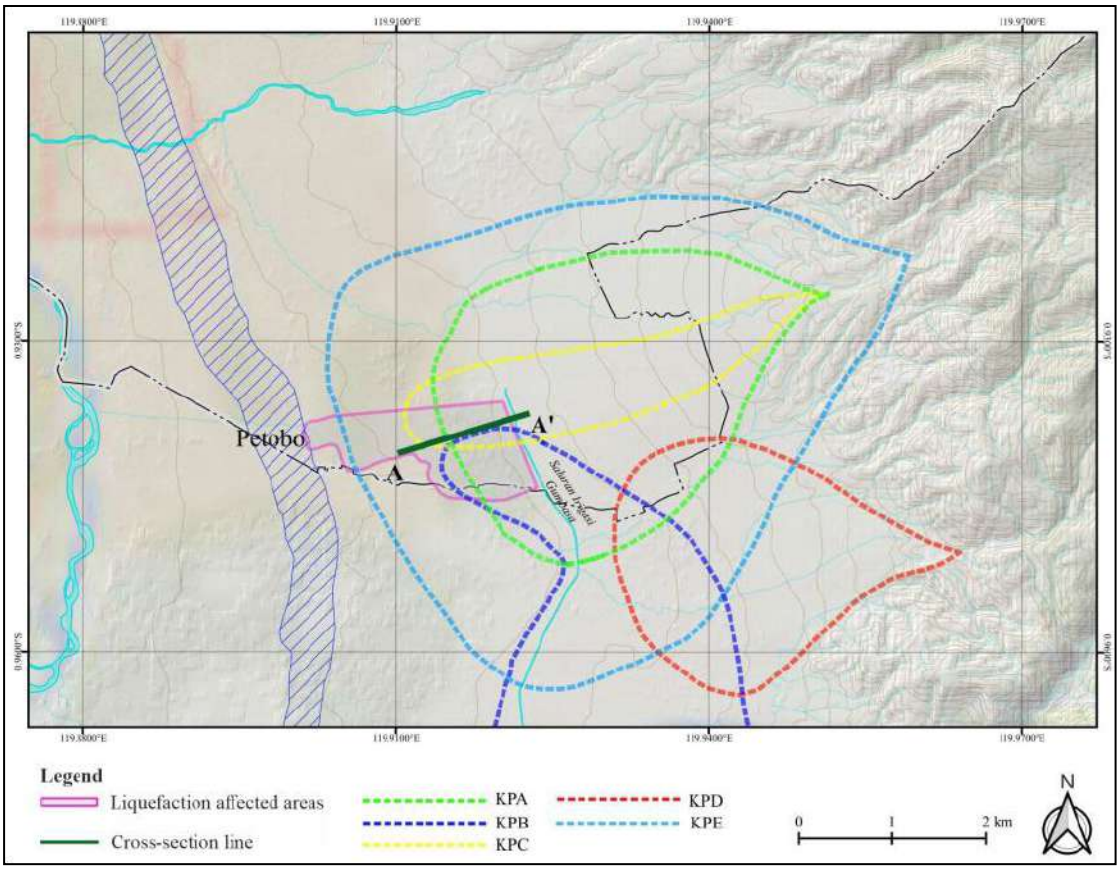

Figure 4.3.21. Reconstruction of the alluvial fan of the affected area in Petobo.

ment with the code F. The downstream section in BH-5 at the top is estimated to originate from the distal alluvial fan of a different system from the alluvial fan in the Petobo impacted area, and is mixed with fluvial processes so that fine-grained lithology is found. Based on the contrasting differences in resistivity values, the affected area has a geological structure in the form of vertical faults filled with fluids with small resistivity values (less than 60 ohms).

Suryaman *et al.* (1995) had identified a confined water zone in Petobo that it had located approximately 2 km downstream of the Petobo landslide crown (Figure 4.3.24). The map was created while the Gumbasa irrigation canal was still active. Two active springs (Ruchijat, 1989) were recorded within the affected area, although it was not stated whether they originated from seepage of the Gumbasa irrigation canal or from the aquifer.

4.3.2.2. Liquefaction Safety Factors in The Petobo Affected Area

Data that used in the analysis are boreholes data and standard penetration tests from Upomo *et al.* (2023) for locations BH-1, BH-4, BH-2, and BH-5. The peak ground acceleration value at Petobo during the September 28th, 2018 earthquake is not available, but Kiyota (2025) stated that the estimated maximum ground acceleration value according to JICA was 471 gal. Based on the assumption that the N-SPT value before and after the earthquake is the same, the calculation results indicate that liquefaction may have oc-

Figure 4.3.22. Gcm facies outcrop in the upstream part of the Petobo affected area which is analogous to the lithology of the KPE alluvial fan (Source: Buana, 2018).

curred in several red lithological layers (Figure 4.3.25a). The layers may liquefaction can reach 20 m in the KPA, KPC, and KPE alluvial fan groups. The general pattern of contractive soil properties starts from BH-1 to BH-2, while BH-5 tends to be dilative, because BH-5 has a mixed lithology from different sources than BH-1, 4, and 2 (Figure 4.3.25b).

The liquefaction potential index in the affected area (Figure 4.3.26) has high liquefaction potential category according to the classification of Iwasaki *et al*. (1981). If a simulation of the critical point or initial liquefaction is carried out, BH-2 and BH-4 are the points which they have the weakest liquefaction compared to other points and only require a force of 0.07g to start liquefaction (Figure 4.3.27).

4.3.2.3. Identification of Weak Layers Susceptible to Liquefaction Induced Landslides in Petobo

Based on post-earthquake ground cracks and water seepage data, lithology, N-SPT values, resistivity values, and the results of calculations of safety factors against liquefaction, the reconstruction of the main slip surface of the liquefaction (Figure 4.3.28) induces flow slide process was at a relatively shallow depth (less than 15 m) and the toe part of the ground movement was around BH-2.

The slip surface may part of the KPC alluvial fan (Sm/Sh facies consisting of silty sand) and KPE (Gcm facies consisting of sandy gravel−gravelly sand). Genetically, KPC alluvial fan has a sand mixed grain size and silt deposited from the primary process of sheet flood which is a characteristic of type II alluvial fans. On the other hand, a secondary process that commonly found in type II alluvial fans is the winnowing process (Blair and McPherson, 1994). It is the natural process of sorting fine material from coarse material by water or wind flow.

4.3.2.4. The role of water pressure from confined aquifers in liquefaction induced landslide

The hypothesis of liquefaction induced landslide at Petobo was not only from the Gumbasa water channel, but there was a strong control from the ruptured confined aquifer, so that it provided large water pressure to the unconfined aquifer zone.

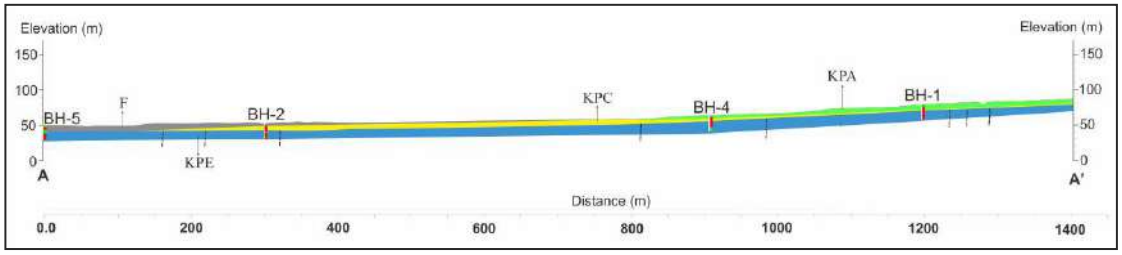

Figure 4.3.23. Cross-section of the geological profile of the Petobo liquefaction affected area from west to east direction.

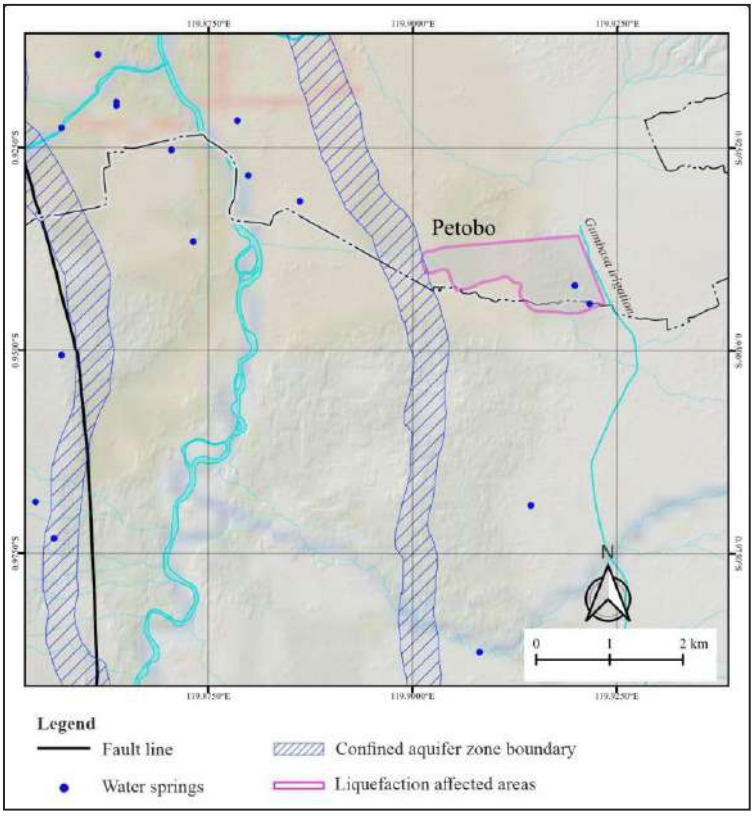

Figure 4.3.24. Confined aquifer surrounding Petobo (Suryaman, 1995).

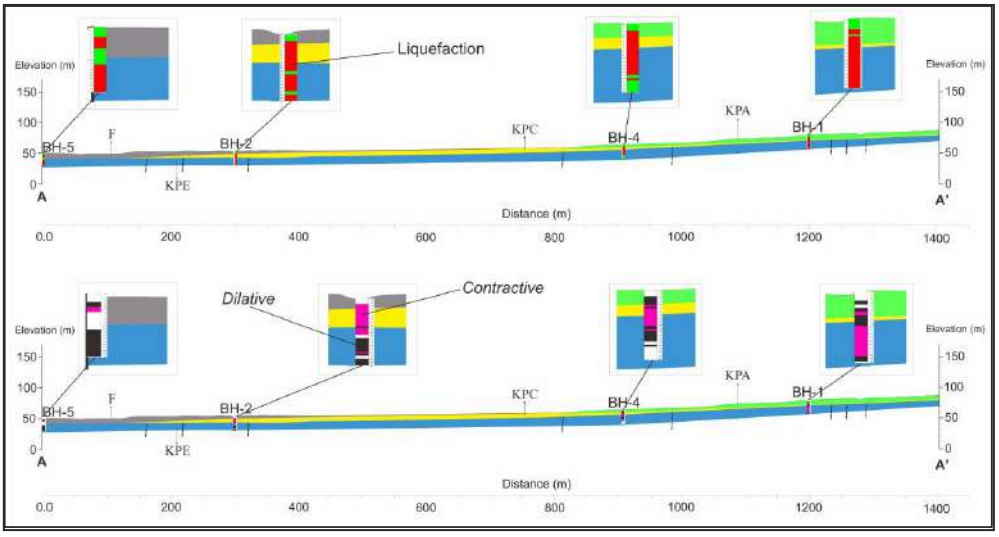

Figure 4.3.25. (a) Reconstruction of lithology that it may liquefaction (red) and (b) reconstruction that is contractive (purple) and dilative (black) in Petobo.

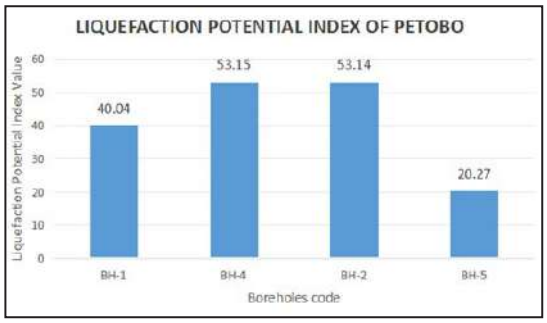

Figure 4.3.26. Liquefaction potential index at locations BH-1, BH-4, BH-2, and BH-5 in Petobo.

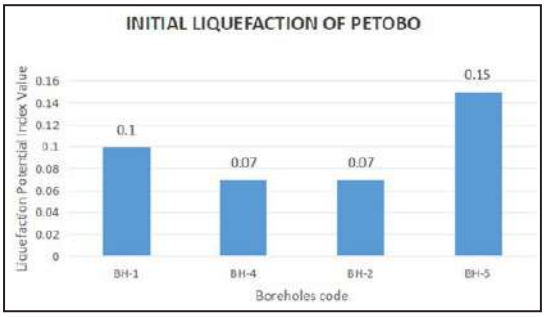

Figure 4.3.27. Initial liquefaction at locations BH-1, BH-4, BH-2, and BH-5 in Petobo.

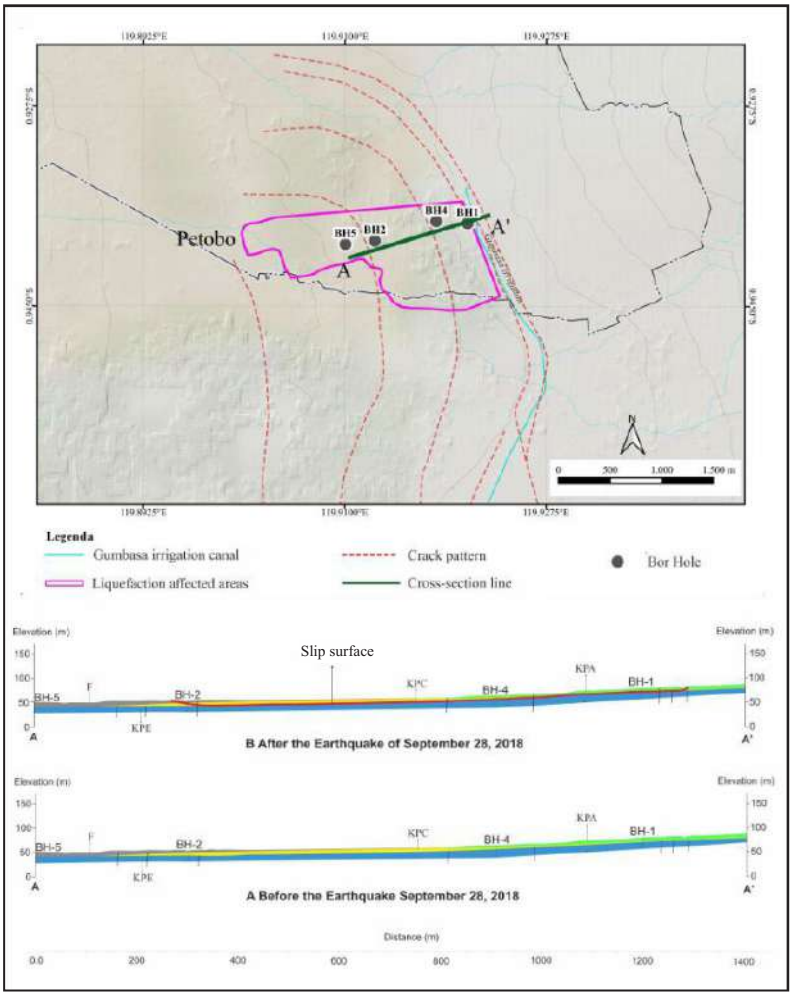

Figure 4.3.28. Reconstruction of the slip surface (red line) of the Petobo, and the results of calculations of safety factors against liquefaction.

Kiyota (2025) stated that the influence of the irrigation channel in the eastern part of The Palu Valley only affected the upper part of the landslide, and had a small effect on the mechanism of landslide, while groundwater rising from the confined aquifer was a strong control of the mechanism of landslide.

Kusumawardani *et al*. (2021) conducted interviews with residents that there was highlight information such as the emergence of warm water in the fracture zone and the presence of hot water in a 130 m deep well near Petobo. The Geological Agency had drilled a well to provide clean water for evacuees in the Petobo temporary shelters and obtained hot water at a depth of 60 m. The well location is approximately 1.4 km from the crown of the upstream Petobo landslide. This indicates that hot temperature of confined aquifer may come from vertical cracks leading to the affected area and mixing with the normal temperature of upper aquifer. Based on the 2016 Kumamoto earthquake, Tsuji *et al*. (2017) stated that the 7.0 Mw Kumamoto earthquake triggered horizontal block movement on a kilometer scale at a depth of 50 m and causing the originally hot well to become blocked, then some hot water emerged through vertical cracks to the ground surface. Furthermore, land movement (lateral spread) occurred due to the liquefaction process.

The September 28th, 2018, earthquake may change groundwater table contour of confined aquifer. Comparison of measurements between 1995 (Suryaman *et al*., 1995) and 2024 (Abdullah *et al*., 2024) indicates a decrease in the groundwater table (Figure 4.3.29).

The phenomenon may effect of subsurface deformation caused by the earthquake that the mechanisms, and its impacts require further detailed study in the future. Water isotope data from shallow wells after the earthquake indicate an abnormal mixing of shallow and deep aquifers.

4.3.3. Liquefaction Characteristic of Balaroa and Petobo

Liquefaction induced landslides at Palu is divided into two parts: the western side (Balaroa) and the eastern side (Petobo, Jono Oge, Lolu, Sidondo, and Sibalaya). Liquefaction induced landslides at Balaroa represents the western part while Petobo is the eastern part of The Palu Valley that both of the have similarities and differences (Table 4.3.2). The same characteristics of the liquefaction induced landslides between Balaroa and Petobo are as follows:

1. Regionally, it lies at an tectonically active condition.
2. Both of them are part of an active alluvial fan.
3. The position lies near plain morphology (slope break area) and the slope is relatively gentle to almost flat.
4. The dominant mineral composition is feldspar and quartz.
5. Toe section is relatively near boundary position of the recharge and discharge groundwater zones.
6. During the September 28th, 2018, earthquake liquefaction lies on weak layer near the ground surface. Then, flow slide was occurred by the opening of vertical cracks mechanism that high water pressure release from ruptured confined aquifer and exert pressure on the weak layers near the ground surface.

The hypothesized mechanism for liquefaction induced landslides at Balaroa and Petobo was explained by Buana *et al*. (2018) with three stages based on visual and electrical resistivity tomography observations. The proposed revised mechanism, developed in 2018 using additional primary and secondary data and several scientific publications, is as follows:

1) Preseismic

   The initial conditions of the Balaroa and Petobo affected areas were part of an active tectonic system that had formed weak condition, such as buried faults. Balaroa may part of an old buried negative flower structure, while Petobo may part of a regional fault that formed concurrently with The Palu Valley dynamics.

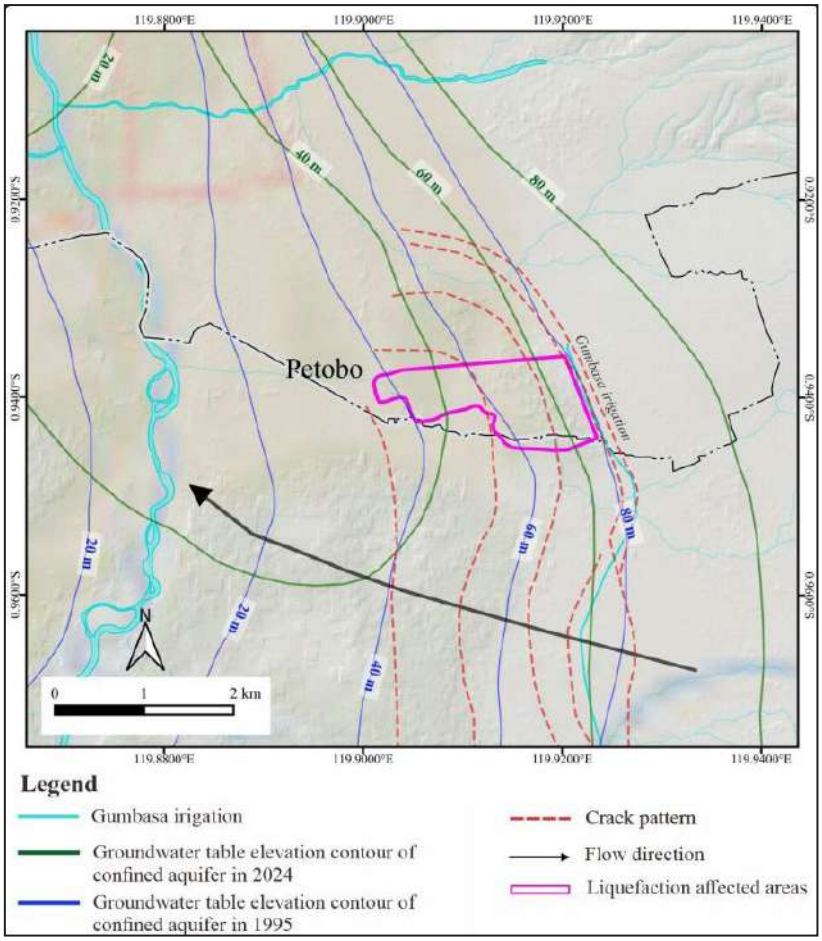

Figure 4.3.29. Groundwater elevation contour changes of confined aquifer before (Suryaman *et al*., 1995)and after the September 28th, 2018 earthquake at Balaroa (Abdullah *et al*., 2024).

Table 4.3.2. Different Character Liquefaction Triggered Flow Landslide in Balaroa and Petobo

No	Description	Balaroa	Petobo
1	Alluvial Fan Type (Blair dan McPherson, 1994)	Type I (*sediment gravity flow Primary procces, dominantly*)	Type II (primary sheetflood processes, dominantly)
2	Facies that have low N-SPT values and suspect to be slip surface	Gmm (*matrix supported, massive gravel*)	Sm (massive sand) dan Sh (sand with horizontal layers)
3	Source rock origin	Dominantly derived from granite/ granodiorite	A mixture of igneous rock products (granite/granodiorite) and metamorphic rock (quartzite, schist, phyllite rock fragments)
4	Crack patterns on ground surface due to earthquakes	The cracks on the surface may part of *a negative flower structure*	The cracks on the surface follow the pattern of the Gumbasa irrigation channels and the topographic contours of the slope

The downstream areas of the Balaroa and Petobo affected areas was border of confined aquifer zone or potentially high water pressure. Resistivity data indicate that ancient vertical fractures are associated with fluids that come from deep confined aquifer. Petobo has a confined aquifer with hot temperatures and depths exceeding 60 m. Water saturation at relatively shallow layers of the Petobo affected area may come from seepage of the Gumbasa irrigation canal.

The Balaroa affected area generally has a high density (N-SPT value > 50), because it is a clast supported gravels facies except for the matrix supported gravels facies which provides a relatively low N-SPT value and it has a weak point for the liquefaction process. In general, the Petobo affected area has a lower soil density value than Balaroa, because it has a different alluvial fan type with a dominant primary sheetflood process. Relatively low N-SPT values are generally found in the sand facies (Sm/Sh).

2) *Co-seismic*

Ground shaking from the ground oscillation process trigger fluidization and then liquefaction in weak layers. According to Obermeier (1996), fluidization is the process when a fluid is forced vertically through a layer of noncohesive sediment at a sufficiently high rate. The layers expand rapidly, porosity increases, and the sediment is no longer supported by grains, but becomes fluid. Then, pore water pressure becomes high and a significant loss of strength occurs, which is known as liquefaction.

Ground shaking from the ground oscillation process trigger ground cracks. Obermeier (1996) mention that ground cracks were caused by hydraulic fracturing, and it can cut the cap layer and cause lateral spreading at Petobo near the ground surface. The crack pattern following the topography and irrigation channels in Figure 4.3.3 that it may a lateral spreading event. Furthermore, the reopening of old and new vertical cracks may occur and cut through to the deeply confined aquifer. The cracks in the Balaroa case may part of the main fault effect that activated the ancient negative flower structure pattern.

3) Post-Seismic

Opened vertical cracks in deeply confined aquifers trigger the release of high water pressure relatively from the confined aquifer. The release of high water pressure damages weak layers near the surface, while it triggers soil liquefaction induced flow slide that it has devastating destructive effects. The process requires a time lag of minutes, according to reports from residents and Mason *et al*. (2020). A typical case for Petobo is the crown of the landslide around the Gumbasa irrigation canal due to the saturation effect of shallow water around the canal.

5. CLOSING STATEMENT

The tectonics of Sulawesi Island are very complex, because they are located at the intersection of three major tectonic plates: Eurasian, Indo-Australian, and Pacific. Since The Early Eocene approximately 55 million years ago, the tectonic evolution of Sulawesi Island has shown complex movements due to the collision of various tectonic plates that control regional geological structures and create a distribution of major faults such as Palu-Koro Fault. The Palu-Koro Fault had been formed during The Pliocene and active to the present day that causes significant deformation of the rock structures along the fault zone. Regional geological conditions of Palu-Koro Fault zone consist of igneous rocks, sedimentary rocks, metamorphic rocks, sedimentary molasses, alluvial deposits, and coastal sediments.

Sulawesi Island, particularly The Palu Bay region, is a highly seismic region due to The Palu-Koro Fault, which extends from the mainland to the sea. Based on the history records since 1905, Palu Bay has seventeen times event of destructive earthquakes from active faults on land, dominantly. The Palu-Koro Fault is divided into four segments: The Makassar Strait, Palu, Suliki, and Moa that extent to seabed and form a pull-apart structure flanked by The East Palu and West Palu Faults. The Palu Earthquake on September 28th, 2018, triggers significant surface fault displacement in Palu City and Sigi Regency. The displacement was largely a sinistral offset of up to 580 cm. The active Palu-Koro Fault cuts through alluvial deposits causing severe damage to buildings along its path. Furthermore, the earthquake also had triggered a secondary hazard such as liquefaction.

Historically, liquefaction in Indonesia has generally been encountered on a small scale such as sandboil, lateral and vertical ground movement, for examples in Yogyakarta, Klaten, Padang, Lombok, and Pidie Jaya. However, the 2018 Palu event was quite different, because liquefaction transform into a massive and relatively large mass of flow liquefaction that is commonly a rare occurrence. This type of liquefaction triggers widespread devastation of infrastructure destruction and loss of life. Liquefaction induced landslides in the western part of The Palu Valley (Balaroa) was associated with fault and in the eastern part (Petobo, Jonooge, Lolu, Sidondo, and Sibalaya) was associated with the Gumbasa irrigation canal. Geologically, the phenomenon is quite unique characteristics, and Badan Geologi proposed it as "Palu Type" liquefaction.

Discussion of three important themes related to “Palu Type” liquefaction from a geological perspective include aspects of quaternary geology and its dynamics, groundwater aspects, and engineering geology aspects. A comprehensive review of “Palu Type” liquefaction focuses on three things, *i.e.* geological characteristics and their relationship to flow liquefaction at Balaroa and Petobo, identification of weak layers and lithological safety factors against liquefaction induced landslide, and the role of water pressure from confined aquifers against liquefaction induced landslide.

Based on geological perspective, "Palu-Type" liquefaction has the following characteristics:

1) Liquefaction induced landslide occurs in alluvial fan landforms that have slopes of less than 3°, and then contact with The Palu Valley plain (slope break area).
2) The lithology consists of unconsolidated material of feldspar and quartz minerals, dominantly it comes from the debris of igneous rocks (granite/granodiorite) and metamorphic rocks.

3) The aquifer type is a multilayered confined aquifer.
4) The weak layers in liquefaction induced landslides is the Gmm facies (matrix-supported, massive gravels) for “type I” alluvial fans (dominated by the primary process of sediment gravity flow) and the Sm facies (massive sand) or Sh facies (horizontal layered sand) for “type II” alluvial fans (dominated by the primary process of sheet flood).
5) Ancient buried vertical cracks existed in the past, and they represent weak zones as pathways for pressurized groundwater release from confined aquifers.
6) The location is passed by an active fault as vibration sources up to 10 km of influence radius.
7) The toe of flow slide is located around the zone of flowing well boundaries.

REFERENCES

Allen, P.A. and Hovius, N., 1998. Sediment supply from uplifted fault blocks in active tectonic settings. *Sedimentology*, *Vol. 45 (3)*, p. 533-548.

Audley-Charles, M.G., 1991. The article discusses the tectonics of the New Guinea area. *Annual Review of Earth and Planetary Sciences*, *Vol. 19 (1)*, p. 17-41.

Badan Geologi (Geological Agency), 2009. *Atlas Zona Kerentanan Likuefaksi Indonesia*. Bandung.

Badan Geologi (Geological Agency), 2009. *Peta Cekungan Sedimen Indonesia berdasarkan data geologi and geofisika*. Pusat Survei Geologi, Bandung.

Badan Geologi, 2018. Laporan Singkat Pemeriksaan Gempa Bumi Palu Tanggal 28 September 2018, Badan Geologi, Kementerian Energi dan Sumber Daya Mineral.

Badan Geologi, *2019. Atlas Zona Kerentanan Likuefaksi Indonesia, cetakan pertama*, ISBN 978-602-9105-78-0, Badan Geologi, Kementerian Energi dan Sumber Daya Mineral.

Bellier, O., Sbrier, M., Beaudouin, T., Villeneuve, M., Braucher, R., Bourles, D., Siame, L., Putranto, E., and Pratomo, I., 2001, High Slip Rate for a Low Seismicity along the Palu Koro Active Fault in Central Sulawesi (Indonesia), Blackwell Science Ltd., *Terra Nova, Vol. 13*, p. 463-470.

Bellier, O., Sébrier, M., Beaudouin, T., Braucher, R., Bourlès, D., and Siame, L., 2001. Active tectonics of the Palu-Koro fault zone, Sulawesi, Indonesia. *Journal of Asian Earth Sciences, Vol. 19 (1)*, 1-18.

Bellier, O., Sébrier, M., Beaudouin, T., Villeneuve, M., Braucher, R., Bourles, D., Siame, L., Putranto, E., and Pratomo, I., 2001. High slip rate for low seismicity along the Palu-Koro active fault in central Sulawesi (Indonesia). *Terra Nova*, *Vol. 13 (6)*, p. 463-470.

Bergman, S.C., Coffield, D.Q., Talbot, J.P., and Garrard, R.J., 1996. Tertiary tectonic and magmatic evolution of western Sulawesi and the Makassar Strait, Indonesia: evidence for a Miocene continent-continent collision. In: Hall, R. and Blundell, D.J. (eds.) *Tectonic evolution of Southeast Asia*. Geological Society of London, p. 391-430.

Bishop, A.W., Green, G.E., Garga, V.K., Andersen, A., and Browns, J.D., 1971. A new ring shear apparatus and its application to the measurement of residual strengtp. *Geotechnique 21 (4)*, p.273-328.

Blair, T.C. and McPherson, J.G., 1994. Alluvial fan processes and forms. In: *Geomorphology of Desert Environments*, p. 354-402. Springer.

Blum, M.D. and Törnqvist, T.E. , 2000. Fluvial responses to climate and sea-level change: A review and look forward. *Sedimentology, Vol. 47*, p. 2-48.

BNPB, 2018. *Kerugian and Kerusakan Dampak Bencana di Sulawesi Tengah Mencapai 13,82 Trilyun Rupiap. Baand Nasional Penanggulangan Bencana, November 22, 2018*. https://bnpb.go.id/berita/kerugian-and-kerusakan-dampak-bencana-di-sulawesi-tengah-mencapai-1382-trilyun-rupiah.

Boggs, S., 2006. *Principles of sedimentology and stratigraphy, 4th ed.*, Pearson Prentice Hall.

Briais, A., Patriat, P., and Tapponnie, 1993. Updated Interpretation of Magnetic Anomalies and Seafloor Spreading Stages in the South China Sea: Implications for the Tertiary Tec-

tonics of Southeast Asia. *Journal of Geophysical Research*, *Vol. 98*, p. 6299-6328.

Broemhead, 1936. *A simple ring shear apparatus. Ground Engineering, Vol.12 (5)*, p.4-44.

Buana, T.W., Hermawan, W., Wiyono, Rahdiana, R.N., 2019. Mekanisme Bencana di Balaroa dan Petobo , In: *Buku Di Balik Pesona Palu, Bencana Melanda Geologi Menata, Cetakan Pertama: 2018*, ISBN: 978-602-9105-76-6, p. 175-186.

Burbank, D.W. and Anderson, R.S., 2011. *Tectonic geomorphology*. Wiley-Blackwell.

Calvert, 1999. The Cenozoic evolution of the Lariang and Karama Basins in Sulawesi is detailed in the Indonesian Petroleum Association's, *Proceedings from the 27th Annual Convention held in Jakarta,* p. 505-511.

Castro, Gonzalo, 1969. Liquefaction of Sand, Dissertation Harvard University Cambridge.

Charlton, T.R., 2000. Tertiary evolution of the eastern Indonesia collision complex. *Journal of Asian Earth Science*, *Vol. 18*, p. 391-430.

Cipta, A., Robiana, R., Griffin, J.D., Horspol, N., Hidayati, S., and Cummins, P., 2016, *A probabilistic seismic hazard assessment for Sulawesi, Indonesia*, Geological Society, London, *Special Publications, 441*, http://doi.org/10.1144/SP441.6.

Cloke, I.R., Milsom, J., and Blundell, D.J., 1999. The implication of gravity data from East Kalimantan and Makassar Straits: a solution to the origin of the Makassar Strait? *Journal of Asian Earth Science*, *Vol. 17*, p. 61-78.

Costa, J.E., 1984. Physical geomorphology of debris flows. In: *Debris Flows/Avalanches: Process, Recognition, and Mitigation*, p. 55-98. Geological Society of America.

Cubrinovski, M., Green, R., Allen, J., Ashford, S., Bradshaw, A., Cox, B., and Wotherspoon, L. 2011. Geotechnical reconnaissance of the 2010 Darfield (Canterbury) earthquake. *Bulletin of the New Zealand Society for Earthquake Engineering, 44 (4)*, p.243-320.

Davidson, J.W., 1991. The geology and perspective of Buton Island, S.E. Sulawesi. Indonesia. *Proceedings Indonesian Petroleum Association, 20th Annual Convention*, p. 209-233

Fortuin, A.R., De Smet, M.E.M., Hadiwasastra, S., Marle, L.J. van, Troelstra, S.R., and Tjokrosapoetro, S., 1990. The study focused on the late Cenozoic sedimentary and tectonic history of South Buton, Indonesia. *Journal ofh-east Asian Earth Sciences*, *Vol. 4 (2)*, p. 107-124.

Gusman, A.R., Supendi, P., Nugraha, A.D., Power, W., Latief, H., Sunendar, H., Widiyantoro, S., Daryono, Wiyono, S.H., Hakim, A., Muhari, A., Wang, X., Burbidge, D., Palgunadi, K., Hamling, I., dan Daryono, M.R., 2019, Source Model for the Tsunami Inside Palu Bay Following the 2018 Palu Earthquake Indonesia, *Geophysical Research Letters.*

Gustiantini, L., Suherman, I.H., Raharjo, P., Purwanto, C., 2024, *Peta Struktur Geologi Teluk Palu*, Kementerian Energi dan Sumber Daya Mineral, Badan Geologi, Balai Besar Survei dan Pemetaan Geologi Kelautan.

Haile, N.S., 1978. Reconnaissance palaeomagnetic results from Sulawesi, Indonesia, and their bearing on palaeogeographic reconstructions. *Tectonophysics, Vol. 46,* p. 77-85.

Hall, R. and Milsom, M.E.J., 2000. Neogene suture in eastern Indonesia, *Journal of Asian Earth Sciences, Vol. 18*, p. 781-808.

Hall, R. and Wilson, M.E.J., 2000. Neogene sutures in eastern Indonesia. *Journal of Asian Earth Sciences*, *Vol. 18 (6)*, p. 781-808.

Hall, R., 1996. Reconstructing Cenozoic SE Asia in Hall, R., and Blundell, D.J., editors' Tectonic evolution ofh-east Asia. *Geological Society of London*, p. 153-184.

Hamilton, W., 1979. Tectonics of the Indonesian Region. U.S. *Geological Survey Professional Paper*, p. 1078-345.

Harvey, A.M., 2005. *Processes of sedimentation on alluvial fans: A critical review*. Earth-Science Reviews, Vol. 72 (3-4), p. 175-193.

Hidayat, S. and Moechtar, H. ,2000. *Penelitian endapan Kuarter bawah permukaan kaitannya dengan kebencanaan di daerah Palu dan*

sekitarnya, Sulawesi Tengah. Pusat Penelitian dan Pengembangan Geologi, Bandung.

Holzer, T.L., 1998. The Loma Prieta, California, Earthquake of October 17, 1989: Liquefaction. U.S. *Geological Survey Professional Paper, 1551-B*.

https://www.tempo.co/politik/tsunami-dan-gempa-palu-donggala-2018-dalam-angka-korban-daya-rusak-dan-lainnya-138090.

Hutchison, C.S., 1989. Geological Evolution of South-East Asia. *Oxford Monographs on Geology and Geophysics, Vol. 13*, 376 pp.

Hvorslev, M.J., 1934. A ring shearing apparatus for the determination of the shearing resistance and plastic flow of soils. *Proceedings of the 1st International Conference on Soil Mechanics and Foundation Engineering*, Harvard University.

Indonesia. *Sains Malaysiana*, *Vol. 3 (1)*, p. 65-86.

Ishihara, 1993. *Liquefaction and flow failure during earthquake. Geotechnique, 43 (4)*, p.73-89.

Jalil, A., Suryanto, W., and Nugraha, H., 2021. Sedimentology and geodynamics of alluvial fans in Palu, Sulawesi. *Indonesian Journal of Earth Sciences, Vol. 40 (2)*, p. 89-102.

Jaya, A. and Nishikawa, O., 2013. Paleostress reconstruction from calcite twin and fault slip data using the multiple inverse method in the East Walanae fault zone: Implications for the Neogene contraction in South Sulawesi, Indonesia. *Journal of Structural Geology*, *Vol. 55*, p. 34-49.

Jaya, A., Nishikawa, O., and Jumadil, S., 2023. Paleoseismic Analysis of the Walanae Fault Zone in South Sulawesi, Indonesia. *Indonesian Journal on Geoscience, Vol. 10 (2).*

Katili, J.A., 1978. *Past and present geotectonic position of Sulawesi, Indonesia, Vol. 45,* p. 289-322.

Kavalieris, I., Leeuwen, T.M. van, and Wilson, M., 1992. Geological setting and styles of mineralisation, north arm of Sulawesi, Indonesia. *Journal of* South-*east Asian Earth Science*, *Vol. 7,* p. 113-129.

Keller, E. A. and Pinter, N., 1996. *Active tectonics, Vol. 19*, Prentice Hall Upper Saddle River.

Kertapati, E., A. Soehaemi, and Djuhanda, A., 1992. *Seismotectonic Map of Indonesia. 1:5,000,000 scale*. Geol. Res. Dev. Centre, Bandung.

Kertapati, E.K., Putranto, E.T., and Bahar, I., 1991. *Katalog gempabumi merusak di Indonesia*. Kelompok Kerja Seismotektonik, Bidang Geologi, P3G, Bandung.

Kiyota, T., Towhata, I., Yasuda, S., Prakoso, W., and Uchimura, T., 2020 Geomorphic and sedimentologic response to the 2018 Sulawesi earthquake in Palu. *Geological Society of America Bulletin, Vol. 132 (9-10)*, p. 1909-1925.

Kramer, S.L., 1996. *Geotechnical Earthquake Engineering*, Prentice Hall Upper Saddle River, New Jersey: 653 pp.

Lee, T.Y., and Lawver, L.A., 1995. Cenozoic Plate Reconstruction of the South China Sea Region. *Tectonophysics, Vol. 251*, p. 85-139.

Leeuwen, T.M. van and Muhardjo 2005. Stratigraphy and tectonic setting of the Cretaceous and Paleogene volcanic-sedimentary successions in northwest Sulawesi, Indonesia: implications for the Cenozoic evolution of western and northern Sulawesi. *Journal of Asian Earth Sciences*, *Vol. 25 (3)*, p. 481-511.

Leeuwen, T.M. van, 1981. The geology of southwest Sulawesi, with special reference to the Blue area, is discussed. Blue area. *The geology and tectonics of Eastern Indonesia*, Vol. *2*, 277-304.

Leterrier, J., Yuwono, Y.S., Soeria-Atmadja, R., and Maury, R.C., 1990. Potassic volcanism The study took place in central Java and south Sulawesi, Indonesia. *Journal ofh-east Asian Earth Sciences*, *Vol. 4 (3)*, p. 171-187.

Letouzey, J., Werner, P., and André Marty, A., 1990. Fault reactivation and structural inversion. Backarc and intraplate compressive deformations. The eastern Sunda Shelf (Indonesia) serves as an example. *Tectonophysics*, *l. 183*, p. 341-362.

Leuwen, Th.M. van, 1981. The geologygy of south-west Sulawesi with special reference to the Biru area. In: Barber, A.J. and Wiryosujono, S. (eds.). *The geology and tectonics of Eastern Indonesia*. GRDC, *Vol. 2*, p. 277-304.

Lupini, J.F., Skinner, A.E., and Vaughan, P.R., 1981. The drained residual strength of cohesive soils. *Geotechnique, 31 (2)*, p.181-213.

Mandl, G., Jong, L.N.J. de, and Maltha, A., 1977. Shear zones in granular material. An experimental study of their structure and mechanical genesis. *Rock Mechanics 9*, p.95-144.

McCaffrey, R., Sutarjo, R., Susanto, R., Buyung, R., Sukarman, R., Husni, B., Sudiono, M., Setudju, D., and Sukamto, R., 1983. Microearthquake survey of the Maluku Sea and Sulawesi, Indonesia. *Bull. Geol. Res. Dev. Centre*, Bandung*, Vol. 7*, p. 13-23.

Metcalfe, I. and Irving, E., 1990. Allochthonous Terrane Processes in-east Asia [and Discussion]. *Philosophical Transactions of the Royal Society of London. Series A, Mathematical and Physical Sciences*, *Vol. 331 (1620)*, p. 625-640.

Metcalfe, I., 1988. Origin and assemblyly of South-east Asian continental terranes. *Geological Society, London, Special Publications*, *Vol. 37 (1)*, p. 101-118.

Metcalfe, I., 1996. conducted a study on the pre-Cretaceous evolution of South-east Asian terranes. *Geological Society, London, Special Publications*, *Vol. 106 (1)*, p. 97-122.

Miall, A.D. ,1992. *The geology of fluvial deposits*. Springer-Verlag.

Miall, A.D., 1996. *The geology of fluvial deposits (2nd ed.)*. Springer.

Moechtar, H., 1994. Coastal plain and fluvial deposits in the Tertiary of central and northern Spain (Doctoral dissertation). Utrecht University. Geologica Ultraiectina No. 123.

Mörner, N.A., 2004. Active faults and paleoseismicity in Fennoscandia, especially Sweden. The study focuses on primary structures and secondary effects. *Tectonophysics*, *Vol. 380 (3)*, p. 139-157.

Natawidjaja, D.N., Mudrik, R., Daryono, Prasetya, G., Philip, U., Liu, L.F., Hananto, N.D., Kongko, W., Triyoso, W., Puji, A.R., Meilano, I., Gunawan, E., Supendi, P., Pamumpuni, A., Irsyam, M., Faizal, L., Hidayati, S., Sapiie,B., Mipi A. Kusuma, M.A., and Tawil, S., 2021. The 2018 Mw7.5 Palu 'supershear' earthquake ruptures geological fault's multisegment separated by large bends: results from integrating field measurements, LiDAR, swath bathymetry and seismic-reflection data, *Geophys. J. Int. Vol. 224*, 985-1002, doi: 10.1093/gji/ggaa498.

Nemec, W., and Postma, G., 1993. Quaternary alluvial fans in the southwestern United States. *Sedimentary Geology, Vol. 81 (1-4)*, 45-67.

Nugraha, A.M.S., Hall, R., and Fadel, M.B., 2002. The Sulawesi Molasse: A revised Neogene stratigraphy for Sulawesi, Indonesia, *Journal of Asian Earth Sciences, Vol. 228*, p. 1-28.

Obruchev, V.A., 1948. *Osnovnyje certy kinetiki i plastiki neotektoniki*. Izvestiya Akademii Nauk UzSSR Sertiya Geologicheskaya.

Omang, A., Solikhin, A., Supartoyo, Minarno, P.A., Cipta,A., Nurfalah, F., and Efendi, R., 2018. *Menghitung Guncangan Gempa Bumi (Dalam Buku Dibalik Pesona Palu, Bencana Melanda Geologi Menata), Cetakan Pertama*, ISBN: 978-602-9105-76-6, Badan Geologi, Kementerian Energi dan Sumber Daya Mineral.

Pakoksung, K., Suppasri, A., Imamura, F., Athanasius, C., Omang, A., and Muhari, A., 2019. Simulation of the Submarine Landslide Tsunami on 28 September 2018 in Palu Bay, Sulawesi Island, Indonesia, Using a Two-Layer Model, *Pure and Geophysics,Vol. 176*, p. 3323 - 3350.

Parkinson, C.D., 1991. The Petrology, Structure, and Geologic History of the Metamorphic Rocks of Central Sulawesi, Indonesia. PhD Thesis, Geological Research in-east Asia, University of London, p. 337.

Patria, A. and Putra, P.S., 2020. Development of the Palu-Koro Fault in NW Palu Valley,

Indonesia. *Geoscience Letters, 7, 1*. https://doi.org/10.1186/s40562-020-0150-2.

Pelynovsky, E., Yuliadi, D., Prasetya, G., and Hidayat, R., 1997. The January 1, 1996 Sulawesi Island Tsunami, Science of Tsunami Hazards, *Int. Journal of Tsunami Society, Vol. 16*, p. 29-38.

Permana, H. and Zen, M.T., 1991. Stratigraphy and sedimentology of Quaternary deposits in Sulawesi, Indonesia. *Indonesian Journal of Earth Sciences, Vol. 2 (1)*, p. 23-37.

Pigram, C.J. and Panggabean, H., 1984. Rifting of the northern margin of the Australian The origin of some microcontinents in eastern Indonesia can be traced back to the rift of the Australian continent. *Tectonophysics*, *Vol. 107 (3)*, p. 331-353.

Posamentier, H.W. and Allen, G.P., 1999. *Siliciclastic sequence stratigraphy: Concepts and applications.* SEPM.

Poulos, S.J., 1981. *The steady state of deformation. Journal of Geotechnical Engineering Division ASCE, 107 (GT 5)*, p.553-562.

Prasetya, G., Budi, S., and Raharjo, B., 2019. Post-earthquake sediment dynamics in Palu: Implications for hazard assessment. *Journal of Asian Earth Sciences, Vol.183*, 103951.

Prasetya, G.S., De Lange, W.P., and Healy, T.R., 2001. The Makassar Strait Tsunamigenic Region, Indonesia, *Natural Hazar, Vol. 24*, p. 295-307.

Priadi, B., Polve, M., Maury, R. C., Bellon, H., Soeria-Atmadja, R., Joron, J. L., and Cotten, J., 1994. Tertiary and Quaternary magmatism in Central Sulawesi: chronological and petrological constraints. *Journal ofh-east Asian Earth Sciences*, *Vol. 9 (1)*, p. 81-93.

Priadi, B., Polve, M., Maury, R.C., Soeria-Atmadja, R., and Bellon, H., 1993. Geodynamic implications of Neogene potassic calc-alkaline magmatism in central Sulawesi: geochemical and isotopic constraints. *Proceedings of the 22nd Annual Convention of the Indonesian Association of Geologists*, *1*, p. 59-81.

Pusgen (Pusat Gempa Nasional), 2017. *Peta sumber dan bahaya gempa Indonesia tahun 2017*, ISBN 978-602-5489-01-3, Puslitbang Perumahan dan Permukiman, Balitbang Kementerian PUPR.

Rangin, C., Dahrin, Quebral, R.M., Pubellier, and the Thetys working group, 1990. A simple model for the tectonic evolution of Southeast Asia and Indonesia region for the past 43 m.y. *Geology Society of France*, *Vol. 6*, p. 889-905.

Robertson, P.K. and Wride, C.E., 1997. Cyclic Liquefaction and Its Evaluation Based on the SPT and CPT. *Technical Report NCEER-97-0022*, p.41-87.

Robiana, R., Athanasius, C., Solikhin, A., Griffin, J., Horspol, N., 2012. *Peta kawasan rawan bencana gempa bumi daerah Sulawesi Tengah*, Pusat Vulkanologi dan Mitigasi Bencana Geologi, Badan Geologi, Kementerian Energi dan Sumber Daya Mineral.

Rusmana, E., Koswara, A., and Simandjuntak, T.O., 1993. *Geology of the Luwuk Sheet, Sulawesi: 250,000.* Geological Research and Development Centre, Bandung.

Sassa, K., 1985. The mechanism of debris flows. *Proceedings of the 11th International Conference on Soil Mechanics and Foundation Engineering, San Fransisco, Calif., Vol.3*, p.1173-1176.

Sassa, K., 1997. A New intelligent type dynamic loading ring shear apparatus. *Landslide News* (Japanese Landslide Society) *(10)*, p.33.

Schumm, S.A., Harvey, M.D., and Watson, C.C., 2000. Incised channels: *Morphology, dynamics and control.* Water Resources Publications.

Seed, H.B. and Idriss, I.M., 1982. *Ground motions and soil liquefaction during earthquakes.* Earthquake Engineering Research Institute.

Seed, P.B. and Idriss, I.M., 1971. A Simplified Procedure for Evaluating Soil Liquefaction Potential. *Journal of the Soil Mechanics and Foundations Division, Vol.97, No. SM9*, p.1249-1273.

Sidi, F., Prasetyo, I., and Hidayah, T., 2018. Sediment supply and depositional systems in tectonically active basins: A case study from

Palu, Sulawesi. *Geosciences Journal, Vol. 22 (4)*, p. 755-767.

Silver, E.A., McCaffrey, R., and Smith, R.B., 1983. Collision, rotation, and the initiation of the evolution of Sulawesi, Indonesia, involved subduction. *Journal of Geophysical Research: Solid Earth (1978-2012)*, *Vol. 88* (B11), p. 9407-9418.

Simandjuntak et al., 1991? P.1

Simandjuntak, T.O., 1992. An Outline of Tectonics of the Indonesian Region. *Geological Newsletter*, Vol. *252 (3)*, p. 4-6.

Simandjuntak, T.O., Surono, and Supandjono, J.B., 1997. *Geological Map of the Poso Quadrangle, Sulawesi, Second Edition*, Geological Research and Development Centre, Bandung, Indonesia.

Simanjuntak, T.O. and Barber, A.J., 1996. Contrasting tectonic styles in the Neogene orogenic belts of Indonesia, p. 185-201. In Hall, R. and Blundell, D.J. (eds.). London. *Tectonic evolution of east Asia. Geological Society Special Publication*. London.

Situmorang, B., 1984. Formation, Evolution, and Hydrocarbon Prospect of Makassar Basin, Indonesia. *Proceedings of the Circum-Pacific Energy and Mineral Resources Conference III*. p. 227-231.

Smith, R.B. and Silver, E.A., 1991. Geology of Miocene collision complex, Buton, Eastern Indonesia. *Geol. Soc. Am. Bull. Vol. 103*, p. 660-678.

Soehaimi, A., 1985, Lawe Earthquake, 5 March 1985, Central Sulawesi (in Bahasa Indonesia). Geological Research and Development Centre, Bandung. internal report, unpublished.

Soehaimi, A.I., Effendi, Setiawan, J.H., and Supartoyo conducted a study in 2005 titled "Investigating the Palolo Earthquake". The earthquake occurred on 24 January 2005 in Central Sulawesi, as documented in an internal report published by the Geological Research and Development Centre in Bandung (in Bahasa Indonesia)

Soesilo, J., 2012. Cretaceous Paired Metamorphic Beltsts in South-east Sundaland. The doctoral dissertation was completed at the Bandung Institute of Technology in Indonesia.

Stevens, C., McCaffrey, R., Bock, Y., Genrich, J., Subarya, C., Puntodewo, S.S.O., and Vigny, C., 1999. Rapid rotations about a vertical axis in a collisional setting are revealed by thePalu fault, Sulawesi, Indonesia. *Geophysical Research Letters*, *Vol. 26 (17)*, p. 2677-2680.

Stewart, I.S. and Hancock, P.L., 1994. Neotectonics. *Continental deformation*, p. 370-409.

Sudradjat, A., 1981. Investigating of Palu Valley, Centre of Sulawesi by Remote Sensing (in Bahasa Indonesia), PhD Thesis, ITB, Bandung.

Sukamto et al., 1973? P.1

Sukamto, R., 1973. *Reconnaissance Geological Map of the Palu Quadrangle, Sulawesi, Scale 1:250,000.* GRDC, Bandung, Indonesia.

Sukamto, R., 1975. The structure of Sulawesi in the light of plate tectonics. *Proc. of the Regional Conference on the Geology and Mineral Resources in east Asia, J*akarta, p. 1-25.

Sukamto, R., 1982. *Geological map of Pangkajene and the western part of Watampone Quadrangle, Sulawesi. Scale 1:250,000*. GRDC, Bandung, Indonesia.

Sukamto, R., Amin, T.C., and Sukarna, D., 2003. *Atlas Geologi and Potensi Sumber Daya Energi Kawasan Indonesia Skala 1:10,000,000.* Pusat Survei Geologi.

Sukamto, R., Simandjuntak, T.O., 1983. Tectonic relationship between geologic provinces of western Sulawesi, eastern Sulawesi, and Banggai-Sula in the light of sedimentological aspects. *Bull. Geol. Res. Dev. Cent. Vol. 7*, p. 1-12.

Sukamto, Sumadirdja, H., Suptandar, T., Hardjoprawiro, S., Sudana, D., 1996. Reconnaissance Geological Map of the Palu Quadrangle, Sulawesi, *Geological Research and Development Centre, Bandung.*

Sukido, Sukarna, D., and Sutisna, K., 2011. *Geological Map of the Pasangkayu Quadrangle, Sulawesi*, Geological Research and Development Centre, Bandung.

Suparan, P. and Rimbaman, 1992. Laporan pendahuluan pemetaan geologi Kuarter Lembar

Palu, Sulawesi Tengah. Pusat Penelitian dan Pengembangan Geologi, Bandung

Supartoyo, Cipta, A., Omang, A., Solikhin, A., Adiminarno, P., 2018. *Munculnya Pergeseran Tanah Konsisten,* In: *Dibalik Pesona Palu, Bencana Melanda Geologi Menata), Cetakan Pertama 2018*, ISBN: 978-602-9105-76-6, Badan Geologi, Kementerian Energi dan Sumber Daya Mineral.

Supartoyo, Surono, dan Putranto, E.T., 2014, *Katalog Gempa bumi Merusak Indonesia Tahun 1612 - 2014 (Edisi Kelima)*, Pusat Vulkanologi dan Mitigasi Bencana Geologi, Badan Geologi, Departemen Energi dan Sumber Daya Mineral, 131 pp.

Surmont, J., Laj, C., Kissel, C., Rangin, C., Bellon, H., and Priadi, B., 1994. New Paleomagnetic constraints on the Cenozoic tectonic evolution of the North Arm of Sulawesi, Indonesia. *Earth and Planetary Science Letters*, *Vol. 121 (3)*, p. 629-638.

Surono and Sukarna, D., 1993. *Geological Map of the Sanana Quadrangle, Maluku. Indonesia* Geological Research Development Centre

Surono and Sukarna, D., 1995. The Eastern Sulawesi Ophiolite Belt, Eastern Indonesia. A review of its origin with special reference to the Kendari area. *Journal of Geology and Mineral Resources, Vol. 46*, p. 8-16.

Surono and Sukarna, D., 1995. The Eastern Sulawesi Ophiolite Belt, Eastern Indonesia. A review of its origin with special reference to the Kendari area. *Journal of Geology and Mineral Resources, Vol. 46*, p. 8-16.

Surono, 1997. A provenance study of sandstones from the Meluhu Formation, east Sulawesi, Eastern Indonesia. *Journal of Geology and Mineral Resources.*

Surono, 1998b. Sedimentology of the oolitic limestone succession of the Paleogene Tampakuran, South-east Sulawesi, Indonesia. *Proc. of the thirty-third Session of the Coordinating Committee for Coastal and Offshore Geosciences Programme in East and Southeast Asia (CCOP)*, 30 October-2 November 1996.

Surono, 2010a. *Geologi Lengan Tenggara Sulawesi*. *Publikasi Khusus, Badan Geologi*, KESDM, 161pp.

Taufiq *et al*., 2019? p. 21

Terzaghi, K.V., 1925. *Erdbaumechanik auf Bodenphysikalischer Grundlage. F. Deuticke* (Leipzig and Wien).

Thein *et al*., 2015? p. 25

Tika, T.E., Vaughan, P.R., and Lemos, L.J.L.J., 1996. *Fast shearing of pre-existing shear zones in soil. Geotechnique 46 (2)*, p.197-233.

Tjia, H.D. and Zakaria, T.H., 1974. Palu-Koro strike-slip fault zone, Central Sulawesi,

USGS (United State Geological Survey), 2018. *M.75 - 70km N of Palu, Indonesia*, https://earthquake.usgs.gov/earthquakes/eventpage/us1000h3p4/executive.

USGS/Wikipedia, 1964? p.2

Wafid, M., Sassa, K., and Fukuoka, P., 2004b. *Deformation of Saturated Sandy Soils under Shearing in Ring Shear Test*. Annuals of Disaster Prevention Research Institute, Kyoto University.

Wafid, M., Sassa, K., Fukuoka, P., and Wang, G., 2004c. *Evolution of Shear Zone Structure in Undrained Ring Shear Tests. Landslides Vol.2*, p.101-112.

Wakita, K., 2000. Cretaceous accretionary-collision complexes in central Indonesia. *Journal of Asian Earth Sciences, Vol. 18*, p.739-749.

Wakita, K., Sopaheluwakan, J., Miyazaki, K., and Zulkarnain, I,. 1996. Tectonic evolution of the Bantimala complex, South Sulawesi, Indonesia. *Geological Society, London, Special Publications*, *Vol. 106 (1)*, p. 353-364.

Wallace, R.C., 1986. Active tectonics. *The work was published under the title "Studies in Geophysics". National Academy of Sciences, Washington, DC*.

Wallace, R.E., 1990. *The San Andreas fault system, California*. Washington, DC: US Government Printing Office.

Walpersdorf, A., Vigny, C., Subarya, C., and Manurung, P., 1998. Monitoring of the Palu-Koro Fault (Sulawesi) by GPS. *Geophysical Research Letters*, Vol.*25 (13)*, p.2313-2316.

Wang, F. and Sassa, K., 2000. *Description of ring-shear apparatus and testing methodology for measurement of excess pore water pressure and saturation (BD ≥ 0.95) following isotropic consolidation at 50 kPa normal stress*. Kyoto University, DPRI.

Watkinson, I.M. and Hall, R., 2017. Quaternary deformation and sedimentation along the Palu-Koro fault, Sulawesi. *Tectonophysics, Vol. 705*, p. 87-101.

Watkinson, I.M., 2011. Ductile flow in the metamorphic rocks of central Sulawesi.*Geological Society, London, Special Publications*, Vol.*355(1)*, p.157-176.

Wilson, M.E.J. and Moss, R., 1999. The study focuses on the Cenozoic paleogeographic evolution of Sulawesi and Kalimantan. *Palaeogeography, Palaeoclimatology, Palaeoecology, Vol. 145*, p. 303-337.

Wood, R.M. and Mallard, D.J., 1992. When is a fault 'extinct'? *Journal of the Geological Society*, *Vol.149 (2)*, p.251-254.

Wu, Z. and Hu, M., 2024. Definitions, Classification Schemes for Active Faults, and Their Application, *Geosciences, Vol. 14*, 68. https://doi.org/10.3390/ geosciences14030068.

Yuwono, Y.S., Bellon, H., Soeria-Atmadja, R., and Maury, R.C., 1985. Neogene and The study focused on Pleistocene volcanism in South Sulawesi. *Proceedings Ikatan Ahli Geologi Indonesia*, *Vol.14*, p.169-179.

Zoback, M.D. and Zoback, M.L., 1991. Tectonic stress field of North America and relative plate motions. *Neotectonics of North America*, *Vol.1*, p.339-366.

AUTHORS AND EDITORS

Authors:
Muhammad Wafid A.N. (Likuefaction - Badan Geologi)
Suyono (Sedimentology - PATGTL)
Taufiq Wira Buana (Geological Engineering - PATGTL)
Sukahar Eka Adi Saputra (Tectonic - PSG)
Akbar Cita (Geomorphology - PSG)
Munib Ikhwatun Iman (Hidrogeology - PATGTL)
Supartoyo (Earthquake - PVMBG)
Rio Alcanadre Tanjung M., (Quatenary Geology- PSG)
Luli Gustiantini (Marine Geology - BBSPGL)
Firman Maliki Abdullah (Hidrogeology - PATGTL)
Ryan Nur Rahdiana (Geological Engineering - PATGTL)
Wawan Hermawan (Geological Engineering - PATGTL)
William Pradana Solu (Geological Engineering - PATGTL)
Athanasius Cipta (Earthquake - PVMGB)
Merry Christina Natali (Earthquake - PVMGB)
Imam Catur Priambodo (Earthquake - PVMGB)
Risna Widyaningrum (Geological Engineering - PATGTL)
Amalfi Omang (Earthquake - PVMGB)
Purnomo Rahardjo (Marine Geology - BBSPGL)
Joko Wahyudiono (Geological Structure - PSG)
Yudhicara (Tsunami - PVMBG)
Irwan Hidayat Suherman (Oseanography - BBSPGL)
Akhmad Solikhin (Earthquake - PVMGB)
Taat Setiawan (Hidrogeology - PAGTL)
Abdullah Husna (Hidrogeology - PATGTL)
Fadlianto Nurfalah (Earthquake - PVMGB)
Exmarwanto (Hidrogeology - PAGTL)
Ibrahim Mandi (Geomorphology - PSG)
Nurmaliah (Geophysics - PSG)
Rohman (Quatenary Geology - PSG)

Editors
Hermes Panggabean (Petroleum - Profesional Geologi)
Wahyu Wilopo (Environment Geology - Universitas Gadjah Mada)
Sri Hidayati (Vulkanology - PVMBG)

Copy Editors
Nenen Adriyani (Profesional)
Atep Kurnia (PSDMBP)

Palu-Type Liquefaction

A Unique Natural Phenomenon in the World, A Comprehensive Geological Review

The earthquake and subsequent liquefaction that occurred in Palu City and its surrounding areas on September 28, 2018, had a devastating impact, particularly in the Petobo, Balaroa, and Jono Oge areas. Based on post-disaster data, the recorded death toll reached 2,081 people, with the highest number of victims in Palu City (1,706 people) as reported by BNPB as of October 25, 2018.

Palu-type liquefaction is a unique and specific phenomenon that occurs in the Palu region, particularly in the Balaroa and Petobo areas, in the form of massive soil flows formed by the complex interaction of geological, hydrogeological, and tectonic factors. This event was triggered by a combination of alluvial fan conditions with loose lithology, the presence of pressurized aquifers, and the formation of vertical fractures due to tectonic activity, which together resulted in destructive post-earthquake ground flows.

Through the studies of sedimentation, structure and tectonics, hydrogeology, and engineering geology presented in this book, it is hoped that it will become a strategic reference for policy makers, academics, disaster practitioners, and the wider community in understanding the risks of liquefaction and developing appropriate mitigation measures. The Geological Agency, as part of the Ministry of Energy and Mineral Resources, which focuses on the investigation and service of energy and mineral resources, is committed to continuously striving to protect the community from various geological disasters.

MINISTRY OF ENERGY AND MINERAL RESOURCES

ISBN 978-634-96502-1-2